UNIVERSIDAD COMPLUTENSE DE MADRID
FACULTAD DE CIENCIAS QUÍMICAS

DEPARTAMENTO DE BIOQUÍMICA Y BIOLOGÍA MOLECULAR

ORGANIZACIÓN BIOQUÍMICA DEL PROTO-ANILLO DE DIVISIÓN BACTERIANO EN SISTEMAS MÍNIMOS DE MEMBRANA-IMPACTO DEL SISTEMA MinCDE DE SELECCIÓN DEL SITIO DE DIVISIÓN.

BIOCHEMICAL ORGANIZATION OF THE PROTO-RING OF BACTERIAL DIVISION IN MINIMUM MEMBRANE SYSTEMS-IMPACT OF THE MinCDE SYSTEM OF DIVISION SITE SELECTION.

Tesis doctoral para optar al grado de Doctor

presentada por

Ana Raso Alonso

Director de Tesis: Prof. Germán Alejandro Rivas Caballero

Madrid, 2018

La presente Tesis Doctoral titulada "*Organización bioquímica del proto-anillo de división bacteriano en sistemas mínimos de membrana-impacto del sistema MinCDE de selección del sitio de división*" ha sido realizada por Ana Raso Alonso, bajo la dirección del Dr. Germán Alejandro Rivas Caballero, en el grupo de Bioquímica de sistemas de la división bacteriana, en el Departamento de Biología Estructural y Química, del Centro de Investigaciones Biológicas del Consejo Superior de Investigaciones Científicas (CIB-CSIC). Esta tesis ha sido financiada por el proyecto "The German Israeli Foundation for Scientific Research and Development (G.I.F.)" (coord.: Prof. Petra Schwille - Max Planck Inst. Biochemistry, Martinsried - y Prof. Mario Feingold - BenGurion University, Beer Sheva, Israel.), y es parte de la colaboración entre los tres laboratorios.

Opta al grado de Doctor

Ana Raso Alonso

Vº Bº del Director de la Tesis

Prof. Germán Alejandro Rivas Caballero

Vº Bº del Tutor de la Tesis

Dr. Francisco Gavilanes Franco

A mi familia

Agradecimientos

Termino esta etapa de mi vida sintiendo un profundo agradecimiento por todas las personas que me han acompañado durante estos años de formación predoctoral. Me siento muy afortunada de haber podido compartir estas experiencias con personas que me han aportado tanto. Para mí ha sido un gran reto recorrer este camino, y no habría sido posible llegar hasta aquí sin el apoyo y la confianza de todas ellas.

A Germán por confiar en mí cuando yo no lo conseguía. Por abrirme la puerta del laboratorio y apoyarme con tanto cariño en todo momento. Gracias por estar tan pendiente de mi bienestar en el laboratorio durante estos años. A Petra Schwille por hacer posible la realización de este doctorado. A Mario Feingold por toda la ayuda dedicada para llevar acabo el proyecto. A Paco Gavilanes por su supervisión desde la Universidad.

Mi agradecimiento a todas la personas que forman parte del laboratorio de Germán, por todo el cariño y apoyo recibido desde el primer momento hasta ahora. A Mercedes por su entusiasmo y su cercanía. Gracias por todo lo que me has enseñado con tanto mimo. Nuestras conversaciones científicas intentando resolver el enigma de la división bacteriana siempre fueron muy estimulantes y enriquecedoras. A Carlos, Begoña y Silvia que desde su profesionalidad y buen hacer me han permitido desarrollarme en mi labor investigadora. Muy especialmente, a Silvia, por todos sus consejos para resolver las dificultades experimentales y por su laboriosa dedicación en la revisión de la presente tesis. A Noelia y Marta, por todos los buenos momentos compartidos y por ser un comando tan estupendo. Gracias Noelia por todo tu esfuerzo ayudándome a purificar ciertas proteínas complicadas. A Michel y Adrián por molestarme tanto por las tardes, ayudarme en los momentos más estresantes de la escritura de la tesis y por ser unos chavales fabulosos. A Sara, Marina y Borja por todo el apoyo durante vuestra estancia en el laboratorio.

A los que formaron parte del grupo de Germán Rivas y ahora se encuentran en otros lugares (Elisa, Rubén, Víctor, Belén y Conchi). Con ellos pude aprender durante mis comienzos en el laboratorio viviendo muy buenos ratos. A toda la gente del CIB con la que he compartido tantas buenas experiencias durante los cafés y las fiestas de primavera (Luque, Ruth, Mariano, Alicia, Aída, Cristina, Pablo, Gonzalo, Albert, Paco, Juan, Alex, Hugo…). Gracias a Luque por ser el mejor “periodista” de El País y por su ingenio dándome sustos. Gracias a Ruth por nuestras conversaciones ecológicas. Gracias a Mariano por sus amorosas rosquillas... En definitiva, gracias a todos por hacer tan agradable el día a día y poner una sonrisa en cada anécdota.

A todas las personas que me acompañaron durante las estancias en Munich. A Ariadna por toda su dedicación dentro y fuera del laboratorio. Gracias por enseñarme tanto y permitirme aprender de tu experiencia. A Silke por su cariño y gran ayuda con los trámites administrativos. A Daniela y Diego por los buenos momentos vividos hablando español 2.0 y siendo el equipo DDA. Muy especialmente a Daniela por toda su ayuda incondicional en persona o vía Skype y por ser una amiga fuera del laboratorio.

A todas esas personas que desde fuera del laboratorio me han ayudado y animado durante esta etapa de mi vida. A Eva, por estar siempre ahí y ser mi confidente en los momentos más duros. A Ana por nuestras enriquecedoras conversaciones científicas y sobre la vida. A Saraih por hacer que los fines de semana en Munich estuvieran llenos de cariño y alegría. A Alicia por ser mi gran apoyo durante la facultad. A Silvia, Ángela, Mikel, Javi, Carmen, Elena, Susana, Fanny, Isa, Carol, Zahid… por enseñarme lo mejor de la amistad. A mi familia Ecuatoriana, por cuidarme tanto y quererme tan honestamente.

Por último, mi especial agradecimiento a mi familia. Por todo el amor transmitido y toda la entrega puesta en que yo haya llegado hasta aquí. A mis padres, por haberme facilitado un entorno donde poder crecer y madurar. Gracias a su ejemplo de honestidad, responsabilidad y esfuerzo, hoy puedo presentar esta tesis doctoral. A mis hermanas, Cristina y Beatriz porque a su lado he crecido feliz. Gracias Tati por ser mi geme. Y a Boris, por ser mi compañero de vida y mi luz en el camino. Mi inmensa gratitud por todo lo compartido.

"Dime y lo olvido,
enséñame y lo recuerdo,
involúcrame y lo aprendo."

Benjamin Franklin

INDEX

Summary

Bacterial cell division in *E. coli* is mediated by a multiprotein machine whose elements interact dynamically at midcell to form the division ring, a structure that drives cytokinesis forming part of the divisome. The first macromolecular assembly of the divisome is the proto-ring, comprising three proteins – FtsZ, FtsA, and ZipA – that associate at the cytoplasmic membrane forming the scaffold structure into which the rest of the essential division proteins are incorporated. FtsZ is a GTPase and its polymerization is closely related to the binding and hydrolysis of GTP. ZipA contains a short amino-terminal region integrated in the membrane and connected to the globular carboxy-terminal domain (through which it interacts with the FtsZ central hub) by a flexible, unstructured linker region. FtsA is an actin-like protein, with a short amphipathic helix that mediates its association to the membrane. The position of the ring at midcell is highly regulated by several negative control systems that inhibit its incorrect formation. One of them involves the self-oscillating MinCDE protein complex, which oscillates from pole to pole, blocking polymerization of FtsZ at both poles.

As the assembly of the proto-ring complex *in vivo* takes place at the inner bacterial membrane, a considerable effort has been (and is being) made to study the assembly properties of FtsZ and its interaction with companion proteins in reconstructions of the proto-ring structured as biomimetic membrane systems. Among them, supported lipid bilayers (SLBs) are well suited to investigate the reactivity (i.e. dynamic interactions) and the membrane structural organization of division proteins by surface sensitive imaging techniques, under biochemically controlled and well-defined experimental conditions.

Following this bottom-up strategy, co-reconstruction of the highly dynamic Min proteins on SLBs *in vitro* has revealed that this complex self-organizes in wave-like patterns, powered by ATP hydrolysis, that travel across the membrane surface. These “waves” exhibit many features of the Min oscillations observed *in vivo.* In addition, the co-reconstitution of FtsZ and FtsA on supported bilayers has shown that FtsA promotes the self-organization of FtsZ fibbers into dynamic patterns, giving rise to coordinated streams and swirling rings with preferential direction.

The main aims in the present thesis can be summarised as follows:

I. Self-organization of membrane-tethered FtsZ in flat supported membranes (Section 4) to understand the mechanisms governing the emergence and steady-state dynamics of FtsZ chiral vortices in supported bilayers.
II. Co-reconstitution of FtsZ-MinCDE complexes in ZipA-containing supported membranes (Section 5) to address the question of how the MinCDE complex regulates the behaviour of FtsZ polymers tethered to the membrane by the proto-ring element ZipA.
III. Co-reconstitution of FtsZ-FtsA-MinCDE complexes in supported membranes (Section 6) to respond to the question of how FtsA influences the coupling between FtsZ polymers and MinCDE complex.

To study the intrinsic role of FtsZ in the formation of dynamic patterns, we thus have revisited the *in vitro* reconstitution of the membrane-targeted chimeric FtsZ variant, FtsZ-YFP-mts, to flat supported membranes (**Section 4**). Our results have demonstrated that under specific conditions the formation of dynamic vortices is intrinsic to FtsZ and thus, the membrane adaptor FtsA is not required for the emergent spatial self-organization dynamics of FtsZ. In addition, this ring formation has only been observed within a narrow range of protein concentrations at the bilayer which is highly modulated by free magnesium and depends upon GTP hydrolysis. Intriguingly, the direction of rotation can be reversed by switching the membrane targeting sequence from the C-terminus to the N-terminus of the protein, implying that the filament attachment must have a perpendicular component to both, curvature and polarity. Remarkably, this chirality switch concurs with previously shown inward or outward membrane deformations by the respective FtsZ mutants. Our results lead to suggest an intrinsic helicity of FtsZ filaments with more than one direction of curvature, supporting earlier hypotheses and experimental evidence.

The specific question addressed in **Section 5** is how the Min system can dynamically modulate the FtsZ polymer network in ZipA-containing bilayers. Our results have determined that the dynamic pattern formation of the Min system modulates the spatial organization of FtsZ polymer networks in membrane-like environments, revealing the anti-correlated coupling between the two systems. The formation of these dynamic FtsZ wave-like patterns required the anchoring of FtsZ filaments to the membrane via ZipA, as well as the recruitment to the membrane of MinC, the element of the Min system that partially impairs FtsZ assembly. Our results can be explained if MinC, when complexed to MinD, has a higher affinity for the central hub of FtsZ than ZipA, which results in the displacement of FtsZ polymers from the membrane. Our coupling assays further revealed that both ZipA surface

density and crowding enhance the coupling between the Z-network and the Min system, as shown by the increase in wave modulation. In this section, we have provided evidences suggesting that ZipA, in addition to its role in proto-ring stability, has a central role in the coupling between the self-oscillating Min system and the remodelling of FtsZ polymers at the early stages of division in *E. coli,* thus contributing to the efficient selection of the division site.

The effect of FtsA protein in the coupling between FtsZ polymers and MinCDE complex in supported lipid bilayer has been analysed in **Section 6**. Firstly, we have optimized the protocol of FtsA purification allowing us to obtain a soluble and active protein, which exists as a mixture of monomers and oligomeric species, and binds membrane lipids with moderate affinity. FtsA-FtsZ self-organization assays on flat supported membranes show that these proteins assemble into dynamic chiral vortices. Co-reconstitution of FtsZ-FtsA-MinCDE complexes resulted in co-migrating MinCDE-FtsZ waves, as revealed by confocal microscopy, similar to the ones previously observed when FtsZ was free in solution in the absence of membrane tethering elements. This behaviour contrasts with the FtsZ polymers waves driven by MinCDE when FtsZ is associated to the membrane by ZipA. These findings suggest that the susceptibility of FtsZ polymers to spatial regulation by MinCDE – driven by MinC - depends on the nature of the FtsZ tethering element, being FtsA or ZipA. Therefore, the dynamic distribution of FtsZ controlled by the MinCDE system is different depending upon which proto-ring protein anchors FtsZ to the membrane. Finally, preliminary results using micro-compartments to reconstruct the MinCDE system together with FtsA-FtsZ filaments have revealed that the spatial confinement of the divisome proteins plays a crucial role in their dynamic behaviour since anti-correlated oscillations from pole to pole of the micro-compartments were found, in contrast with that observed in flat membranes.

Resumen

La división celular bacteriana en *E. coli* está mediada por una maquinaría multiproteica (divisoma) cuyos componentes se ensamblan dinámicamente en el punto medio de la célula para formar el anillo de división, el cual desencadena la citocinesis bacteriana. El primer complejo macromolecular del divisoma es el proto-anillo constituido por tres proteínas, FtsZ, FtsA y ZipA, que se asocian a la membrana citoplasmática formando la estructura de andamiaje a la que se incorporan el resto de las proteínas esenciales de división. FtsZ es una GTPasa y su mecanismo de polimerización está estrechamente relacionado con la unión e hidrólisis de GTP. ZipA se estructura en un dominio transmembrana amino-terminal y un dominio globular C-terminal (zona de interacción con el *central hub* de FtsZ), conectados ambos por un segmento flexible. La proteína FtsA presenta homología estructural con la actina y consta de una corta hélice anfipática que permite su anclaje a la membrana. El posicionamiento del anillo Z está estrechamente regulado mediante varios sistemas de control negativo, con el fin de inhibir su incorrecta localización en la membrana bacteriana. Uno de ellos es el complejo de proteínas MinCDE, el cual oscila de polo a polo de la célula, bloqueando la polimerización de FtsZ en dichos polos.

El ensamblaje del proto-anillo *in vivo* tiene lugar en la membrana bacteriana interna, por ello se ha realizado (y se sigue haciendo) un esfuerzo considerable para estudiar las propiedades de ensamblaje de FtsZ y su interacción con el resto de proteínas del divisoma, reconstruyendo el proto-anillo en sistemas biomiméticos de membrana. Entre ellos, las bicapas lipídicas soportadas (SLBs) constituyen un sistema adecuado para investigar la reactividad (es decir, las interacciones dinámicas) y la organización estructural de las proteínas de división en la membrana, mediante técnicas de imagen sensibles a la superficie, bajo condiciones experimentales bien definidas y bioquímicamente controladas.

Siguiendo esta estrategia *bottom-up*, la co-reconstitución *in vitro* de las proteínas MinCDE en SLBs ha revelado que este complejo se auto-organiza formando patrones oscilatorios, mediados por la hidrólisis de ATP, que viajan a través de la superficie de la membrana. Estas "ondas" poseen muchas características observadas en las oscilaciones de las proteínas Min *in vivo*. A su vez, la reconstitución de FtsZ y FtsA en bicapas lipídicas soportadas ha demostrado que FtsA promueve la auto-organización de fibras de FtsZ originando patrones dinámicos y anillos que giran con una dirección preferencial.

Los objetivos generales de esta tesis se resumen a continuación:

I. Autoorganización de la variante de FtsZ que se auto-ensambla a la membrana en bicapas soportadas planas (Sección 4), para comprender los mecanismos que gobiernan la aparición y la dinámica del estado estacionario de los vórtices quirales de FtsZ en bicapas soportadas.
II. Co-reconstitución de los complejos FtsZ-MinCDE en membranas con ZipA integrada (Sección 5), para abordar la cuestión de cómo el complejo MinCDE regula el comportamiento de los polímeros de FtsZ anclados a la membrana a través del elemento del proto-anillo ZipA.
III. Co-reconstitución de los complejos FtsZ-FtsA-MinCDE en membranas soportadas (Sección 6), para responder la pregunta de cómo FtsA influye en el acoplamiento entre los polímeros de FtsZ y el complejo MinCDE.

Con el fin de estudiar el papel intrínseco de FtsZ en la formación de patrones dinámicos, hemos revisado la reconstitución *in vitro* de la variante quimérica de FtsZ que se auto-ensambla a la membrana, FtsZ-YFP-mts, en membranas soportadas planas (**Sección 4**). Nuestros resultados han demostrado que, bajo condiciones específicas, la formación de vórtices dinámicos es intrínseca a FtsZ y, por lo tanto, el anclaje de FtsZ a la membrana a través de FtsA no es estrictamente necesario para la dinámica de auto-organización espacial de FtsZ. Además, la formación de anillos dinámicos solo se ha observado dentro de un estrecho intervalo de concentración de FtsZ en la bicapa, lo cual depende de la concentración de magnesio libre y de la hidrólisis de GTP. La dirección de rotación de dichos anillos puede invertirse al cambiar la posición de la secuencia de anclaje a membrana del extremo C-terminal al N-terminal de la proteína. Esto implica que la secuencia de unión a membrana de FtsZ debe tener un componente perpendicular tanto a la curvatura como a la polaridad del filamento de FtsZ. La opuesta quiralidad de los anillos cuando la secuencia de anclaje a membrana se posiciona en un extremo u otro de la proteína concuerda con las deformaciones de membrana hacia dentro o hacia fuera observadas previamente por las variantes quiméricas de FtsZ. Nuestros resultados sugieren que los filamentos de FtsZ muestran una naturaleza helicoidal intrínseca con más de una dirección de curvatura, lo cual respalda las hipótesis anteriores y es coherente con el trabajo experimental.

En la **Sección 5** se ha pretendido conocer cómo el sistema Min puede modular dinámicamente la red de polímeros de FtsZ en bicapas con ZipA integrada. Los resultados obtenidos han revelado que la formación de patrones dinámicos del sistema Min modula la

organización espacial de las redes de polímeros de FtsZ en entornos biomiméticos de membrana, revelando el acoplamiento anti-correlacionado entre los dos sistemas. La formación de dichos patrones dinámicos requiere tanto el anclaje de los filamentos de FtsZ a la membrana a través de ZipA como el reclutamiento a la membrana de MinC, responsable de inhibir la formación del anillo Z. Estos resultados pueden ser explicados si MinC, al formar complejo con MinD, muestra una mayor afinidad por el *central hub* de FtsZ que ZipA, originando la exclusión de los polímeros de FtsZ de la membrana. A su vez, el incremento de la densidad superficial de ZipA y la formación de redes de polímeros de FtsZ en presencia de Ficoll 70 favorecen el acoplamiento entre las ondas de Min y las de FtsZ, dando como resultado un mayor desplazamiento de FtsZ, en zonas donde la concentración de MinC es máxima. Estos resultados demuestran que la formación de ondas dinámicas del sistema Min es suficiente para modular la organización espacial de los polímeros de FtsZ en sistemas mínimos de membrana, revelando el acoplamiento entre los dos sistemas. Por último, en esta sección hemos proporcionado evidencias que sugieren que ZipA, además de su papel en la estabilidad del proto-anillo, tiene un papel central en el acoplamiento entre el sistema Min y la reorganización de los polímeros de FtsZ en las primeras etapas de la división de *E. coli*, contribuyendo así a la eficiente selección del sitio de división.

El efecto de la proteína FtsA en el acoplamiento entre los polímeros de FtsZ y el complejo MinCDE en bicapas lipídicas soportadas ha sido analizado en la Sección 6. En primer lugar, hemos optimizado el protocolo de purificación de FtsA, lo que nos ha permitido obtener una proteína soluble y activa, que existe como una mezcla de monómeros y especies oligoméricas, y que se une a los lípidos de membrana con una afinidad moderada. Los ensayos de auto-organización de FtsA-FtsZ en membranas soportadas planas muestran que estas proteínas se auto-ensamblan originando vórtices dinámicos y quirales. La reconstitución de los complejos FtsZ-FtsA-MinCDE en membranas lipídicas soportadas permitió la detección mediante microscopía confocal de ondas MinCDE-FtsZ dinámicas que migran conjuntamente. Dicho comportamiento es similar al observado previamente, cuando FtsZ permanecía libre en solución en ausencia de elementos de anclaje a la membrana. Sin embargo, este resultado difiere del acoplamiento observado cuando FtsZ está asociado a la membrana por ZipA, donde las ondas de los polímeros de FtsZ impulsadas por MinCDE se detectaron en anti-fase respecto a las del complejo Min. Estos hallazgos sugieren que la susceptibilidad de los polímeros de FtsZ a la regulación espacial mediante el sistema Min, impulsada por el efecto de MinC, depende de la naturaleza del elemento de anclaje de FtsZ a la membrana (FtsA o ZipA). Por lo tanto, la distribución dinámica de FtsZ mediada por el sistema MinCDE es alterada en función de la proteína del proto-anillo que ancle FtsZ a la membrana. Finalmente, la reconstitución del sistema MinCDE junto con los filamentos FtsA-

FtsZ en micro-compartimentos ha permitido determinar de forma preliminar que el confinamiento espacial de las proteínas del divisoma desempeña un papel crucial en su comportamiento dinámico. El acoplamiento de los sistemas FtsZ-MinCDE detectado dentro de los micro-compartimentos fue en anti-fase, en contraposición con lo observado en membranas planas.

Abbreviations

ADP, ATP	Adenosine di-, tri-phosphate
A.U.	Arbitrary units
BCA	Bicinchoninic acid
C-terminus	Carboxyl-terminus
CHAPs	3-((3-cholamidopropyl) dimethylammonio)-1-propanesulfonate
DLS	Dynamic light scattering
E. coli	*Escherichia coli*
Ficoll 70	Poly(sucrose-*co*-epichlorhydrin)
FRAP	Fluorescence Recovery After Photobleaching
FtsZ	Filamenting temperature sensitive mutant Z
FtsA	Filamentous temperature sensitive mutant A
GDP, GTP	Guanosin 5´di-, tri-phosphate
GFP	Green Fluorescent Protein
GUV	Giant Unilamellar Vesicles
IPTG	Isopropylthio-β-galactoside
m	Modulation parameter
MLVs	Multilamellar Vesicles
mts	membrane-targeting-sequence
N-terminal	Amine terminal
PDMS	Polydimethylsiloxane
SDS-PAGE	Sodium dodecyl sulfate polyacrylamide gel electrophoresis
SLBs	Supported Lipid Bilayers
SUMO protein	Small Ubiquitin-related Modifier protein
SUVs	Small Unilamellar Vesicles
TIRFM	Total Internal Reflection Fluorescence Microscopy
YFP	Yellow Fluorescent Protein
ZipA	FtsZ interacting protein A

1. INTRODUCTION

1.1. Bacterial cell division in *Escherichia coli*

The understanding of the specific processes and mechanisms that are involved in bacterial cell division, constitute a very interesting objective for the bioscientific research field. In recent years, the emergence of antibiotic-resistant microbial populations has generated a growing interest in developing new strategies to confront pathogenic bacteria. The fact that bacterial division proteins are essential for cell proliferation makes them potential targets for broad-spectrum antibiotic compounds, still underexploited. For this reason, the study and characterization of the bacterial proliferation mechanisms are essential (Reija *et al.*, 2011) (Vicente *et al.*, 2006).

The research on cell division in bacteria, in comparison to the studies in eukaryotes, has several advantages due to the lack of prominent intracellular structures (Lutkenhaus *et al.*, 2012). ***Escherichia coli*** (*E. coli*) has been extensively studied and employed as a standard model system in microbiology since its cell cycle regulation is relatively simple, it is easily grown and manipulated, and its genome has been sequenced. *E. coli* is a rod-shaped gram-negative bacterium and its typical size is around 1×3 μm.

In the **bacterial cell cycle**, mass growth, chromosome replication, and cell division are the three major processes that provide the formation of two progeny cells, each with a copy of the chromosome (Dewachter *et al.*, 2018). **Bacterial cell division** is a fundamental biological process that occurs by the partition of a mother cell into two daughter cells. This essential process, known as **cytokinesis**, provides the force to split cells and is spatially regulated to faithfully partition the genetic material. In all organisms, cytokinesis must be tightly coupled to the cell cycle so that each daughter cell receives a complete copy of the genome (Margolin, 2005) (Romberg and Levin, 2003).

An extensive characterization of the **bacterial envelope** is required since membranes are essential components of bacterial cells and have both functional and structural roles. Previous studies established that the cell contains three layers in *E. coli*: the cytoplasmic or inner membrane (IM, 4nm thick lipid bilayer), the outer membrane (OM, 4nm thick bilayer) and the peptidoglycan layer (PG, 6 nm thick) that maintains the shape of the cell and resides between the cytoplasmic membrane and the outer membrane (**Figure 1.1**). PG is the main component of the bacterial wall and is located in the periplasm (10 nm thick) that is the space between the cytoplasmic and outer membrane. Importantly, PG protects cells from

the mechanical stress that results from high intracellular turgor (Nanninga, 1998) (Erickson and Osawa, 2017) (Monteiro *et al.*, 2018).

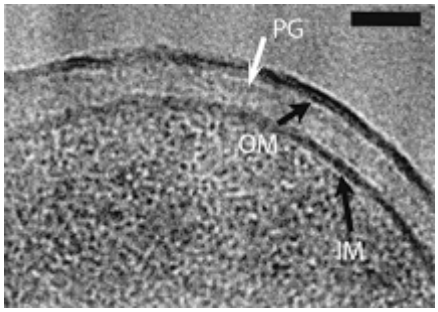

Figure 1.1. CryoEM of the cell envelope of *E. coli*. The black arrows point to the IM and OM. The PG is the lightly stained narrow band indicated by the white arrow. The periplasm is the lighter stained zone between the OM and IM. Bar is 50 nm. Figure adapted from (Erickson and Osawa, 2017).

The bacterial membrane does not only represent a passive physical barrier, but also provides a highly dynamic platform for the interplay between lipids, membrane binding proteins and cytoskeletal elements (Loose and Schwille, 2009). In particular, bacterial division requires accurate identification of the cell division site, positioning of the division machinery on the bacterial membrane, and coordinated constriction of the inner membrane and the bacterial cell wall.

There are several molecular mechanisms coordinating chromosomal positioning with cell division that strictly **regulate** in time and space for bacterial cell division. In particular, two regulatory systems, the Min system and nucleoid occlusion (NO), play crucial roles in controlling temporal and spatial establishment of the division machinery in *E. coli*. (Ortiz *et al.*, 2016).

- ***Assembly of E. coli divisome during bacterial cell division***

Bacterial cell division in *E. coli* is carried out by macromolecular assemblies whose components transiently interact to form, toward the end of the cell cycle, a contractile ring at midcell. This division ring (**divisome**) formation is initiated by the self-assembly of FtsZ protein at midcell (**Figure 1.2**). **FtsZ** is the most abundant and conserved element of the bacterial cell division machinery and the first protein recruited to the division site, where it assembles in filaments forming the **FtsZ ring** (also called Z ring) (Haeusser and Margolin, 2016). Cells depleted of or lacking functional FtsZ do not divide and grow into long filaments that eventually lyse (Hurley *et al.*, 2016). The Z ring serves as a scaffold for assembly of the

divisome, a complex macromolecular structure composed of over 20 known proteins in *E. coli* that drives cytokinesis (den Blaauwen *et al.*, 2017). The proteins that constitute the core of the divisome (FtsZ, FtsA, ZipA, FtsK, FtsQ, FtsL, FtsB, FtsW, FtsI, and FtsN) are essential for cell division (Rico *et al.*, 2013). Assembly of the division machinery is a multi-step process involving two sets of factors: the so-called 'early and late' division proteins. The early proteins include FtsZ and its membrane anchors FtsA and ZipA.

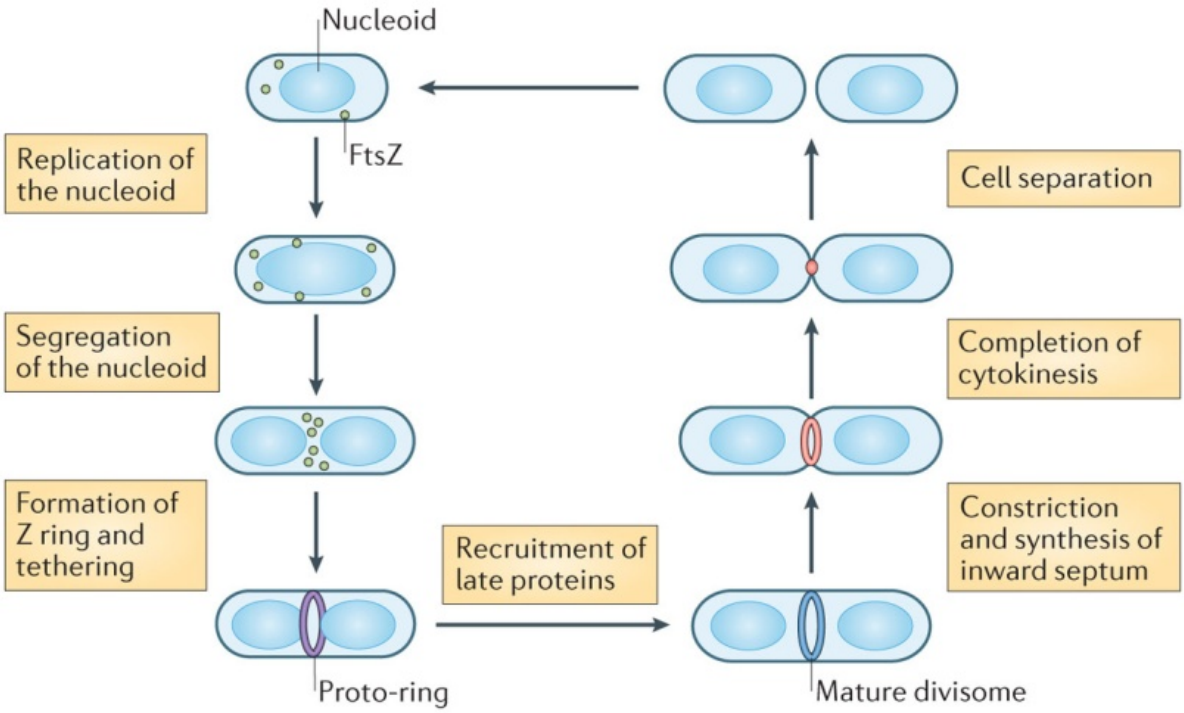

Figure 1.2. Overview of bacterial cytokinesis. In a new-born cell, FtsZ is present as unassembled monomers or short oligomers (green beads). *Escherichia coli* cell replicate and segregate its chromosome, which is organized as nucleoids. Toward the end of chromosome segregation, FtsZ polymerizes and is tethered to the inner face of the cytoplasmic membrane at the cell centre by specific FtsZ-interacting proteins (FtsA and ZipA). This three division proteins are concentrated at midcell and organize into the Z ring, forming the essential divisome proto-ring, which is attached to the membrane. After the recruitment of at least ten membrane-associated proteins (including FtsN, FtsK, FtsBLQ, FtsW and FtsI), the ring progresses to a mature divisome, which coordinates the constriction of the inner membrane and outer membrane with the functions of targeted cell wall hydrolases and ingrowing septal peptidoglycan. The result is the separation of a bacterial cell into two daughter cells of approximately equal size. Figure adapted from (Haeusser and Margolin, 2016).

FtsZ reversibly interacts with the amphitropic protein FtsA and the bitopic membrane protein ZipA at the cytoplasmic membrane to form the **proto-ring**, the first essential molecular assembly of the division machinery (**Figure 1.3**) (Rivas *et al.*, 2013) (Rico *et al.*, 2013). Either FtsA or ZipA can attach FtsZ to the membrane, but no localization of FtsZ occurs if both are absent (Pichoff and Lutkenhaus, 2002). Interestingly, four non-essential Zap proteins (FtsZ-associated proteins) have been described to promote and stabilize the FtsZ

ring (Huang *et al.*, 2013). The proto-ring formation is followed by a time delay that can occupy up to 20% of the cell cycle, after which the 'late division proteins', some of them required for synthesis of the septal wall, assemble (den Blaauwen *et al.*, 2017). After its assembly, completion of the divisome, possessing a septal peptidoglycan synthesising complex and connected to other periplasmic and outer membrane proteins (Vicente *et al.*, 2006), results in the production of a septum that ultimately splits the cell in two almost equal halves.

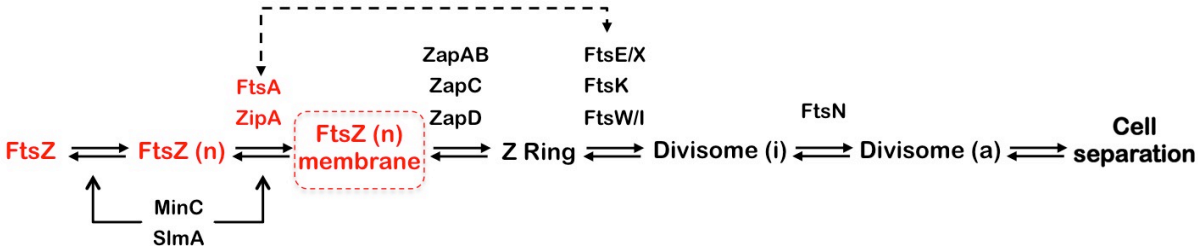

Figure 1.3. Assembly of the Z ring and maturation into the divisome in *E. coli*. FtsZ polymers (FtsZ[n]) are tethered to the membrane by FtsA and ZipA, which leads to the formation of the Z ring. Although not essential, several FtsZ interacting proteins (ZapA-D) localize to the ring and promote its integrity. Antagonists of FtsZ assembly, MinC/D and SlmA, are positioned away from midcell so that it is permissive for Z ring formation. When enough FtsA is present at the Z ring the remaining proteins are recruited (divisome [i]. The arrival of the essential division protein FtsN signals the divisome is complete (divisome [a]) and activation of septal PG (peptidoglycan) synthesis occurs. Figure adapted from (Lutkenhaus *et al.*, 2012).

The initiation of **FtsZ assembly** must be tightly **controlled** both temporally and spatially to prevent aberrant septation. In particular, the positioning of FtsZ filaments, forming the Z ring at cell centre, is highly controlled by FtsZ concentration at midcell, the initiation of DNA replication and the nucleoid segregation control (Romberg and Levin, 2003). The negative regulation is directed by complex site selection mechanisms, among them nucleoid occlusion (NO) and the MinCDE proteins (Loose *et al.*, 2011;Rowlett and Margolin, 2013;Wu and Errington, 2011). **Nucleoid occlusion** prevents FtsZ polymerization, and therefore the cell constriction, in the vicinity of the bacterial chromosome (Adams and Errington, 2009), (Lutkenhaus *et al.*, 2012;Wu and Errington, 2011). This negative regulation of the Z ring is mediated by SlmA protein that specifically binds to *E. coli* chromosome DNA (**Figure 1.4.A**). The spatiotemporal **oscillations of the Min proteins** from pole to pole establish a localization signal for FtsZ, which can only polymerize and initiate cytokinesis in the region with the lowest inhibitor concentration, that is, the middle of the cell (**Figure 1.4.B**) (Kretschmer and Schwille, 2016). Accordingly, Z rings near the poles of the cell were found when mutant cells without the Min system were employed, but not in wild-type cells (Pichoff and Lutkenhaus, 2001).

Recently, it has been observed that Min system and NO defective cells are still capable of establishing a medial division site with remarkable precision (Bailey *et al.*, 2014) (den Blaauwen *et al.*, 2017). Indeed, it has been observed that two additional regulation systems control the spatial position of the Z ring in bacterial dividing cells. First, the replication terminus region of *E. coli* chromosome which forms a compact entity (Ter macrodomain) constitutes a positive regulation mechanism in *E. coli* that promotes assembly of the Z ring in its immediate vicinity and guides cell division proteins toward the replication terminus region of the chromosome. In this process, the **Ter linkage** is the anchor that coordinates localization of both the Z ring and the Ter macrodomain region of the chromosome (**Figure 1.4.C**). Lastly, DNA translocase **FtsK** leads to positioning the DNA and localize the chromosome relative to the divisome (**Figure 1.4.D**) (Mannik and Bailey, 2015).

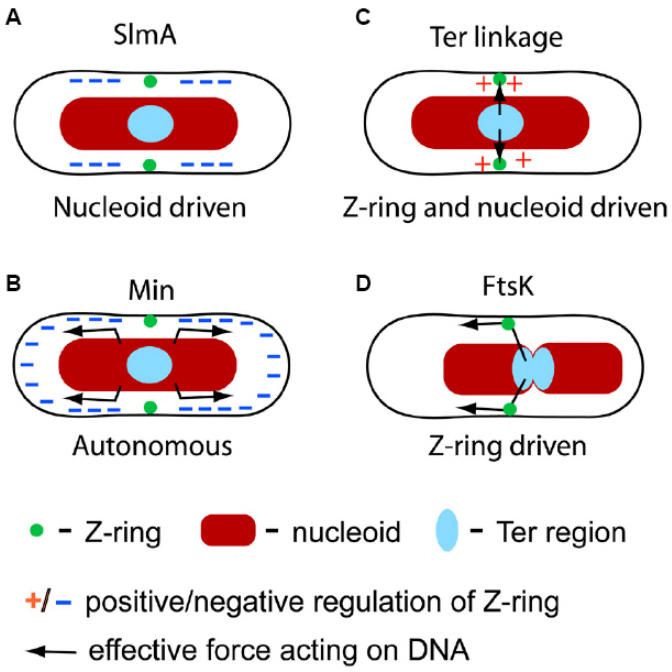

Figure 1.4. Four different regulation mechanisms of Z ring formation during bacterial cell division. (A) SlmA-dependent nucleoid occlusion (NO). **(B)** MinCDE system complex. **(C)** Ter linkage. **(D)** FtsK translocase. Figure adapted from (Mannik and Bailey, 2015).

Recent studies based on high-resolution imaging of *E. coli*, have shown that the structure of the **divisome** is a toroid that contains at least three concentric rings: the inner layer(s), that seems to have a regulatory role, include ZapB and MatP (a DNA-binding protein involved in the condensation and segregation of the chromosome). The middle proto-ring is the assembly scaffold; this ring may also provide some of the force necessary for constriction, as it contains FtsZ, FtsA, and ZipA. And finally, there is the outer ring, containing FtsQ, FtsL,

FtsI, and FtsN, which are involved in peptidoglycan synthesis and ingrowth (**Figure 1.5**) (Soderstrom and Daley, 2017).

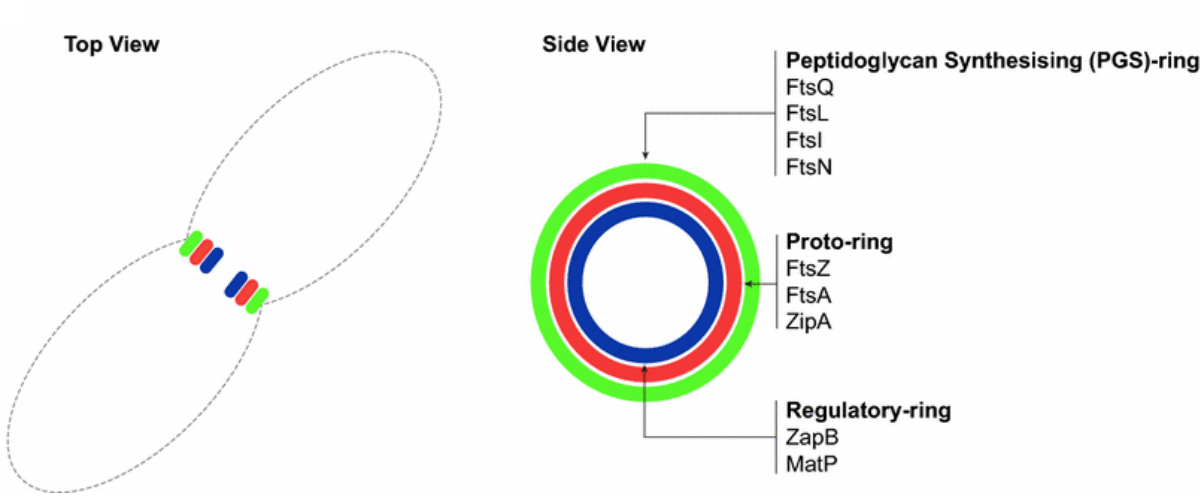

Figure 1.5. Schematic representation of concentric divisome rings observed in *E. coli*. Left panel: Schematic representation (top view) of the three concentric divisome rings that are spatially separated at the septum. Right panel: Side view of the concentric rings containing different sets of proteins. Figure adapted from (Soderstrom and Daley, 2017).

- ***Divisome disassembly and constriction force generation in bacterial cytokinesis***

Although bacterial cell division in *E. coli* has been studied for decades, some mechanistic details are still missing. For instance, the precise **divisome disassembly process** is still hardly known. Söderström and co-workers described that division machinery disassembly occurs in a coordinated process that is initiated by FtsZ, which disassembles from the division septum before full closure of cell envelope (Soderstrom *et al.*, 2014). Once the fusion of the inner membrane has been accomplished, ZipA and FtsA disassemble, followed by FtsL, FtsQ then FtsI and a subpopulation of FtsN. Lastly, the remaining FtsN molecules disassemble, the daughter cells separate, and a new round of division can be initiated. This sequence of events is remarkably similar to the assembly process, indicating that disassembly follows a first-in, first-out principle (**Figure 1.6**) (Soderstrom *et al.*, 2016).

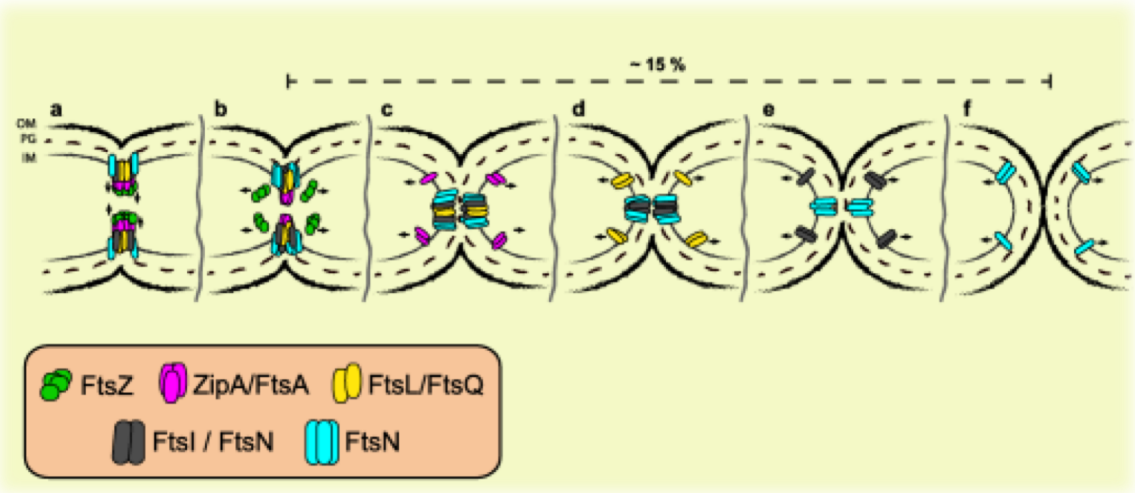

Figure 1.6. A model for the stepwise disassembly of the *E. coli* divisome. (a) The divisome remains intact for most of the constriction process. (b) Disassembly is initiated by FtsZ, which disassembles from the division septum whilst the cytoplasm is still connected. (c–e) Once the inner membrane has fused, ZipA and FtsA disassemble, followed by FtsL, FtsQ then FtsI and a sub-population of FtsN. (f) Then, the disassembly of the remaining FtsN molecules allows the daughter cells separation. Figure adapted from (Soderstrom *et al.*, 2016).

Currently, a question that is catching special interest in the bacterial cell division research field is how the **constrictive force** could be generated during the septum invagination process that conduce to the complete cell constriction. Although several hypotheses regarding this key aspect have been discussed for decades, further investigations need to be performed.

The **force-generating role of FtsZ** has been postulated in many works. From this perspective, the continuous rearrangement of the FtsZ polymers in the vicinity of the cell membrane at the division site provides the main force driving membrane constriction. Thus, the Z ring constitutes a force-generating structure where FtsZ generates a constrictive force to oppose turgor pressure, as well as a scaffold to localize the division machinery and coordinate the cell wall synthesis at the division septum (Rico *et al.*, 2013) (Holden S., 2018). In contrast, other authors have suggested that the critical, conserved role of FtsZ may not be its ability to generate a driving force for cytokinesis, but to regulate the spatiotemporal dynamics of other divisome components, in particular proteins involved in septal cell wall formation. Thus, FtsZ could act as a **signal-processing hub** to coordinate cell wall synthesis, ensuring that the cell divides smoothly at the correct time and place, and with the correct septum morphology (Coltharp and Xiao, 2017). Cytokinesis occurs in two coordinated phases. First, FtsZ filaments in the treadmilling patch may deform the membrane, namely, the **FtsZ driving force** may be the main responsible for the initial invagination of the cell membrane. In a second step, **PG synthesis provides the driving**

force since this permits the cell wall to follow the inner membrane until the complete constriction is achieved (**Figure 1.7**) (Bisson-Filho *et al.*, 2017) (Holden S., 2018) (Monteiro *et al.*, 2018).

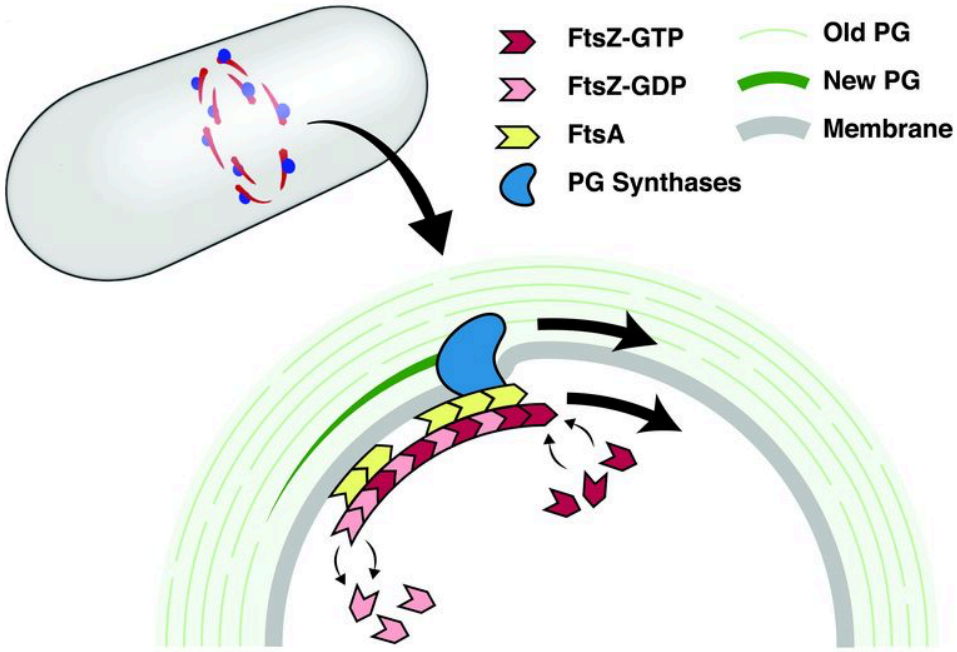

Figure 1.7. Model for coupling between FtsZ treadmilling and PG synthesis in *Bacillus subtilis* cell division. The dynamic Z ring contains multiple FtsZ filaments associated to the membrane by FtsA that treadmill around the future division site and recruits PG synthases and other proteins involved in cytokinesis. The FtsZ treadmilling rate control both the rate of PG synthesis, building sequentially smaller uniform arcs of PG, and cell division. Figure adapted from (Bisson-Filho *et al.*, 2017).

1.2. *E. coli* proto-ring elements

The main element in bacterial division, FtsZ, along with other division proteins forms a ring positioned at midcell that initiates cell division and membrane constriction. Two are the proteins that seem to be essential in *E. coli* for FtsZ anchoring to the membrane, FtsA and ZipA.

- ***FtsZ, the central component of the bacterial cell division machinery***

The essential cell division protein FtsZ is a 40 kDa GTPase widely conserved in bacteria and archaea and considered the ancestral homologue of eukaryotic tubulins (Hurley *et al.*, 2016). FtsZ and tubulin present homologue structures with strikingly similar protein folds and GTP binding interactions (Romberg and Levin, 2003).

FtsZ is a soluble cytoplasmic protein with no significant affinity for phospholipid bilayers. For its anchoring to the cytoplasmic membrane, FtsZ interacts through its carboxy-terminal region with the other proto-ring proteins, ZipA and FtsA (Pichoff and Lutkenhaus, 2002). Apparently, both of these proteins can support the attachment of FtsZ to the membrane, but no localization of FtsZ at the membrane occurs if both are absent (Geissler *et al.*, 2007) (Pichoff *et al.*, 2012).

The FtsZ crystal structure determined for FtsZ from the thermophilic archaeon *Methanococcus jannaschii* displayed two globular domains connected by a central core α helix, the H7 helix (**Figure 1.8**). The GTPase catalytic site is formed during filament assembly by the addition of the synergy T7 loop from the incoming subunit. The carboxy terminal domain comprises a structured folded part, followed by a flexible unstructured region, of variable length in FtsZ from different bacteria, and a short alpha helix C-terminal end (the central hub). The unstructured part participates in lateral interactions between FtsZ protofilaments, whereas the central hub is involved in the interaction with at least six cell division proteins: the membrane anchors FtsA and ZipA, the FtsZ polymerization inhibitors MinC and SlmA, the FtsZ-stabilizing protein ZapD and the ClpX moiety of the ClpXP protease involved in FtsZ degradation (Ortiz *et al.*, 2016) (Huang *et al.*, 2013).

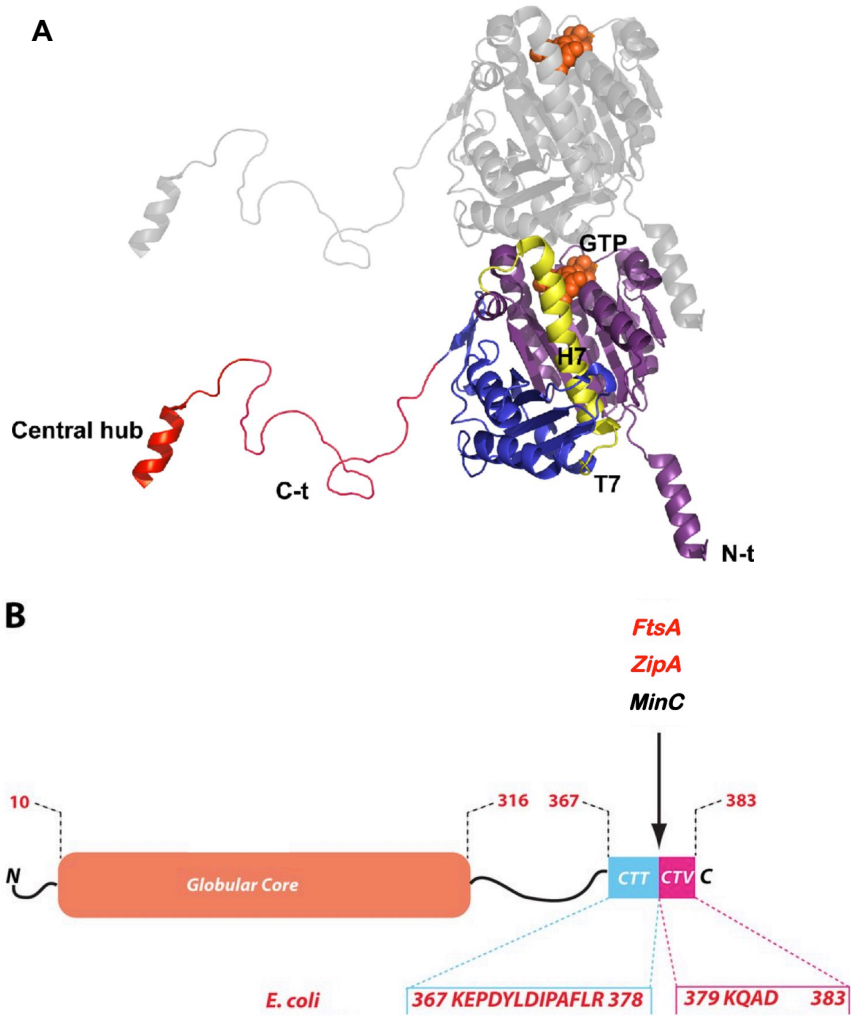

Figure 1.8. Model of FtsZ structure. (A) FtsZ dimer modelled from the *Methanococcus jannaschii* crystal structure. The bottom monomer shows the N-terminal domain (amino acids 1–220) (purple) and the carboxy-terminal domain (amino acids 221–383) (blue). Both folded domains are connected by the catalytic H7 helix followed by the T7 loop (both in yellow). Once GTP (orange) is coupled to the GTP-binding site, the T7 loop achieves the correct positioning of the phosphate activating the hydrolytic activity. The highly variable C-terminal linker (red) is depicted here as a free-drawn unstructured peptide since is not defined in the crystal. The structure of the central hub at the C-terminal end (also coloured in red) is based on the structure of the interacting region of the *E. coli* FtsZ protein with the globular domain of ZipA. Figure and text were adapted from (Ortiz *et al.*, 2016). **(B)** Schematic domain organization of *E. coli* FtsZ. The C-terminal linker (CTL) comprises a 50-amino acid flexible linker (amino acids 316-367) and a 17-amino acid peptide (the central hub) that includes the amino acid residues of the conserved CTT (C-terminal tail) and the variable C-terminal end (CTV). The central hub sequence allows the interaction between FtsZ and FtsA, ZipA or MinC. Figure adapted from (Huang *et al.*, 2013).

As it has been mentioned above, during the bacterial cell cycle, FtsZ exhibits a series of different behaviours: assembly to form the Z ring at midcell, maintenance of the ring through continuous subunit turnover, and constriction and disassembly of the ring (Romberg and Levin, 2003).

Over the last few decades, **FtsZ polymerization** has been extensively studied ***in vitro***. The protomeric unit of FtsZ is a monomer, which binds magnesium with low affinity (Rivas *et al.*, 2013). In the presence of GDP, FtsZ oligomerizes to form linear single-stranded oligomers according to a Mg^{2+}-linked non-cooperative indefinite self-association mechanism. In contrast, the assembly of FtsZ monomers to form narrow-size distributed single stranded filaments following a cooperative process is concerted by GTP and Mg^{2+} and stimulated by the presence of K+ (**Figure 1.9, upper panel**) (Mingorance *et al.*, 2010). This cooperative polymerization mode is evidenced by the fact that a constant amount of unpolymerized protein is always found within FtsZ polymer solutions, indicating that there is a critical concentration (around 1 μM) above which polymerization is triggered. Below this concentration, no polymers are detected (Erickson *et al.*, 2010) (Reija *et al.*, 2011). These protofilaments are structurally flexible and tend to further associate into higher order polymers sufficiently plastic to adopt multiple geometries (multi-stranded fibbers, bundles, circles, toroids, etc) depending upon experimental conditions (**Figure 1.9, bottom panel**) (Gonzalez *et al.*, 2003) (Erickson *et al.*, 2010). *In vivo* these lateral associations of FtsZ filaments are favoured by the presence of other cell division proteins (Ortiz *et al.*, 2016). Negative stain Electron Microscopy (EM) techniques allowed to establish that when FtsZ is assembled at steady state with GTP, thin protofilaments that are one subunit wide and 100–200 nm (25–50 subunits) long were formed (Erickson and Osawa, 2017).

Although ultrastructural characterization of assembled FtsZ filaments *in vivo* still remains unclear, recent super-resolution fluorescence microscopy and electron cryotomography studies of FtsZ state that Z rings are a largely patchy heterogeneous structure, appearing as large nodes of high concentration separated by thinner regions of low concentration where FtsZ forms bands of 5–10 filaments wide completely encircling *E. coli* division site (Coltharp and Xiao, 2017;den Blaauwen *et al.*, 2017;Holden S., 2018). Additionally, current models stress the importance of the presence of **lateral interactions between FtsZ protofilaments** that loosely arrange to form a Z ring composed of dynamic clusters of short, overlapping protofilaments (Meier and Goley, 2014). *In vitro* studies determined that these lateral associations are affected by protein concentration, pH, the presence of divalent cations (calcium and/or magnesium) and the effect of crowding agents (**Figure 1.9**) (Erickson *et al.*, 2010). It was earlier demonstrated that high concentrations of inert polymers like Ficoll 70, used to mimic the crowded cellular interior, favour the assembly of FtsZ into bundles with slow depolymerization (Gonzalez *et al.*, 2003).

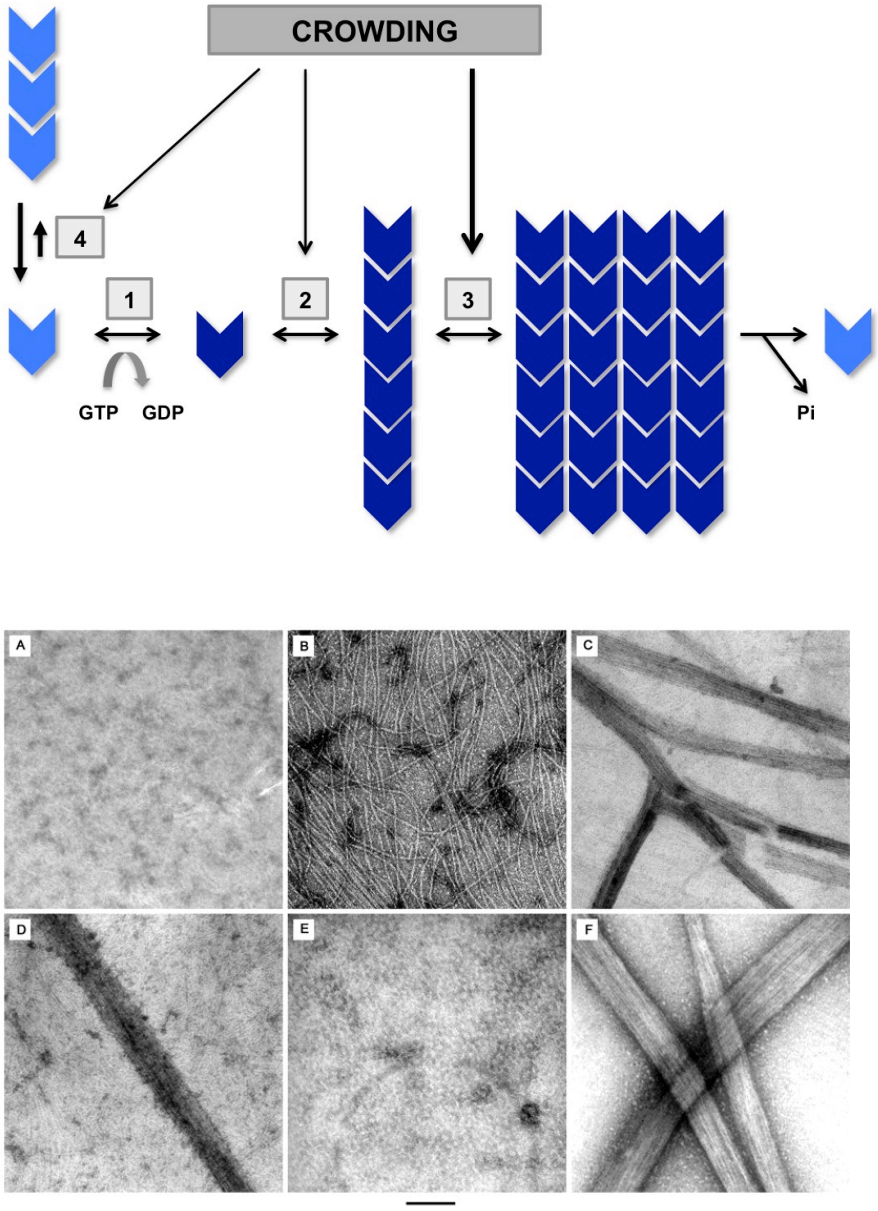

Figure 1.9. FtsZ polymerization mediated by crowding. **Upper panel:** Model for the assembly of FtsZ under conditions resembling the crowded bacterial interior. FtsZ-GDP and FtsZ-GTP are represented with light blue and dark blue, respectively. **(1)** Nucleotide exchange in soluble FtsZ monomer. **(2)** Cooperative formation of FtsZ protofilaments. **(3)** FtsZ assembly into ribbons enhanced by macromolecular crowding. **(4)** Magnesium-linked oligomerization of FtsZ in its GDP state at low ionic strength. **Bottom panel:** Electron microscopy images of FtsZ assembly in the absence and in the presence of macromolecular crowders. **(A)** FtsZ assembly is not triggered in the absence of potassium (1 g/L FtsZ in 50 mM Tris-HCl, 100 mM NaCl, pH 7.4, plus 1 mM GTP and 200 g/L Ficoll 70). **(B)** FtsZ assembled in the presence of 1 mM GTP and potassium. FtsZ filaments are mostly straight although some have intermediate curvature. **(C-F)** In the presence of macromolecular crowders FtsZ-GTP assemble into multi-stranded fibbers. **(C)** Formation of polymers, some of them interconnected, with a width of 40–100 nm (0.2 g/L FtsZ plus 2 mM GTP and 220 g/L Ficoll 70). **(D)** Similar results were observed when dextran was used to simulate crowding (0.1 g/L FtsZ plus 2 mM GTP and 200 g/L dextran T70). **(E)** 0.5 g/L FtsZ plus 0.5 mM GTP and 200 g/L Ficoll 70 after 1-h incubation at 30ºC. **(F)** In the presence of Ficoll 70 and the nucleotide analog GMPCPP, which is hydrolysed more slowly than GTP, FtsZ fibbers were also detected (0.5 g/L FtsZ plus 0.1 mM GMPCPP and 200 g/L Ficoll 70). The bar scale is 100 nm. Figure adapted from (Gonzalez *et al.*, 2003).

The structural plasticity of FtsZ polymers is explained by a **highly dynamic behaviour**. Their assembly and disassembly, linked to GTP hydrolysis, are considered crucial for Z ring function and happen rapidly on the time-scale of seconds. Moreover, the dynamic exchange between FtsZ molecules in the polymers and FtsZ monomers or short oligomers in the cytoplasm has been established in the *E. coli* cytokinetic ring. The halftime for replacement of FtsZ subunits has been found to be between 8 and 30 s, as indicated by fluorescence recovery after photobleaching (FRAP) experiments on cells (Chen and Erickson, 2005). This dynamic nature of the Z ring makes it susceptible to regulation by numerous protein factors that modify the rates of assembly and disassembly of the filaments (Erickson *et al.*, 2010) (Mingorance *et al.*, 2010) (Monterroso *et al.*, 2013).

The observation that individual FtsZ molecules remain stationary in polymers points out that the progressive movement of FtsZ polymers is consistent with a **treadmilling mechanism** where one end of a polymer steadily grows (polymerization) while the other end of the same polymer steadily shrinks (depolymerization) (Niu and Yu, 2008) (Loose and Mitchison, 2014). Treadmilling requires a difference in the rate of net polymerization and depolymerization at the so-called plus and minus ends of the filaments (**Figure 1.10**) (Wagstaff *et al.,* 2017). Indeed, treadmilling of FtsZ *in vitro* has been observed on supported lipid bilayers where FtsZ filaments move by GTP- hydrolysis-driven asymmetric filament polymerization and depolymerization (Loose and Mitchison, 2014) (Holden S., 2018). In *E. coli*, FtsZ forms motile filaments that were recently found to treadmill circumferentially around the division plane *in vivo*, and that the treadmilling motion of FtsZ drives cell division and septal cell wall synthesis (Yang *et al.*, 2017) (Bisson-Filho *et al.*, 2017).

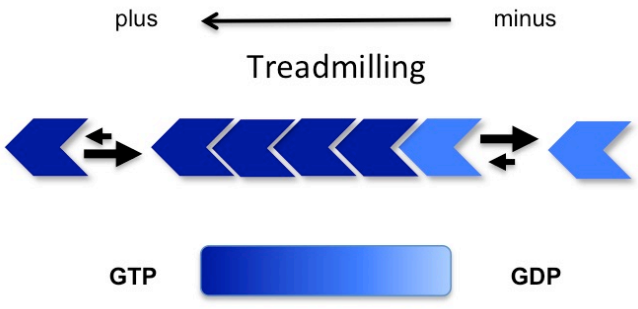

Figure 1.10. Model of FtsZ filament treadmilling. Schematic drawing of a polar single-stranded FtsZ filament with FtsZ-GTP subunits represented in dark blue and FtsZ-GDP subunits in light blue. FtsZ can grow at one end (plus) and shrink at the other end (minus) at the same rate. Black arrows indicate rates roughly in proportion to their width.

The requirement of force generation by Z rings can probably be much smaller than expected previously. Recently, Osawa and Erickson proposed that a substantial constriction force at the division site is generated by combination of FtsZ pulling from the inside and excess membrane production pushing membrane inward (**Figure 1.11**) (Osawa and Erickson, 2018).

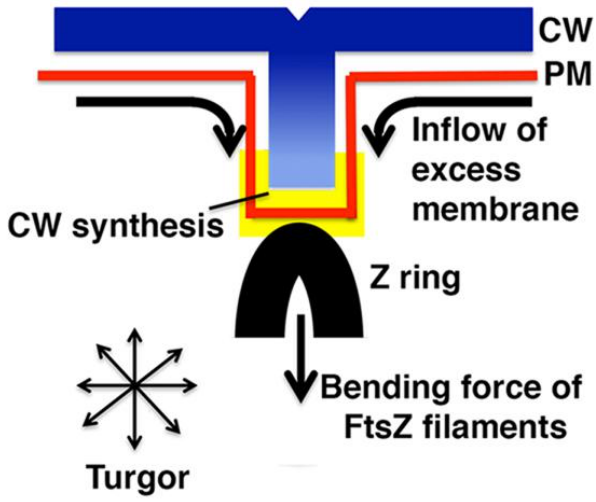

Figure 1.11. A model showing how excess of phospholipid production can play a key role in Z ring constriction. First, FtsZ filaments bend the plasma membrane (PM) from the inside. Then, peptidoglycan assembly pushes the PM from the outside and excess membrane synthesis pushes the membrane to expand inward. The combined force of FtsZ pulling and membrane pushing could divide bacteria even against turgor pressure. Figure adapted from (Osawa and Erickson, 2018).

- ***ZipA, the bitopic membrane protein that tethers FtsZ to the bacterial membrane***

ZipA is essential in Gram-negative gammaproteobacteria, remaining evenly distributed in the inner membrane but concentrated in the septum during division (Rueda *et al.*, 2003) (Huang *et al.*, 2013). It is an essential bitopic integral inner membrane protein, which contains a short amino-terminal region that is integrated in the membrane and connected to the carboxy terminal FtsZ-interacting domain by a flexible, unstructured linker region (Ortiz *et al.*, 2016) (**Figure 1.12**). In *E. coli,* ZipA functionally overlaps with FtsA in tethering FtsZ to the membrane (Huang *et al.*, 2013). ZipA may be a stronger membrane anchor for FtsZ than FtsA, as both interactions (ZipA with the membrane and ZipA with FtsZ) are stronger than the equivalent interactions provided by FtsA (Rico *et al.*, 2013).

Interestingly, although a single amino acid substitution in FtsA (FtsA* mutant) renders ZipA non-essential in *E. coli*, allowing efficient growth and division in its absence (Adams and

Errington, 2009), it has been detected that ZipA also protects FtsZ from degradation by the protease system ClpXP, suggesting a specific function of ZipA in proto-ring stability, as this role cannot be fulfilled by FtsA or the gain-of-function FtsA* mutant (Pazos *et al.*, 2013) (Geissler *et al.*, 2003). Additionally, it has been recently determined that ZipA is required for FtsZ-dependent cell wall synthesis at midcell during the transition from cell wall elongation to septum invagination in wild-type *E. coli* (Huang *et al.*, 2013) (Potluri *et al.*, 2012).

Previous studies in solution determined that the soluble recombinant ZipA (sZipA) lacking the transmembrane domain was able to bind with micromolar affinity GDP-FtsZ (Martos *et al.*, 2010). In addition, reconstitution studies proposed that ZipA can recruit FtsZ monomers to the membrane and polymerize there in contrast to FtsA that only recruits FtsZ polymers (Loose and Mitchison, 2014).

Another important role of ZipA in bacterial division seems to be the stabilization of FtsZ filaments that promotes higher order FtsZ structures formation under certain conditions (Hale *et al.*, 2000) (Pazos *et al.*, 2013). Furthermore, experiments using giant unilamellar vesicles allowed to establish that interaction between sZipA and FtsZ is sufficient to promote membrane constriction when both proteins are encapsulated together with GTP (Cabré *et al.*, 2013).

- ***FtsA, probably the principal membrane anchor for the Z ring***

FtsA is an actin-like peripheral membrane protein that contains a conserved C-terminal amphipathic helix that interacts with the lipid bilayer and anchors itself to the membrane. (Pichoff and Lutkenhaus, 2005). FtsA has two critical roles in bacterial cell division. Thus, along with ZipA, FtsA tethers FtsZ filaments to the membrane. Besides, ZipA and FtsA are required for recruitment of all the downstream division proteins to the Z ring (Ortiz *et al.*, 2016).

The broad conservation of FtsA, the ability of Z rings to assemble in the absence of ZipA, the ability of ftsA mutant, FtsA*, to bypass the need for ZipA, and the direct interaction between FtsA and some downstream proteins suggest that FtsA is the primary factor required for anchoring FtsZ to the membrane in *E. coli* (Huang *et al.*, 2013).

In *E. coli*, the FtsA:FtsZ ratio is crucial for proper cell division since small changes could inhibit septum formation. This ratio is roughly 1:5, with around 700 molecules of FtsA and

3200 molecules of FtsZ per cell, which would correspond to concentrations of 1–2 and 5–10 μM, respectively (Beuria *et al.*, 2009).

Although FtsA is a member of the actin family, it lacks one of the four subdomains of actin and has an additional one (1C) (**Figure 1.12**). The assembly of the divisome is controlled by this additional domain since FtsA devoid of it localizes efficiently at the Z ring but is unable to recruit the late cell division proteins (Rico *et al.*, 2004). In addition, domain 2B seems to contribute to the FtsA-FtsZ interaction (Huang *et al.*, 2013) (Pichoff and Lutkenhaus, 2007). Targeting of FtsA to the membrane by the amphipathic helix in its C-terminal is essential for its function, but the sequence of this membrane target does not have a direct role in the interaction with FtsZ, because it can be replaced with a MinD membrane targeted sequence with no significant effect on FtsA-FtsZ interaction (Pichoff and Lutkenhaus, 2005). The predicted structure of FtsA C-terminal helix is a motif commonly present in amphitropic proteins displaying higher affinity for anionic phospholipids.

A previous study accomplished the purification of *E. coli* FtsA from inclusion bodies where a controlled refolding step was required. When the lipid-binding properties of this protein were measured, the apparent affinity of FtsA binding to the inner membrane resulted ten-fold higher than to phospholipids, suggesting that inner membrane proteins could modulate FtsA-membrane interactions (Martos *et al.*, 2012).

Furthermore, FtsA was capable to bind ATP with very low affinity and *in vitro* studies with others organisms reported that FtsA assembles into non dynamic filaments (Szwedziak *et al.*, 2012). Nevertheless, no ATPase activity has been reported yet, and therefore further studies are needed to clarify the physiological role for this nucleotide-interaction ability.

Recently, the co-reconstitution of wild-type FtsZ and FtsA on supported lipid bilayers has revealed that FtsA promotes the self-organization of FtsZ filaments into dynamic patterns, giving rise to coordinated streams and swirling rings with preferential directions, due to treadmilling dynamics, as revealed by total internal reflection fluorescence microscopy, TIRFM (Loose and Mitchison, 2014). Interestingly, FtsA does not modify the FtsZ GTPase activity but depolymerizes FtsZ bundles similarly to that previously observed for mutant FtsA (FtsA*) (Beuria *et al.*, 2009). In contrast, this dynamic behaviour was not observed when FtsZ was tethered to the membrane through ZipA, or when a hybrid version of FtsZ that binds autonomously to the membrane through an amphipathic helix at its C-terminus (FtsZ-YFP-mts, see below) was used. Form these observations, Loose and Mitchison concluded that FtsA could play a crucial role in these dynamics, not only recruiting FtsZ polymers to the

membrane but also destabilizing them by biochemical mechanisms yet to be identified (Loose and Mitchison, 2014).

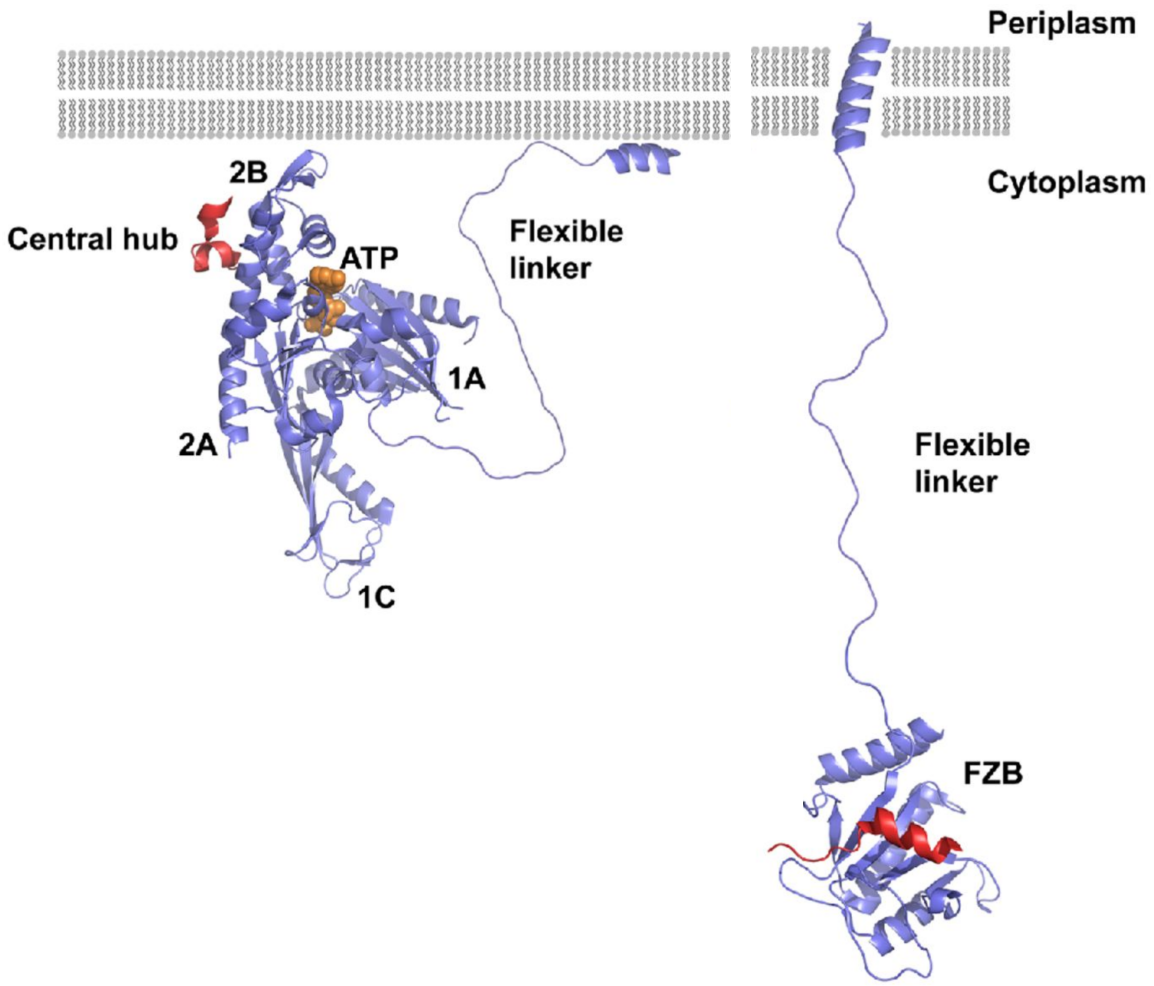

Figure 1.12. Crystal structures from the *Thermotoga maritima* FtsA (left) and *E. coli* ZipA (right). FtsA contains four different subdomains: 1A, 2A, 2B and 1C. The ATP-binding site formed by the interaction of the subdomains 1A, 2A and 2B shows ATP (orange) bound inside it. The central hub of FtsZ (red) is shown bound to the 2B FtsA subdomain. The flexible linker of FtsA is depicted here as a free-drawn unstructured peptide. The amphipathic helix or mts (blue) attaches FtsA to the cytoplasmic membrane. ZipA is shown with its C-terminal globular domain, the FZB, bound to the FtsZ central hub (red). The flexible linker of ZipA is depicted here as a free-drawn unstructured peptide. The transmembrane segment (blue) is an alpha helix which anchors ZipA to the membrane. Figure adapted from (Ortiz *et al.*, 2016).

- ***Membrane-tethered FtsZ construct***

As mentioned before, FtsZ is a cytoplasmic protein that needs to be anchored to the membrane by FtsA or ZipA. To provide autonomous membrane attachment and bypass these natural anchors, a **membrane-targeted FtsZ chimeric (FtsZ-YFP-mts) protein** was constructed by inserting a membrane targeting sequence (mts) that attaches FtsZ directly to the membrane (**Figure 1.13**) (Osawa *et al.*, 2008). This mts corresponds to the amphipathic

helix from MinD, one of the elements of the bacterial division site-selection MinCDE complex peripherally attached to the membrane. Previous studies showed that this membrane-targeting sequence [FIEEEKKGFLKRLFGG] from MinD, consists of a positively charged, hydrophobic region that promotes the binding to membranes enhancing the electrostatic interaction of MinD with anionic phospholipids (Renner and Weibel, 2012).

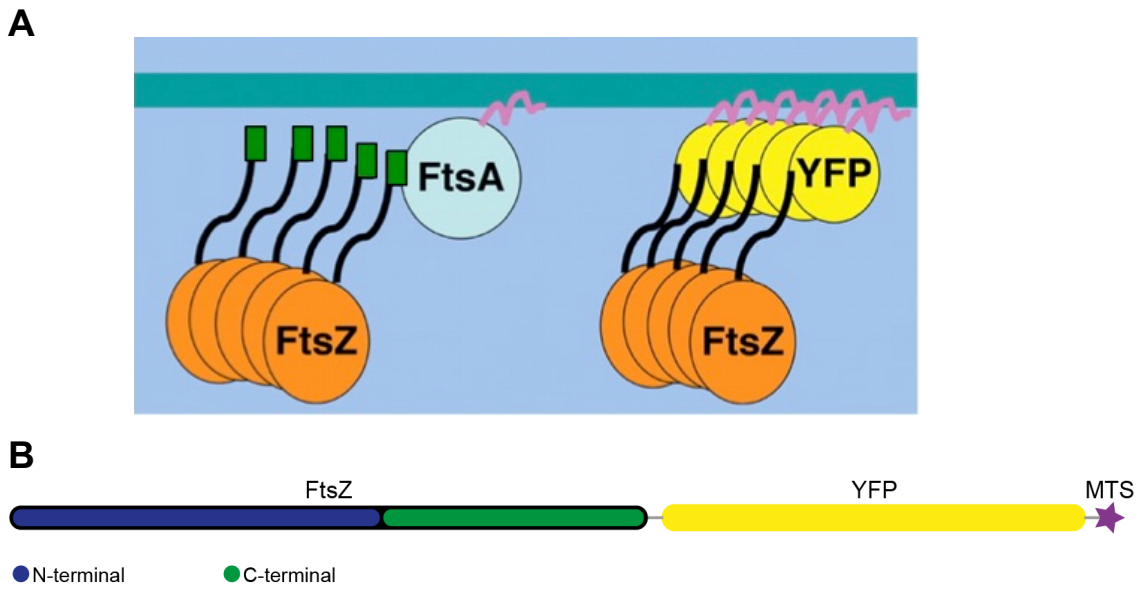

Figure 1.13. Schematic representation of chimeric FtsZ (A) FtsZ is tethered to the membrane by FtsA, a natural anchor. The C-terminal peptide (green) of FtsZ binds FtsA, and FtsA interacts with the membrane by its amphipathic helix (pink line). To mimic this natural membrane FtsZ attachment, a chimeric FtsZ was constructed (FtsZ-YFP-mts). In this protein, the FtsA-binding peptide is replaced with yellow fluorescent protein (YFP) and an amphipathic helix (pink line). **(B)** Chimeric FtsZ consists of a N-terminal and a sliced C-terminal (1-366 aa). Notice that FtsZ central hub was replaced by YFP (yellow) and an amphipathic helix from MinD (purple star). The molecular weigh of this construct is 68 kDa. Figure adapted from (Osawa *et al.*, 2008).

Furthermore, Osawa and Erickson designed a FtsZ construct (mts-FtsZ-YFP) where the membrane tether is switched to the N-terminal, which is on the opposite side of the FtsZ subunit (Osawa and Erickson, 2011). Using biomimetic membrane systems, Osawa and Erickson observed that FtsZ-YFP-mts and mts-FtsZ-YFP, in the presence of GTP, were able to assemble and deform membranes (Osawa *et al.*, 2008) (Osawa *et al.*, 2009).

Importantly, Arumugam and co-workers (Arumugam *et al.*, 2014) stated that FtsZ-YFP-mts filaments on supported lipid bilayer systems showed rapidly exchanging subunits with a half time of 10 s, similar to the rate of exchange in the Z ring *in vivo* (Anderson *et al.*, 2004) and single filaments in solution (Chen and Erickson, 2005). However, it is noteworthy that the differences between an autonomous FtsZ attachment or FtsZ anchoring through ZipA or

FtsA to the membrane, may have an impact on the structural organization of the polymers, *e.g.*, in the spacing of the protofilaments. Indeed, Cryo-EM images of reconstituted FtsZ in the presence of FtsA showed protofilaments in lateral contact, with a 7-9 nm spacing (Szwedziak *et al.*, 2014), while the negative stain images of FtsZ-YFP-mts showed a spacing of around 5 nm (Milam *et al.*, 2012), suggesting that FtsA may enforce the larger separation of protofilaments.

1.3. The Min system: spatial regulators of cell division

The Min system is highly conserved and widely distributed across diverse bacterial species. Min proteins form a well understood geometric positioning system for the Z ring in *E. coli* that defines the cell's geometric middle and prevents polar septations (**Figure 1.14**) (Lutkenhaus *et al.*, 2012). Mutant cells lacking Min proteins are prone to divide asymmetrically giving rise to mini-cells with deficient DNA since the Min system suppresses assembly of the Z ring at the cell poles (Rowlett and Margolin, 2013).

This system comprises three proteins (MinD, MinE, and MinC) that exhibit reproducible and stable pole-to-pole **oscillations *in vivo*** on a typical time scale of about 1 min (Hu and Lutkenhaus, 1999). Together, MinD and MinE account for the dynamic behaviour of the system, which arises from self-organization and exchange of protein subunits between the membrane and the cytosol. MinC (inhibitor of FtsZ assembly) is passively transported with the MinDE wave and its concentration exhibits a time-averaged local minimum at midcell, allowing Z ring formation at this position (Kretschmer and Schwille, 2016) (Hu and Lutkenhaus, 1999) (Meinhardt and de Boer, 2001).

To clarify the order of events in space and time and the generic features required for pattern formation, Min proteins oscillations have been successfully **reconstructed *in vitro***, using supported lipid bilayers that mimic the cytoplasmic membrane of the bacterial cell. In this biomimetic system, detected dynamic MinCDE waves are characterised by a wavelength, velocity and temporal period (Loose *et al.*, 2011). These waves have characteristics that mimic the *in vivo* oscillation, including a maximum concentration of MinE at the trailing edge of the wave, estimated to be in a 1:1 ratio with MinD (Loose *et al.*, 2011). Furthermore, it is known that the spatial scale (wavelength), velocity and period of Min waves *in vitro* as well as the Min oscillation period *in vivo* are sensitive to the MinE/ MinD concentration ratio, and these oscillation patterns are defined by a similar speed, about 0.5 nm/s (Loose *et al.*, 2008).

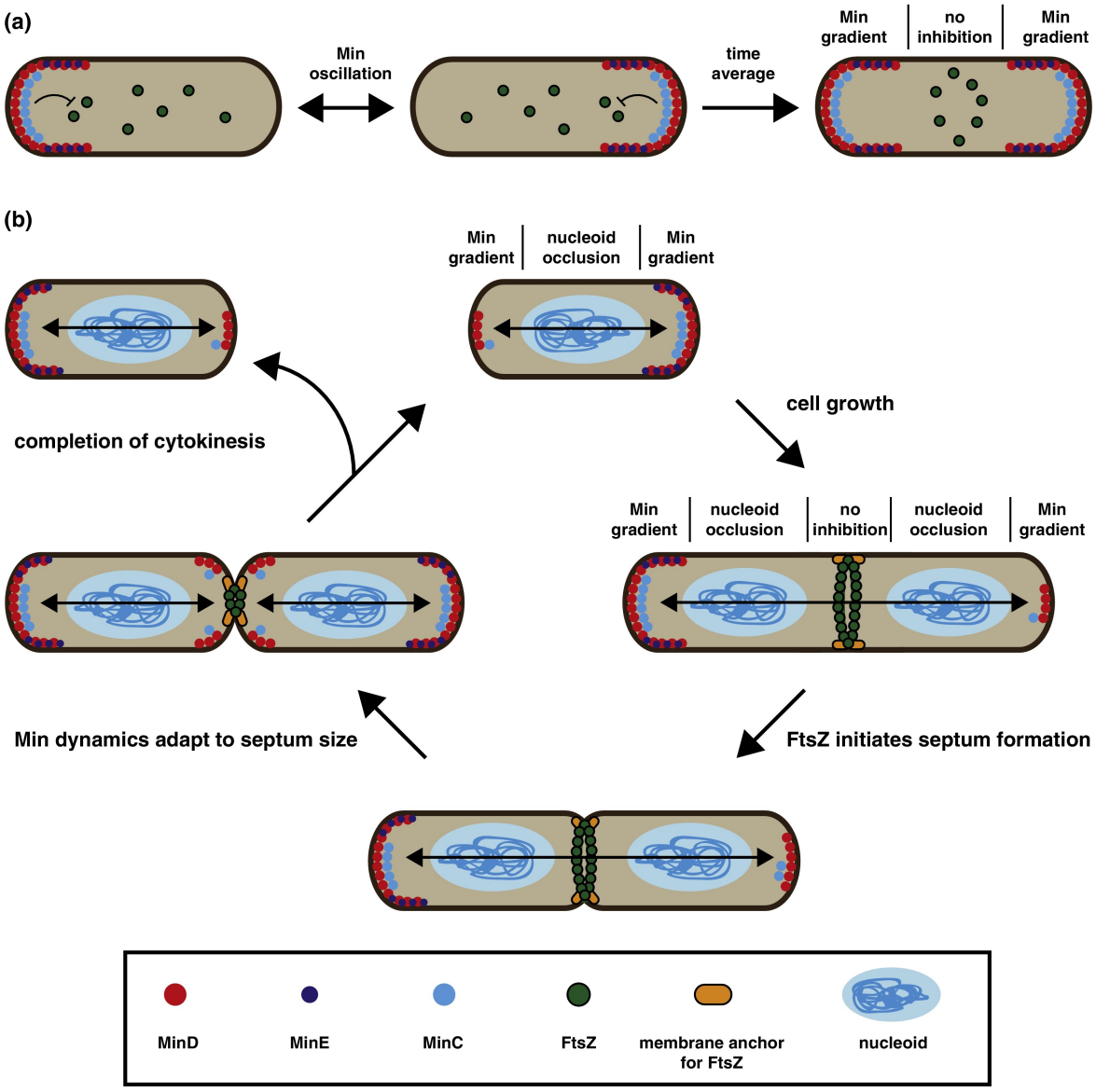

Figure 1.14. Scheme of Min oscillations in *E. coli* and their adaptation to the progress of cytokinesis. (a) Min proteins oscillate from pole-to-pole forming a time-averaged concentration gradient, which directs FtsZ polymerization to the cell middle through the inhibitory action of MinC. **(b)** In short cells, FtsZ polymerization is inhibited by the Min system at the poles and nucleoid occlusion near the chromosome. Once cells exceed a certain length, an inhibitor-free region is established at midcell that allows for polymerization of FtsZ, which is anchored to the membrane via adaptor proteins FtsA and ZipA. FtsZ assembles into the Z ring at midcell and initiates septum formation. In constricting cells, the Min dynamics switch from a pole-to-pole oscillation to a half-cell-to-half-cell oscillation and finally to a double oscillation. This ensures stable inheritance of Min proteins and oscillatory dynamics to the daughter cells. Figure adapted from (Kretschmer and Schwille, 2016).

MinD is a reversibly membrane-bound ATPase that presents a membrane targeting sequence (mts); a 19 amino-acid long amphipathic helix at the C-terminal end of the protein. Upon ATP binding, MinD dimerizes and exposes its mts, which peripherally attaches to the membrane in a cooperative manner. Importantly, binding of MinD to the membrane shows

cooperative behaviour arising from protein–protein interaction of the membrane-bound species (Hu and Lutkenhaus, 2001) (Suefuji *et al.*, 2002).

MinE is a dimer when it binds to membrane-bound MinD. This binding drives a conformational change to an active, membrane-associated state of MinE, which stimulates the ATPase activity of MinD, triggering the detachment of MinD from the membrane (**Figure 1.15**) (Loose *et al.*, 2011) (Kretschmer and Schwille, 2016). MinE has been reported to form a ring-like structure predominantly close to midcell, the so-called 'E-ring', comprising a sharply defined band of MinE that travels behind MinD and MinC (Martos *et al.*, 2012). It is thought that the localization of MinCD at midcell is impaired by this E-ring, hence allowing FtsZ filaments assembly at this location.

The lipid composition of the bacterial membrane could control the spatial assembly of the Min protein machinery in *E. coli* cells. *In vitro* studies using quartz cristal microbalance (QCM) demonstrated that binding affinity of MinD and MinE for lipid bilayers increase with increasing concentration of anionic phospholipids, which reduces MinD ATPase activity. These results indicate that anionic lipids, which are concentrated at the cell poles, increase the retention of MinD and MinE explaining their longer residence time at this region of bacterial cells (Renner and Weibel, 2012).

MinC is an inhibitor of FtsZ polymerization, composed of two functional domains of similar size forming a dimeric protein. MinC is recruited to the cell membrane by MinD and is topologically regulated by MinE, which, as stated, undergoes an oscillation along with MinC and MinD between the poles of the cell (Lutkenhaus, 2007) (Park *et al.*, 2018). The C-terminal domain ($MinC^C$) binds MinD and FtsZ. The amino-terminal domain ($MinC^N$) directly interacts with the globular domain of FtsZ. It has been proposed that MinC first binds to FtsZ filaments using its C-terminus and then $MinC^N$ attacks the FtsZ H10 helix and "breaks" the longitudinal bond (Shen and Lutkenhaus, 2009). Although, $MinC^N$ antagonizes polymerization *in vitro* and blocks Z ring assembly *in vivo*, it does not affect its GTPase activity or polymerization ability. $MinC^C$ decreases filament bundling and can localize at the Z rings and block cell division when MinD is present (Ghosal *et al.*, 2014).

MinD recruits MinC to the membrane forming copolymeric filaments. These membrane-bound MinCD copolymers constitute the active inhibitor complex that spatially regulates Z ring assembly. *In vivo* studies using MinD mutants established that MinC activation by MinD is more than just recruitment of MinC to the membrane. The mechanism of MinC activation

by MinD, and how the MinCD inhibitor complex regulates Z ring assembly remains unclear (Ghosal *et al.*, 2014).

MinC links MinD-MinE and FtsZ systems by virtue of its binding to MinD and its depolymerizing activity on FtsZ polymers. FtsZ and Min proteins constitute a self-organized system in which energy is consumed independently by two different components: the MinD-MinE system, in which MinD hydrolyses ATP, and the FtsZ system, whose dynamics are based on GTP hydrolysis.

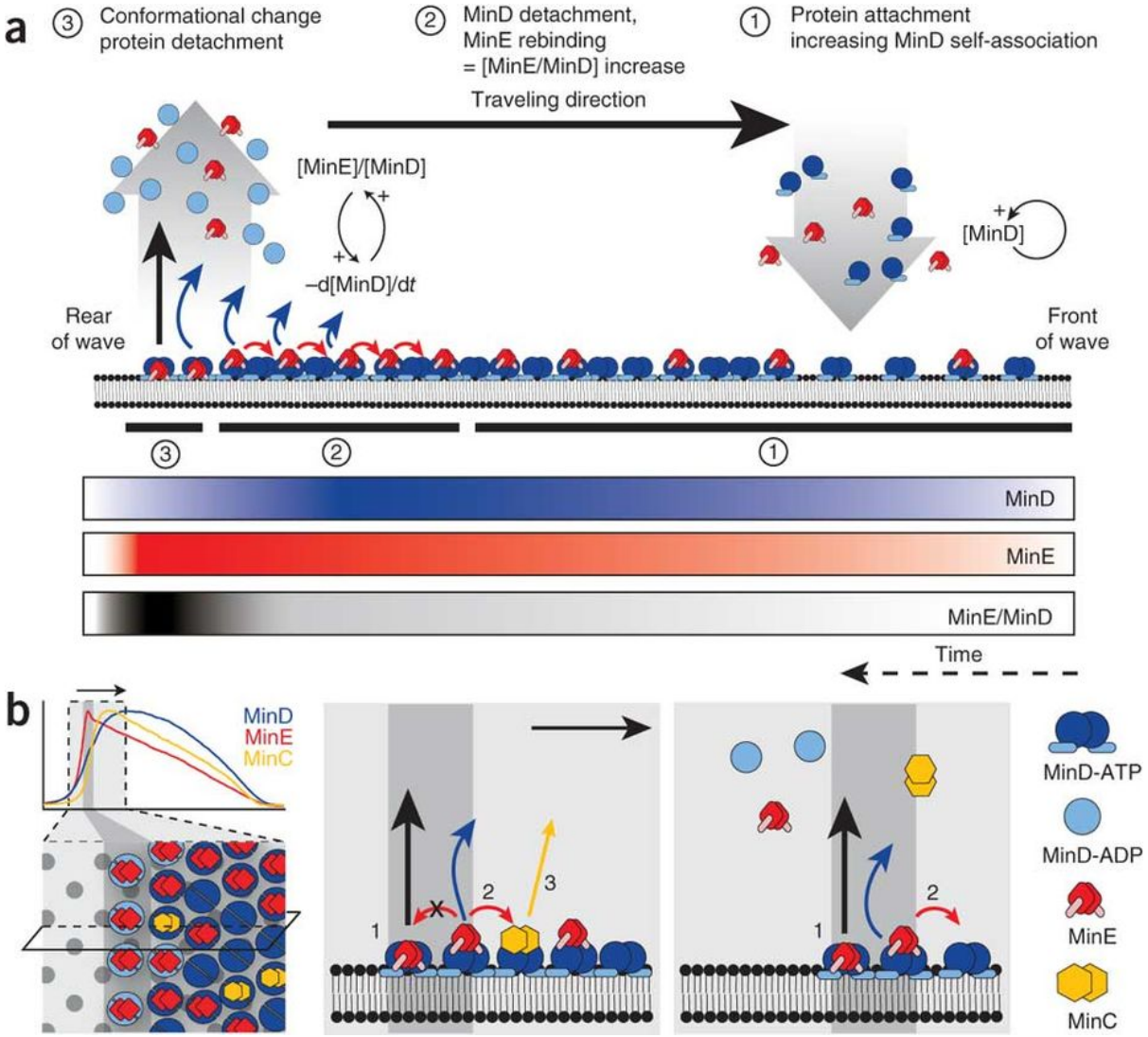

Figure 1.15. Model of Min-protein pattern propagation. (A) First, MinD-ATP binds cooperatively to the membrane and MinE dimers present in solution start to bind to membrane-bound MinD. Here, at the front of the wave the concentration of MinE is too low to trigger a predominant MinD membrane detachment. At a sufficiently high [MinE]/[MinD] density ratio, protein detachment starts to dominate. At a [MinE]/[MinD] ratio of about 1, interaction of MinE with the membrane induces a conformational change, which results in the displacement of MinC from the MinD carpet before the MinD–MinE complex itself detaches from the membrane. **(B)** Illustration of the order of events at the

rear of the protein wave. Shown are top (left) and side (middle and right) views of Min proteins bound to the membrane. As seen in the side view, before detachment from the membrane, either MinE forms a complex with MinD, which is present in an altered conformation involving membrane binding by MinE (1), or MinE rebinds to a neighbouring membrane-bound MinD, if available (2). Because the density of membrane-bound MinD is higher toward the front of the wave, rebinding MinE is biased in this direction, giving rise to the local saturation of MinD with MinE. After detachment of MinC from MinD (3), MinE can occupy the overlapping binding site on MinD. Figure adapted from (Loose *et al.*, 2011).

1.4. Reconstruction of minimal divisome in biomimetic membrane systems

A biological system can be regarded as a combination of individual functional elements; hence, an extraction of these components could be performed to simplify the complete system. The **bottom-up synthetic biology strategy** aims to reconstitute biological parts and systems with increasing levels of complexity toward a minimal cell-like scaffold. Notably, the reconstruction of the bacterial cell division has been accomplished by developing the required technology to mimic different elements of the bacterial cell.

Because the assembly of the bacterial cell division machinery takes place at the inner bacterial membrane, considerable efforts have been made to study the assembly properties of FtsZ and its interaction with companion proteins in reconstructions of the proto-ring on **biomimetic membrane systems** (Martos *et al.*, 2012) (Natale *et al.*, 2013) (Jimenez *et al.*, 2013). Importantly, these minimal membrane systems that can be used as scaffolds to reconstruct the molecular machinery of the bacterial divisome, have helped to advance in the molecular description of how bacteria manage to precisely control the timing and the topology of division. *In vitro* reconstitution experiments in biomimetic membranes systems provide an effective strategy to test the biophysical properties of the elements of the division machinery and their fundamental interactions and enzymatic activities, since biochemical and biophysical parameters can be controlled precisely in well-defined environments (Martos *et al.*, 2012) (Rivas *et al.*, 2014).

In order to test the functional properties of proto-ring subsets, minimal membrane systems, from nanodiscs and supported bilayers to microbeads and free standing vesicles, have been used as scaffolds to reconstitute the division machinery (**Figure 1.16**) (Martos *et al.*, 2012); (Rivas *et al.*, 2014).

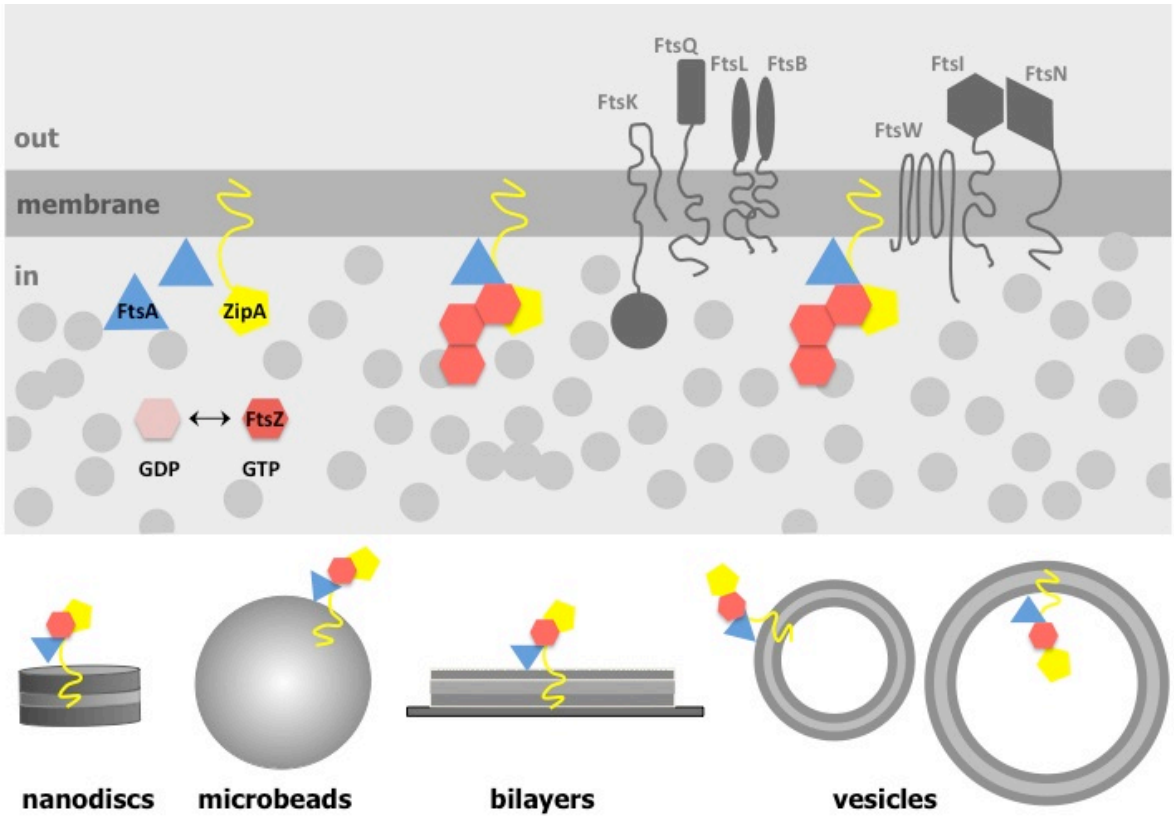

Figure 1.16. Diagram illustrating the molecular assembly of the proto-ring elements in *E. coli* cells (top panel) and the reconstitution of protein assemblies in minimal membrane systems (bottom panel). Nanodiscs, lipid-coated microbeads, supported lipid bilayers and vesicles constitute different synthetic membrane systems employed to reconstruct the *E. coli* division proteins. Figure adapted from (Martos *et al.*, 2012).

In the present thesis, the main minimal membrane system selected to study the protein cell division interactions has been the **supported lipid bilayers** (SLBs). This synthetic approach is well suited for investigating the reactivity (*i.e.*, dynamic interactions) and the membrane structural organization of division proteins by surface-sensitive imaging techniques under biochemically controlled and well defined experimental conditions (Loose and Schwille, 2009). Remarkably, thermal fusion of small liposomes and the Langmuir–Blodgett film deposition are the most popular methods to prepare SLBs (Richter *et al.*, 2006). In addition, in these experimental setups the solid supports are usually made of glass, which offers an optically transparent and flat surface.

The investigation of the protein interactions reconstituted in supported membranes and their dynamic processes can be accomplished in detail using fluorescence microscopy. One of the most popular fluorescence based imaging methods is confocal microscopy which offers a high spatial resolution since it measures only the fluorescence of thin sample sections. Additionally, total internal reflection fluorescence microscopy (TIRFM) exploits the unique

properties of an induced evanescent wave in a thin section immediately adjacent to the coverslip allows enhancing the resolution and it is extremely useful to study the dynamics of single lipid and protein molecules in membranes and the dynamic interactions of soluble proteins with these membranes (Garcia-Saez and Schwille, 2010).

In addition, to analyse and measure the binding affinities of the membrane tethered FtsZ chimeric and of FtsA for membranes, **lipid coated microbeads** were employed in this thesis. This system provides a rigid support that is chemically and physically stable with uniform curvature. Thus, the affinity of refolded FtsA for the bacterial cytoplasmic membrane was studied previously using microbeads (Martos *et al.*, 2012). More recently, a quantitative study of the effect of the nucleotide and receptor density on the binding of FtsZ to ZipA containing lipid-coated microbeads has been published (Sobrinos-Sanguino *et al.*, 2017).

- ***Reconstitution of the proto-ring proteins in membrane systems***

A decade ago, Osawa and Erickson reconstituted FtsZ filaments in liposomes *in vitro*, using membrane-tethered FtsZ chimeric. Such an FtsZ construct was found to become internalized and accumulated in narrow regions of tubular liposomes, forming static ring-like structures (**Figure 1.17; model a**). Although GTP was necessary, its hydrolysis was not, indicating that the formation of the filaments on the membrane was the only factor responsible for the observed deformation of the vesicles. Interestingly, when FtsZ-YFP-mts was added to the outside of liposomes, the protein that was bound to the membrane produced concave depressions. This membrane bending was in the same direction as the Z ring inside liposomes (**Figure 1.17; model b**) (Osawa *et al.*, 2008) (Osawa *et al.*, 2009).

In another work, reconstituted copolymers of wild-type FtsZ and the FtsZ chimera were found to preferentially align along the surface of micro-structured SLBs, as visualized by atomic force microscopy (AFM) and total internal reflection fluorescence microscopy (TIRFM) (**Figure 1.17; model c**) (Arumugam *et al.*, 2012).

Subsequently, when another FtsZ mutant version with the mts cloned to the N-terminal was applied to the outside of liposomes, it generated convex bulges, bending the membrane in the direction opposite to the concave depressions (**Figure 1.17; model d**) (Osawa *et al.*, 2009). Furthermore, around the outside surface of tubular liposomes, mts-H-FtsZ-YFP assembled “inside-out” Z rings that were highly dynamic, and generated a constriction force that squeezed the tubular liposomes from outside (**Figure 1.17; model e**) (Osawa and

Erickson, 2011). In addition, using bilayer-coated glass capillaries, mts-H-FtsZ-YFP filaments aligned almost perpendicularly to the longitudinal axis of the glass rod showing that FtsZ assembled into inherently curved and twisted filaments supporting a helical geometry (**Figure 1.17; model f**) (Arumugam *et al.*, 2012).

The reconstruction of the Z rings using its native membrane anchors, FtsA and ZipA, has been also attempted applying different minimal membrane systems. For instance, when a mixture of FtsZ-GTP and a mutant of FtsA (FtsA*) was added inside of liposomes, Z rings that encircled liposomes and occasionally achieved complete constriction and septation were detected (**Figure 1.17; model g**) (Osawa and Erickson, 2013). Interestingly, FtsZ static assemblies were also found when wild type FtsZ and its natural membrane anchor FtsA were co-reconstituted inside liposomes (**Figure 1.17; model h**) (Jimenez *et al.*, 2011). Additionally, co-reconstitution of FtsZ and FtsA on supported membranes revealed that FtsA drives the self-organization of FtsZ polymers into dynamic patterns, consistent with treadmilling of dynamic polymers (**Figure 1.17; model i**) (Loose and Mitchison, 2014).

On the other hand, studies employing permeable giant vesicles showed that wild-type FtsZ assembly inside ZipA-containing giant vesicles yielded dynamic structures resulting in vesicle shrinkage (**Figure 1.17; model j**) (Cabré *et al.*, 2013). Furthermore, the polymerization of the natural FtsZ protein in the external face of ZipA-containing giant vesicles resulted in membrane deformation (**Figure 1.17; model k**) (Martos *et al.*, 2012). Besides that, FtsZ polymers bound to SLBs through a soluble variant of ZipA, lacking the transmembrane region, formed two-dimensional networks that retained their capacity to dynamically restructure, as revealed by AFM (**Figure 1.17; model l**) (Mateos-Gil *et al.*, 2012) (Lopez-Montero *et al.*, 2012).

Membrane targeting method	Membrane system/ Assay(s)	Outcome	Model
membrane FtsZΔC-YFP-MTS FtsZΔC-MTS	Protein inside tubulated vesicles	Z-ring formation and constriction	 a
	Protein outside spherical vesicles	Concave depressions, membrane tubulation	 b
	Protein on lipid bilayers assembled on curved substrate	Alignment of FtsZ filaments with preferred curvature	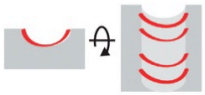 c
MTS-FtsZΔC-YFP	Protein outside spherical vesicles	Convex bulges	 d
	Protein outside tubulated vesicles	"Inside-out" Z-ring formation and constriction	 e
	Protein on lipid bilayers-coated glass capillaries of different diameters	Alignment of FtsZ filaments with preferred curvature	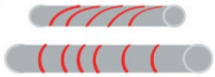 f
FtsZ-YFP FtsA*	Protein inside unilamellar vesicles embedded in agarose	Z-ring formation, constriction, and fission	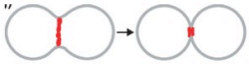 g
FtsZ FtsA	Protein inside giant unilamellar inner membrane vesicles	Lumenal accumulation of FtsZ-FtsA bundles	 h
	Protein on supported lipid bilayers	FtsA and FtsZ self-organize into dynamic patterns	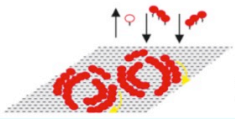 i
FtsZ ZipA	Protein inside giant unilamellar vesicles	FtsZ and ZipA induce vesicle shrinkage and cell membrane invagination	 j
	Protein outside giant unilamellar vesicles	Membrane tubulation of vesicles containing ZipA driven by native FtsZ polymers	 k
	Protein on supported lipid bilayers	ZipA-FtsZ dynamic networks	 l

Figure 1.17. Biomimetic membrane systems for studying FtsZ assembly and force generation *in vitro*. In graphical representations of outcomes, membranes are depicted in grey and FtsZ is depicted in red. FtsZΔC: FtsZ lacking its C-terminal FtsA-binding peptide; FtsA*: R286W hypermorph mutant of FtsA. Notice that membrane system model diagrams are labelling (**a-l**) for easier reading in the main text. Figure adapted from (Meier and Goley, 2014). The information incorporated in this thesis are emphasized in blue.

- ***MinCDE complex reconstitution in minimal membrane systems***

In recent years, a synthetic minimal approach, in which the Min cycling behaviour was successfully transferred to artificial membranes, has powered a great progress towards the understanding of the biochemical basis of the Min system (Loose *et al.*, 2008). *In vitro* reconstitution of MinDE in the presence of ATP on **supported lipid bilayers** (SLBs) showed that the Min proteins assemble as spatiotemporal patterns propagating across the bilayer surface (**Figure 1.18**). The formation of dynamic protein patterns requires a reversible binding of the Min proteins to the membrane. In this regard, self-organization in the Min system arises from an interplay of two opposing mechanisms: cooperative binding of MinD to the membrane, and accelerated MinD detachment due to persistent MinE binding (Loose *et al.*, 2011) (Martos *et al.*, 2013) (Martos *et al.*, 2012).

Min waves were also reconstructed in free-standing **giant unilamellar vesicles (GUV)** membranes which display higher fluidity since the average diffusion of lipids and other molecules within the membrane has been shown to be several times faster than in supported bilayers. Interestingly, the propagation velocity and wavelength of Min waves on GUVs are three times higher than those reported on supported bilayers, but the wave period is conserved (Martos *et al.*, 2013). Furthermore**, microdroplets** interfaced by lipid monolayers were employed as a simple 3D mimic of cellular compartments to reconstitute Min protein oscillations (Zieske *et al.*, 2016).

Interestingly, **dynamic FtsZ oscillations** have been reported in *E. coli* elongated cells, with the period of oscillation similar to that of the Min proteins (Thanedar and Margolin, 2004). Although the driving force to account for the large mobility was not known, it was suggested that it was driven by Min proteins complex. FtsZ waves were also observed *in vitro* when membrane-tethered FtsZ chimeric networks (FtsZ-YFP-mts) were reconstructed together with the Min system. This strategy was used to study in detail the role of the GTPase activity of FtsZ on the inhibition driven by MinC (Arumugam *et al.*, 2014) and to demonstrate how the protein gradient resulting from the oscillation of the Min system efficiently drives FtsZ-YFP-mts assembly to the middle of cell-shaped micro-compartments (Zieske and Schwille, 2014).

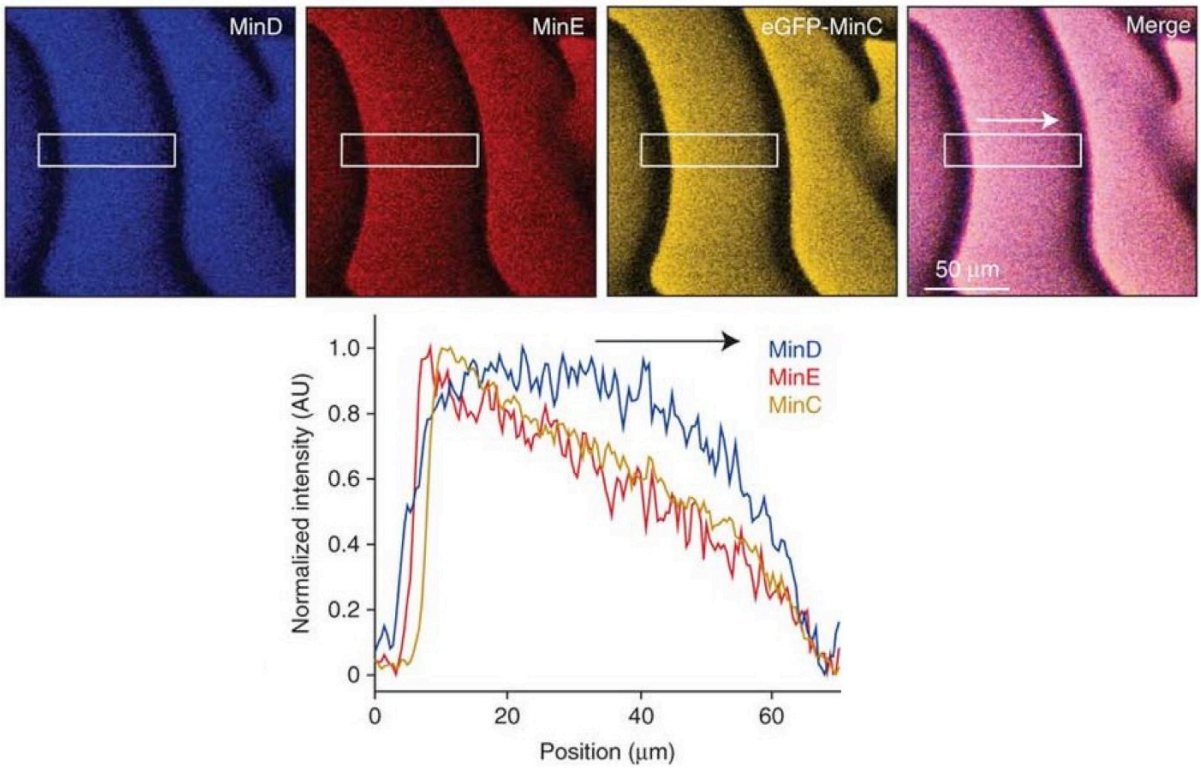

Figure 1.18. Min complex surface waves *in vitro*. Upper panels: Confocal images of self-organized Min protein waves on a supported lipid membrane (MinD (0.8 µM with 10 mol % MinD-Cy3), MinE (1.2 µM MinE with 10 mol % MinE-Cy5) and MinC (0.08 µM, with 40 mol % His-eGFP–MinC)). **Bottom panel:** Fluorescence intensity profiles of MinD, MinE and MinC acquired from the rectangular region shown in the confocal images. Figured adapted from (Loose *et al.*, 2011).

2. OBJECTIVES

The general aim of the present doctoral thesis has been to characterise the self-organization behaviour of FtsZ when is reconstituted in supported membranes and to elucidate the effect of the site-selection MinCDE complex on these self-organization processes. To overall project has been organized into three sub-projects covering complementary and interconnected aspects of the main objective.

I. Self-organization of membrane-tethered FtsZ in flat supported membranes (Section 4) to understand the mechanisms governing the emergence and steady-state dynamics of FtsZ chiral vortices in supported bilayers, as minimal membrane system. The specific aims of this sub-project have been 1) the biochemical characterization of membrane tethered FtsZ variant (FtsZ-YFP-mts) in solution and in membrane systems; and 2) the analysis of FtsZ-mts self-organization in bilayers, to elucidate whether FtsZ by itself is able to self-organize into dynamic vortices and if this is the case, determination of the biochemical factors that control their emergence.

II. Co-reconstitution of FtsZ-MinCDE complexes in ZipA-containing supported membranes (Section 5) to address the question of how the MinCDE complex regulates the behaviour of FtsZ polymers tethered to the membrane by the proto-ring element ZipA. The specific aims have been 1) to study the dynamic reorganization of FtsZ polymers by the action of MinCDE in supported bilayers containing the full-length ZipA protein; and 2) to determine the influence of factors as ZipA surface density or excluded volume effects due to crowding on the FtsZ-Min coupling.

III. Co-reconstitution of FtsZ-FtsA-MinCDE complexes in supported membranes (Section 6) to address the question of how FtsA influences the coupling between FtsZ polymers and MinCDE complex. The specific aims of this subproject have been 1) the optimization of the protocol of FtsA production to biochemically characterise the protein, in terms of association state and lipid-binding properties; and 2) the co-reconstitution of the FtsA-FtsZ-MinCDE system in flat membranes and in micro-compartments, to determine the impact of the proto-ring element serving as membrane tether of FtsZ on FtsZ-MinCDE coupling.

3. MATERIALS AND METHODS

3.1. Materials

Reagents, salts and buffer components were purchased from Sigma, Merck or Invitrogen. All reagents were of analytical or spectroscopic grade. *E. coli* polar lipid extract was acquired from Avanti Polar Lipids (Alabama, USA). Bradford and BCA colorimetric protein quantitation assays were from Bio-Rad (California, USA) and Pierce (Illinois, USA), respectively. BioBeads were from Bio-Rad. 1.5 glass coverslips were from Menzel (Germany). Ultraviolet-curable glue was from Norland Optical Adhesive 63, (Norland Products, Cranbury, NJ). 5ml HiTrap Q HP column, 5ml HisTap FF column and 5ml HiTrap Desalting column were purchased from GE Healthcare. Alexa Fluor 488 succinimidyl ester, Alexa Fluor 647 succinimidyl ester and Alexa Fluor 647 C_2 maleimide dyes were acquired from Molecular probes (Invitrogen). GTP was purchased from Sigma-Aldrich. Nano-body GFP-Booster Atto647N was from ChromoTek, (Germany). BIOMOL® GREEN reagent for phosphate detection was from Enzo, Life Science. PDMS base Sylgard™ 184 and curing agent were from Dow Corning GmbH, Germany. Chloro-trimethylsilane was purchased from Sigma–Aldrich. Silica beads (nominal diameter ~5 μm, 10.2% suspension in DI water solution) were from Bangs Laboratories, Inc. (Fishers, IN).

3.2. Overexpression, purification and labelling of proteins

3.2.1. FtsZ

E. coli FtsZ (40.3 kDa) overproduction and purification was carried out following the Ca^{2+} -induced precipitation method, published in (Rivas *et al.*, 2000). Briefly, the protein was subjected to two cycles of polymerization/depolymerization by addition of Ca^{2+} and GTP and after centrifugation, the pellet was resuspended and further purified by ionic exchange chromatography (HiTrap Q HP column). Purity of the protein was confirmed by SDS-PAGE. FtsZ activity was evaluated by a GTPase activity assay, as described below.

3.2.2. ZipA

E. coli His_6-ZipA (38.6 kDa) was purified as previously described (RayChaudhuri, 1999). Briefly, the protein was expressed from a pET-15ZIP expression vector and transformed into *E. coli* strain BL21. The protein was purified by immobilized nickel affinity chromatography (His-Bind Resin). ZipA in storage buffer (Tris-HCl 40 mM pH 8.0, NaCl 500 mM, Triton X-100 0.02 % v/v) was aliquoted and stored at -80ºC.

3.2.3. Membrane-tethered FtsZ construct

Plasmids corresponding to **FtsZ-YFP-mts** and **mts-H-FtsZ-YFP** were kindly provided by Dr. Harold P. Erickson (Durham, US). **FtsZ*[T108A]-YFP-mts** was obtained by site-directed mutagenesis using 5'- GGTGGTGGTGCCGGTACAGGT-3' and 5'-ACCTGTACCGGCACCACCACC-3' oligonucleotides. These three proteins were purified according to the protocol described in (Osawa and Erickson, 2009). Briefly, the proteins were expressed from a pET-11b expression vector and transformed into *E. coli* strain BL21. FtsZ-YFP-mts and FtsZ*[T108A]-YFP-mts were overexpressed at O/N 20ºC. In the case of the mts-H-FtsZ-YFP protein overexpression was conducted O/N at 37ºC. Cells were lysed by sonication and subsequently centrifuged. Then, protein was precipitated from the supernatant by adding 30% ammonium sulfate and incubating the mixture for 30 min on ice (with slow shaking). After centrifugation and resuspension of the pellet, the protein was purified by anion exchange chromatography using a HiTrap Q HP column. Purity of the protein (60 kDa) was confirmed by SDS-PAGE and mass spectrometry.

3.2.4 FtsA

To obtain FtsA (45.3 kDa), an optimization of a prior FtsA purification protocol (Loose and Mitchison, 2014) was required. Briefly, FtsA-SUMO plasmid (pML29) was kindly provided by Dr. Martin Loose (IST Austria) and was transformed in C41 cells. Protein expression was induced by adding 1 mM of IPTG, and keeping the cells overnight at 18ºC. After cell lysis by sonication, the lysate was purified by immobilized nickel affinity chromatography using 5ml HisTap FF column. His**-**SUMO**-**FtsA was eluted with an imidazole gradient and the main protein peak was found at 200 mM imidazole. At this point, CHAPs detergent as added at 10 mM (final concentration) to the eluted protein. This zwitterionic detergent is useful for membrane protein solubilisation while maintaining protein activity. CHAPs is soluble over a wide range of pH values (2 to 12) and is easily removed from solution by dialysis because it has a high critical micelle concentration (CMC).

After different cleavage tests the His-SUMO tag was separated from FtsA by incubation of His-SUMO-FtsA (around 50 µM) with equimolar concentration of 50 µM SUMO Protease at 4ºC during 2 h, with slow shaking. Then, the protease and released tag were removed from the untagged FtsA by using a His-Bind Resin. Untagged FtsA protein was eluted with 50 mM HEPES at pH 8, 500 mM KCl, 10 mM $MgCl_2$, 10% glycerol, 50 mM imidazole, 10 mM CHAPs and 1 mM ADP. The protein was afterwards subjected to a concentration step using Vivaspin Centrifugal Concentrators to reach around 20 µM FtsA. Finally, CHAPs detergent (10 mM) that was in the protein buffer was removed using a Hi-Trap Desalting column. FtsA

in storage buffer (50 mM HEPES at pH 7.5, 500 mM KCl, 10 mM $MgCl_2$, 10% glycerol, and 1 mM ADP) was aliquoted and stored at -80ºC. Protein concentration was quantified by Bradford assay (at 595nm). The purity of protein was evaluated by PAGE-SDS.

3.2.5 MinCDE system

His_6-MinC, His_6-eGFP-MinC, His_6-MinD, His_6-eGFP-MinD and His_6-MinE were purified as described elsewhere (Loose *et al.*, 2011;Loose *et al.*, 2008) in the Core Facility of Max Planck Institute of Biochemistry (Martinsried, Germany).

3.2.6 Protein labelling

FtsZ was labelled in the amine groups with Alexa Fluor succinimidyl ester probes as previously described (Reija *et al.*, 2011). Assembled FtsZ was employed for the labelling process. In addition, Alexa Fluor 647 C2 maleimide dye, a thiol-reactive probe, was used to label **FtsA** in the cysteine residues. Briefly, FtsA was labelled using equimolar concentration of Alexa 647-C_2 maleimide for 10 min (with continuous shaking at 4ºC). The unreacted dye was removed with a Hi-Trap Desalting column equilibrated in 50 mM Hepes, 500 mM KCl, 10 mM MgCl, 10% glycerol, 1 mM ADP, pH 7.5. After protein elution of the labelled protein, FtsA concentration was quantified by Bradford Assay and Alexa 647 dye concentration by absorbance measurements, using the absorption coefficient of the dye at 650nm. Final protein concentration was around 10-20 μM. The degree of labelling of the proteins was typically 0.2–0.9 mol fluorophore/mol protein in all cases.

3.3. Biochemical characterization of proteins in solution

3.3.1. Sedimentation velocity

Sedimentation velocity experiments were carried out at 38,000 rpm and at 20ºC in an XL-I analytical ultracentrifuge (Beckman-Coulter Inc.) equipped with a UV-vis detection system, using an An-50 Ti rotor and 12 mm double-sector centerpieces. Sedimentation profiles were registered every 5 min at the appropriate wavelength. The sedimentation coefficient distributions were calculated by least-squares boundary modelling of sedimentation velocity data using the c(s) method as implemented in the SEDFIT program (Schuck, 2000). These S-values were corrected to standard conditions (water, 20ºC and infinite dilution) using the software SEDNTERP (van Holde, 1985). The frictional ratio, f/f0, was calculated for the monomer using this software.

Sedimentation velocity analysis of **FtsZ-YFP-mts** was performed at 0.5 g/L protein concentration in 50 mM Tris-HCl, 150 mM KCl, pH 7.5 buffer. Different conditions of GTP and Mg^{2+} concentrations were employed. Sedimentation profiles were registered at 515nm. In the case of **FtsA**, sedimentation velocity analysis was performed at 0.2 g/L of FtsA in 50 mM Hepes, 500 mM KCl, 5 mM $MgCl_2$, pH 7.5 buffer. Two different nucleotides were employed: ATP (1 mM) and ADP (1 mM). Sedimentation profiles were registered at 280nm.

3.3.2. FtsZ GTPase activity assays

GTPase activities of the different variants of FtsZ were determined by measuring released inorganic phosphate using BIOMOL® GREEN assay. FtsZ GTPase activity was determined using FtsZ at 5 μM and measuring phosphate concentration in the sample as a function of time, after adding 1 mM GTP. Measurements were performed every 20 s for a total time of 140 s. After 15 minutes of incubation with BIOMOL® GREEN, the absorbance of the samples at 620 nm was measured using Varioskan plate reader. The concentrations of phosphate were calculated according to a phosphate standard curve. This same procedure was followed for the samples where FtsZ was incubated along with liposomes (4 mg/ml).

3.3.3. Dynamic light scattering assays (DLS)

DLS experiments were performed on a Protein Solutions DynaPro MS/X instrument (Wyatt) at 25ºC using a 90º light scattering cuvette. Previous to measurements, samples equilibrated in SLB-buffer were centrifuged during 10 minutes at 100000× *g*. Data were collected and exported as text files with Dynamics V6 Software (Wyatt Technology Corp.), and analysed using user-written scripts and functions in MATLAB (ver. 7.10, MathWorks, Natick, MA). For a single scattering species, the autocorrelation function can be analysed by a single exponential. In our case, to better describe the polydispersity observed for FtsZ species, autocorrelation functions were analysed as earlier described (Monterroso *et al.*, 2012) by an empirical exponential function:

Equation 3.1:

$$ACF = ACF_{\infty} + (ACF_0 - ACF_{\infty}) \exp\left[-(D_{app} q^2 \tau)^{\beta} \right]^2$$

where, ACF_0 and ACF_{∞} respectively denote the values of the autocorrelation function in the short and long time limits, D_{app} is the apparent average diffusion coefficient, τ is time, β is a parameter that decreases from unity with the width of the distribution of diffusion coefficients and, then, allows assessing polydispersity of the sample and q is the scattering vector at

90º, defined as

Equation 3.2: $$q = \frac{4\Pi n_0}{\lambda_0} \sin\left(\frac{\Pi}{4}\right)$$

where n_0 and λ_0 are the solvent refractive index and the wavelength of incident light, respectively.

3.4. Membrane systems assays

3.4.1. ZipA-proteoliposomes

Full-length purified ZipA was reconstituted in *E. coli* polar lipid extract liposomes according to the standard method described by Rigaud and coworkers (Rigaud and Levy, 2003). Briefly, a fraction of purified ZipA was solubilized in 0.2% Triton-X100. The mixture was added to small unilamellar vesicles (SUVs) made of *E. coli* polar lipids (see below) already solubilized with Triton-X100 (1.5 detergent/lipid molar ratio) and then incubated for 1 h, at 4ºC under mild stirring. The detergent was removed gradually in 4 successive dialysis of 2 h /4ºC each. In each dialysis step, 10 mg BioBeads per milligram of Triton-X100 were added. After complete detergent removal, the reconstituted proteoliposomes were fractionated and stored at -80 ºC. In order to determine the ZipA:lipid ratio of the proteoliposomes, we used in parallel the methods of quantification of inorganic phosphorus (Rouser *et al.*, 1966) and BCA assay to quantify the amount of lipid and protein respectively.

3.4.2. Small unilamellar vesicles (SUVs)

E. coli polar lipid extract, initially dissolved in chloroform, was dried under nitrogen flow. Chloroform traces were further removed by 1-hour vacuum. The lipids were rehydrated with 150 µl of SLB-buffer (50 mM Tris-HCl, 150 mM KCl, pH 7.5) to reach a lipid concentration of 4 mg/ml. The hydrated film was vortexed to obtained multilamellar vesicles (MLVs). Finally, the vesicle solution was sonicated in an ultrasonic bath for about 10 minutes, obtaining small unilamellar vesicles suspension.

3.4.3. Supported lipid bilayers (SLBs) and ZipA-containing bilayers

Glass coverslips were cleaned in air plasma, except for the experiments on the coupling of MinCDE and FtsZ propagating waves in ZipA-SLBs, where cleaning involved sonication for 10 min using ethanol. Then, a homemade cylindrical plastic chamber was stuck on the coverslip using ultraviolet-curable glue. SLBs and ZipA-containing bilayers (ZipA-SLBs) were

obtained by vesicle fusion, from SUVs or proteoliposomes respectively, on the glass surface as previously described (Brian and McConnell, 1984). A suspension of SUVs or proteoliposomes (0.5-1 mg/ml) diluted in SLB-buffer was added to the glass bottom chamber together with 2 mM $CaCl_2$, to promote vesicle fusion and deposition of the bilayer. All the preparations were incubated at 38ºC for 20 min and then washed with pre-warmed SLB-buffer to remove non-fused vesicles. The last washing step was done with the specified reaction buffer and the final volume of the samples was always 200 µl.

3.4.4. Self-organization assays in minimal membranes

3.4.4.1. FtsZ-YFP-mts self-organization assays on SLBs

FtsZ-YFP-mts was added to a final concentration of 0.5 µM or 0.2 µM to the supported lipid membrane. In the case of **FtsZ*[T108A]-YFP-mts** and **mts-H-FtsZ-YFP**, 0.2 µM and 1 µM of protein was employed, respectively. FtsZ polymerization was induced by adding GTP to a final concentration of 4 mM. Experiments were also carried out using 0.4 mM and 0.04 mM GTP to study the effect of nucleotide concentration in FtsZ-YFP-mts filaments self-organization on the membrane. The experiments were performed in the buffer: 50 mM Tris-HCl at pH 7.5, 150 mM KCl and $MgCl_2$ (5 mM or 1 mM).

3.4.4.2. Self-organization assays on ZipA-SLB

- *Surface density of ZipA (ρ_{ZipA}) reconstructed in ZipA-SLBs*

The surface density of ZipA (ρ_{ZipA}) in these bilayers was controlled by varying the ratio ZipA:lipid on the proteoliposomes. The ρ_{ZipA} values corresponding to the ZipA-SLBs used in this work are summarized in **Table 3.1**.

ZipA/lipid (molar ratio)	1:1200	1:1600	1:2500	1:4500	1:5500
Distance between two ZipA molecules (nm)	30	35	43	58	64
ZipA content (molar %)	0.083	0.062	0.040	0.022	0.018

Table 3.1: Five different surface densities of ZipA (ρ_{ZipA}) reconstructed in ZipA-SLBs. For each condition assayed, the number of lipids per ZipA molecule in the bilayer, the theoretical average distance between two ZipA molecules, and the ZipA content in the bilayer (molar %) are displayed.

Considering a rod-shaped bacteria with dimensions (2 x 0.8) µm (Sundararaj *et al.*, 2004) and taking into account that the number of ZipA copies per cell is ~1000–1500 (Rueda *et al.*, 2003), the estimated distance between two ZipA molecules, assuming they were distributed uniformly, would be ~50 nm. This situation is compatible with an early stage of the division

process in which the Min system starts its pole-to-pole oscillation but the Z ring is not targeted at midcell yet. This value is equivalent to an ~1:3200 ZipA/lipid molar ratio or 0.03 molar % of ZipA.

- *Self-organization assays of FtsZ-Min proteins on ZipA-SLB*

For these experiments exchange of the SLB-buffer for the Z-buffer (50 mM Tris-HCl, 500 mM KCl, 5 mM $MgCl_2$, pH 7.5) was carried out in a last washing step. The proteins of the MinCDE complex were used at the following conditions: 0.75 μM MinD, 0.75 μM MinE and 0.06 μM MinC (traced by ~40% of eGFP-MinC) and supplemented with 2.5 mM ATP. The experiments were carried out at 23ºC. For the coupling assays, Min proteins were incubated on ZipA-SLBs in Z buffer, and then 2 μM FtsZ (15% FtsZ-Alexa 647) was added along with 3 mM GTP. To maintain FtsZ polymers at steady-state during the time scale of the experiments, 1 U/mL acetate kinase, and 15 mM acetyl phosphate (enzymatic GTP-regenerating system) was incorporated as previously described (Gonzalez *et al.*, 2003). In the crowding assays, samples containing preassembled FtsZ networks on ZipA-SLBs were supplemented with Ficoll 70 at the corresponding concentrations.

3.4.4.3. Self-organization assays of FtsA and FtsZ filaments

For this experiment, 0.5 μM unlabelled FtsA and 1.5 μM FtsZ labelled with Alexa 647 were employed. First of all, FtsA and FtsZ were mixed in a tube and slowly added to the sample with the previously formed SLB, in the presence of 2.5 mM ATP. GTP (4 mM) was incorporated in the last step. All the experiments involving FtsA and FtsZ in SLBs were performed in the buffer: 50 mM Tris-HCl at pH 7.5, 150 mM KCl and 5 mM $MgCl_2$

3.4.4.4. Self-organization assays of FtsA-Min proteins-FtsZ system in flat membranes

As self-organization of FtsA and FtsZ polymers on SLBs was observed at 0.5 μM of FtsA and 1.5 μM FtsZ, those were the concentrations of the proteins employed to study the behaviour of FtsZ-MinCDE coupling in supported *E. coli* lipid bilayers when FtsA acts as the membrane anchor.

To probe that the MinCDE system was able to self-organize when FtsA was attached to the membrane, FtsA (0.5 μM) was added to the reaction buffer (50 mM Tris-HCl, 150 mM KCl, 5 mM $MgCl_2$, pH 7.5) in the presence of ATP (2.5 mM), and then, MinCDE protein system (0.5 μM MinD, 0.5 μM eGFP-MinD, 1 μM MinE, 0.06 μM MinC) was incorporated on top of the supported lipid membranes and incubated for at least 3h.

Once complete MinCDE oscillations waves were detectable by a confocal microscope on the membrane in the presence of unlabelled FtsA, FtsZ-Alexa 647 together with GTP (4 mM) and the regeneration system (1 U/mL acetate kinase and 15 mM acetyl phosphate) were incorporated to the sample. At least 30 min incubation was required to observe a new self-organization of the MinCDE system.

3.4.4.5. Self-organization assays of FtsA-Min proteins-FtsZ system in micro-compartments

Reconstitution of self-organized oscillations of MinCDE-FtsZ proteins in the presence of FtsA was also performed in membrane-clad soft-polymer compartments. For this study, we prepared PDMS microstructures essentially as previously described (Zieske and Schwille, 2014) (**Figure 3.1**). Briefly, resist micro-patterns were produced on silicon wafers using photolithographic techniques (Zieske and Schwille, 2013). To prevent sticking of PDMS to the wafer, Si wafers were coated with chloro-trimethylsilane. PDMS was mixed with the curing agent at a ratio (monomer to cross-linker) of 10:1 and degassed under vacuum. The PDMS mixture was then poured on top of the wafer. A PDMS layer of about 30 µm thin was made by gently pressing the coverslip to placed on top. After curing the PDMS at 80°C overnight, the glass cover slip with the thin, micro structured layer of PDMS attached was peeled off. Before the micro-structured PDMS was used as a membrane support, it was sonicated for 5 min in ethanol, washed with water, air dried, and treated with air plasma. After cleaning and plasma treatment, a plastic ring was glued on top of the PDMS microstructures. *E. coli* supported lipid membranes within the micro-compartment, which adapt to the topography of the underlying PDMS support, were produced as described above (section 3.4.3). Then, ATP, FtsA and MinCDE complex (using same concentrations as in section 3.4.4.4.) were added to a buffer volume of 200 µl on top of the supported lipid membranes. After incubation, dynamic Min patterns travel on top of the membrane and oscillations inside the micro-compartments were observed. At this point, FtsZ along with GTP and the enzymatic GTP regeneration system were added to the same sample. When Min-FtsZ travelling waves were detected, the buffer reservoir was manually and carefully reduced using a pipette, such that the buffer remained only in the micro fabricated chambers. The upper level of the PDMS supports (outside of the compartments) was dry and residual biomolecules, such as remaining lipids and Min proteins were immobile (**Figure 3.1.D**). The protein concentrations stated in **Figure 6.9** refer to the concentrations before buffer aspiration. Under these conditions, independent protein oscillations were observed inside each compartment (see section 6**, Figure 6.9**).

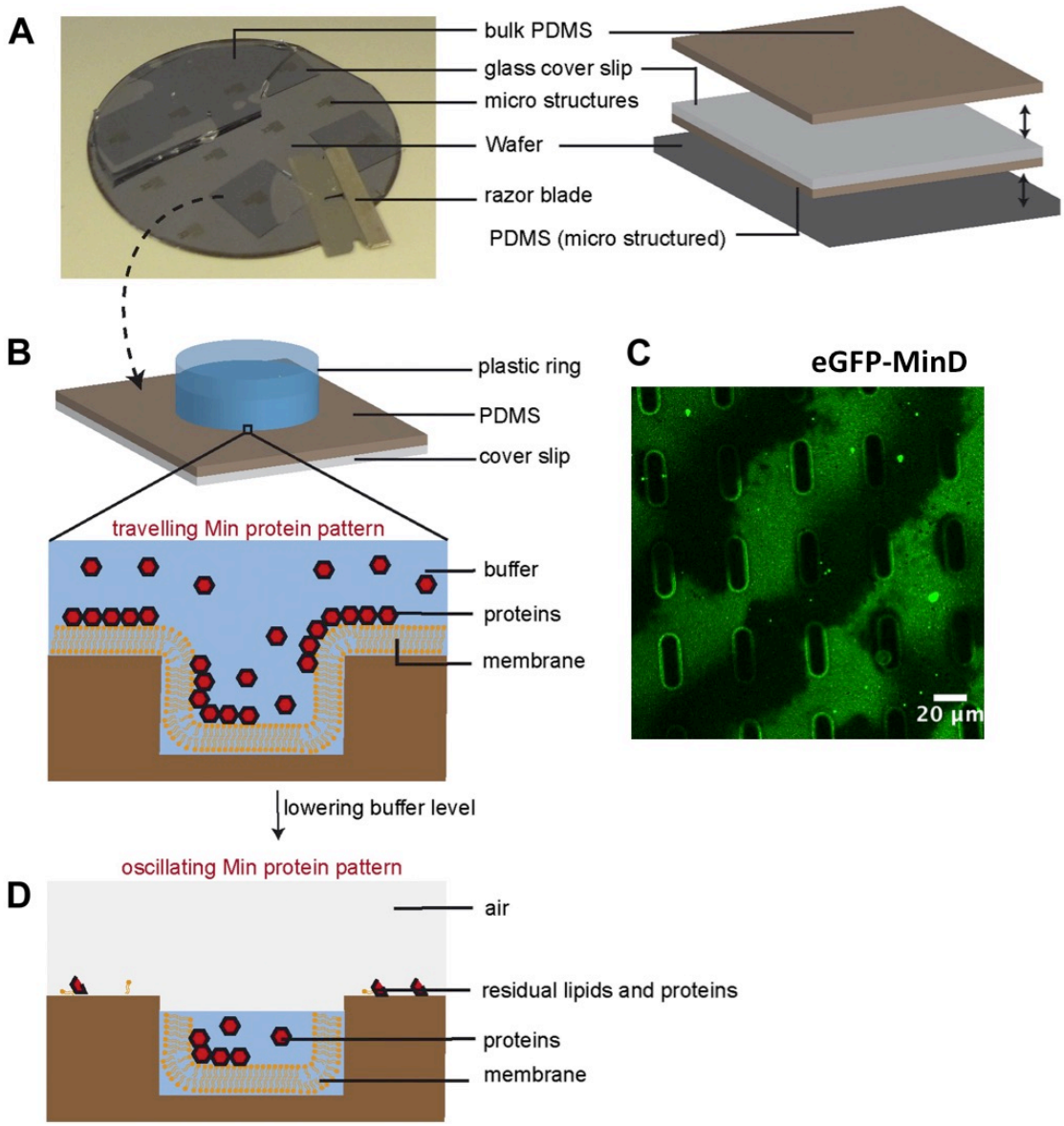

Figure 3.1. Experimental setup of micro-compartments system for Min protein oscillations. A) Schematic image of the setup. **B)** A plastic ring was glued on top of the PDMS microstructures. *E. coli* lipid supported bilayers were produced on PDMS microstructures by vesicle fusion techniques. Then proteins, ATP and GTP were added on top of the supported lipid membranes. **C)** Confocal fluorescence micrograph showing MinCDE self-organization patterns on the membrane outside micro-compartments. All the micro-compartments used in this thesis were 35 µm long, 10 µm wide and 10 µm deep. **D)** The buffer level was reduced below the upper rim of the micro-compartments and the top of the chambers was open with a buffer/air interface. Figure adapted from (Zieske and Schwille, 2014).

3.5. Fluorescence Microscopy

3.5.1. Confocal microscopy

Image acquisition was performed on a Zeiss (Jena, Germany) LSM780 confocal laser scanning microscope equipped with a Zeiss Plan-Apochromat 40X/NA 1.2 W corr and Plan-Apochromat 20X/NA 0.8 objectives.

3.5.1.1. Imaging analysis and processing

Images corresponding to the self-organization assays reported in sections 5.1. and 6.1. were processed and analysed using Image J program (http://rsb. info.nih.gov/ij/). Images were coloured in red and green to facilitate identification of the labelled protein. The FtsZ waves reported in section 5 were quantified by a modulation parameter, m, defined as the relative difference between the maximum and minimum fluorescence intensity measured within the wave: $m = (F_{max} - F_{\min})/F_{max}$ (**Figure 3.2 and Figure 5.9**). Measurements were taken using the 633 nm laser line at 0.8% laser power in the photon-counting mode. The *m* values presented correspond to the mean values of at least four independent experiments.

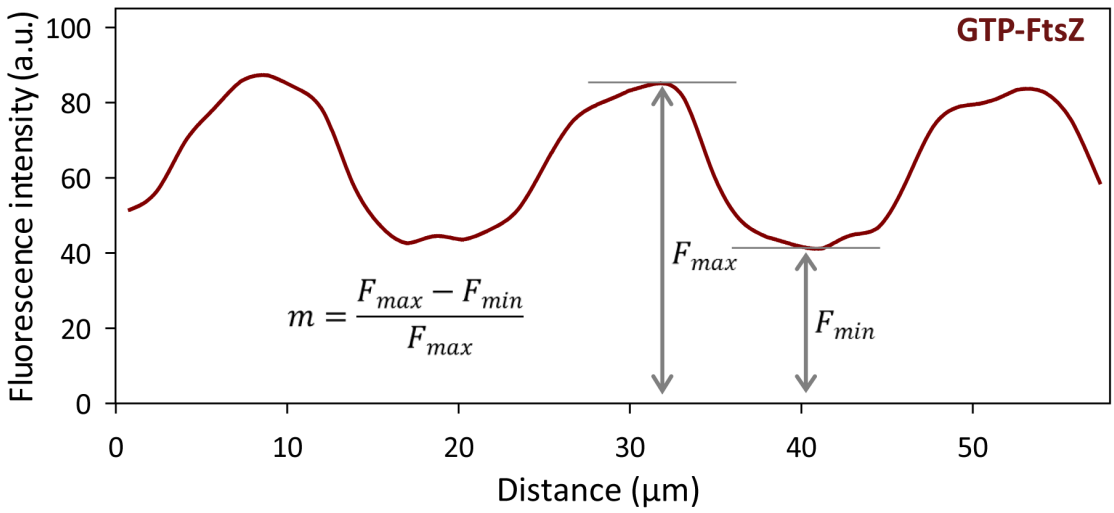

Figure 3.2: Representative smoothed fluorescence intensity profile corresponding to FtsZ-Alexa647-GTP in the sample show in Figure 5.9. The definition of the FtsZ wave modulation parameter *m* is the relative difference between the maximum and the minimum fluorescence intensity measured within the wave.

3.5.1.2. Image correlation

A sequence of images of ZipA-SLB with FtsZ under variable conditions (see section 5) was acquired with the Zeiss LSM 780 microscope. The correlation *g(τ)* between the fluorescence intensity in the same pixel at a time difference of τ was calculated as (Wiseman and Petersen, 1999):

Equation 3.3:

$$g(\tau) = \frac{1}{n_{ij}} \sum_{ij} F_{ij}(t) F_{ij}(t+\tau)$$

where $F_{ij}(t)$ is the intensity in the pixel (i, j), n_{ij} is the number of elements in the sum, and the time t indexes the images in the sequence. Before correlation, an average image, calculated over the whole sequence, was subtracted from all images $F_{ij}(t)$ to eliminate the static features in images. The correlations were found to decay exponentially, and therefore were fitted to a single exponential function, with the decay of correlation characterised by the half-time $\tau_{1/2} = \tau_c \ln 2$ (**Figure 3.3**).

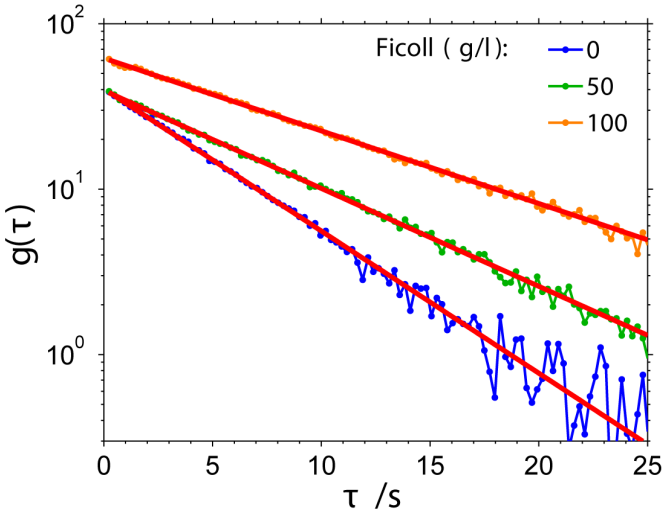

Figure 3.3: Image correlation decay plot. Example of typical fluorescence correlation decays FtsZ on SLB (Equation 3.3) at three different Ficoll 70 concentrations with exponential fits.

3.5.1.3. Fluorescence recovery after photobleaching (FRAP)

For the bleaching experiments, a Zeiss Plan- Apochromat 40x/NA 1.2 W corr objective was used. After a time series of pre-bleaching images was recorded, a circular area of 5 µm diameter (region of interest) on the bilayer was photobleached by 30 iterations of the 633 nm laser under 100% laser power for 2 min. The fluorescence recovery curves were corrected and normalized for the bleaching caused by imaging and then fitted by a single exponential curve: $I(t) = A(1 - e^{-\tau t})$, where $I(t)$ is the fluorescence of the bleached region at time t, A is the mobile fraction, and $\tau_{1/2} = \ln 2/k$.

3.5.2. Total internal reflection fluorescence microscopy

High resolution imaging of single molecules and real-time kinetic measurements were performed by total internal reflection fluorescence microscopy (TIRFM). In TIRF experiments the excitation light is confined to a thin region of the specimen (less than 200 nanometres from the coverslip surface), thus increasing the resolution of the images. Chimeric membrane-tethered FtsZ and FtsA-FtsZ self-organization experiments were performed on a

WF1 GE DeltaVision Elite® total internal reflection fluorescence microscope (GE Healthcare Life Sciences, Germany) equipped with an OLYMPUS 100x TIRF objective (NA 1.49). The UltimateFocus feature of DeltaVision Elite maintains the focus plane constant in time. FtsZ-YFP-mts was excited with a 488 nm diode laser (10 mW, before objective) Fluorescence imaging was performed using a standard FITC filter set. Images were acquired with a PCO sCMOS 5.5 camera (PCO, Germany) controlled by the softWoRx® Software (GE Healthcare Life Sciences, Germany). For time-lapse experiments, images were acquired every 3 or 10 s, with a 0.05 s exposure time, with light illumination shuttered between acquisitions.

3.5.2.1 Image analysis and processing

Image analysis was carried out using MATLAB 2015 (MATLAB and Image Processing and Computer Vision Toolbox Release 2015a, The MathWorks, Inc., Natick, Massachusetts, (United States.) and Fiji/ImageJ (Rasband, W. S., ImageJ, US National Institutes of Health, Bethesda, http://rsb.info.nih.gov/ij/, 1997–2007). Images correspond to average of 5-10 frames from a time-series experiment. For the kymograph analysis, time-series acquisitions were filtered using a standard mean filter and drift corrected (Image J). A Matlab script allowed to define a ring by providing two coordinates and every ring was automatically fitted to a circle with radius r. Then, three trajectories corresponding to three concentric circles having radii r, r+1 and r-1 are determined. At this point, the script reads the time-series data and calculate a kymograph for each time point and trajectory. The final kymograph corresponds to the average of the three different trajectories.

3.5.2.2. Single-molecule imaging and residence time measurement

Single molecule imaging was performed using a standard Cy5 filter set. FtsZ-YFP-mts previously incubated 1:1 with the nano-body GFP-Booster Atto647N for at least 1 hour at 4°C under agitation. To filter out non-bound nano-body, the protein was ultrafiltrated in a 30 kDa Amicon unit. The GFP-Booster Atto647N was excited with a 640nm diode laser (30 mW, before objective). After 10 minutes upon GTP addition, a significant number of spots in the single molecule channel (Atto 647N) were observed and imaged at a rate of 1 fps or 3 fps with 0.3 s exposure time. To improve imaging conditions, we added 10 nM protocatechuate-dioxygenase (PCD), and 2 mM 3,4-protocatechuicacid (PCA) as an oxygen scavenging system. To determine the position of every single molecule and calculate its residence time, we employed a Matlab routine designed by Weimann & Ganzinger (Weimann *et al.*, 2013). Briefly, a band pass filter was used to remove low and high frequency noise. Then, single molecule positions with intensity above a user-defined threshold were determined by their brightness-weighted centroid. The detection algorithm is

highly efficient for detecting particles with a signal to noise ratio above 1.5. The user-defined threshold was chosen to detect the largest number of spots and kept constant for all experiments. Single molecules were tracked among consecutive frames in an area given by a radius of 10 pixels (pixel size = 0.042 μm). Thus, the residence time is defined as the time that the particle stays in this area before its signal vanishes.

To calculate the mean residence time, we calculated the probability as a function of time *t* to obtain a loss of signal event at times ≤ *t* (cumulative probability, see **4.3. Annex, Figure 4.3. Annex.A**). We fitted to a double exponential function $Ae^{-kt} + Be^{-k_p t}$ where k refers to the inverse of the mean residence time and k_p corresponds to the photobleaching rate. A and B are constrained since the photobleaching contribution is limited to be between 0.2- 0.25 in the fitting routine for all conditions (Matlab). The photobleaching rate was calculated as $k_p = 0.031 s^{-1}$ using a single exponential fit as shown in **Figure 4.3. Annex.B**. Events shorter than 2 frames are below the accuracy of our method and were not included in the statistics. The cumulative probability was measured for 5 different experiments having total number of events (N) in each experiment. For GDP forms: 5 mM Mg^{2+}, N varies in the range of 3000 - 5300 events (1 fps) and 660 - 8800 events (3 fps). 1 mM Mg^{2+}, N= 3000 - 11000 (3 fps). For GTP forms: 0.04 mM GTP, N = 1300 - 3000 (1 fps). 4 mM GTP, N= 1200 - 6700. In the case of FtsZ*[T108A]-YFP-mts at 4 mM GTP, N= 180 - 800.

3.6. Microbeads coating and quantification of binding

Microbeads were coated with the *E. coli* lipid mixture following the method described by Sobrinos-Sanguino (Sobrinos-Sanguino *et al.*, 2017), with modifications (**Figure 3.4**). First, the lipid amount content per microbeads was estimated, assuming a single bilayer, from the surface area of 1 g of beads and the surface of the polar head of a lipid molecule (taking the value reported for phosphatidylcholine in a bilayer (Hauser, 2000), 0.65 nm^2). The required amount of lipid coating the microbeads was dried under nitrogen flow to evaporate the chloroform in which they were dissolved and the lipid film was then rehydrated with the required volume of SLB-buffer to form MLVs. Lipid incubation at 37ºC for 1 hour with two vortex cycles was performed to resuspend the dried lipids. In parallel, microbeads, of around 5 μm diameter, were washed by three successive centrifugations (5 min at 10000 g per cycle) and suspension steps in an ethanol/water mixture (3:7 v/v). After a final centrifugation, the microbeads were resuspended in a 1% ethanol solution and centrifuged again. Lastly, all the supernatant was removed using a Speed-Vac device. To obtain lipid coated microbeads, these washed beads were suspended in SLB-buffer with 5 mM Mg^{2+} and then, mixed with

the prepared solution of *E. coli* lipids. The mixture was incubated for at least 1 h, at 4ºC, to allow spontaneous fusion of the MLVs onto the surface of the bead. The lipid excess was removed by subsequent washing steps. Microbeads were finally resuspended in SLB-buffer with 5 mM Mg^{2+} to get the necessary microbeads stock concentration.

Samples consisted on increasing concentrations of lipid coated beads incubated for 10 min with a constant concentration of protein. For **FtsZ-YFP-mts** binding affinity quantification experiments, the protein (1 μM) was measured in the presence of GTP (4 mM) or in its absence, when the protein is bound to GDP (described as FtsZ-GDP in the results section). In the binding affinity experiments accomplished for **FtsA** (0.5 μM) measurements were conducted in the presence of 1 mM ATP or in its absence (described as FtsA-ADP in the results section).

Binding of the protein to the lipid surface was quantified by measuring, after centrifugation, the fluorescence intensity corresponding to the amount of unbound protein remaining in the supernatant in a fluorescence plate reader (Varioskan Flash, Thermo), with 495 and 520 nm excitation and emission wavelengths, respectively. Fluorescence intensity of membrane-tethered FtsZ corresponded to the yellow fluorescence protein (YFP) sequence included in the construct. FtsA was labelled with Alexa Fluor 488 dye to be detected. The linearity of the signal of the labelled protein with its concentration was verified in both cases.

Protein binding to lipid bilayers can be described defining an apparent association constant, *K* (the reciprocal of the lipid concentration at which half of the protein amount is bound), which does not require any assumptions about the adsorption mechanism:

Equation 3.4:

$$\frac{[\mathrm{Protein}]_B}{[\mathrm{Protein}]_T} = \frac{\mathrm{K}\,[\mathrm{Lipid}]_{\mathrm{acc}}}{1 + [\mathrm{Lipid}]_{\mathrm{acc}}}$$

where $[Protein]_B$, $[Protein]_T$, $[Lipid]_{acc}$ are the concentrations of bound protein, total protein and accessible lipids, respectively. Equation 3.4 was fitted to the recovered isotherms using user-written functions in MATLAB (Ver. 7.10, MathWorks).

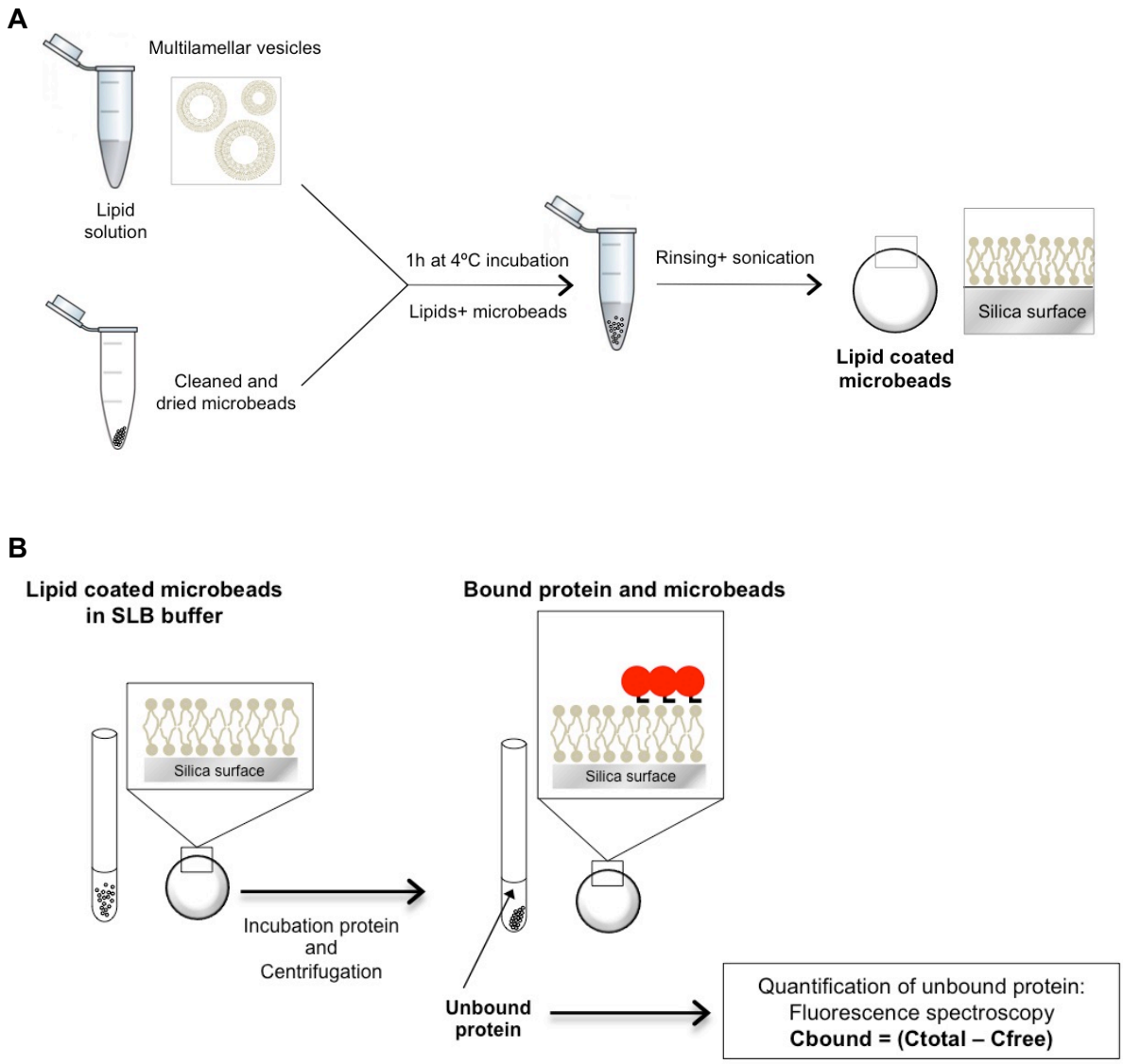

Figure 3.4. Schematic drawing of protein-lipid affinity quantification using microbead systems. (A) Experimental procedure for coating silica microbeads with *E. coli* lipids. **(B)** Steps for quantification of a protein (in this thesis, FtsA or FtsZ-YFP-mts) binding to the *E. coli* lipid coated microbeads. Figure adapted from (Sobrinos-Sanguino *et al.*, 2017).

4. Treadmilling analysis reveals new insights into dynamic FtsZ ring architecture

FtsZ, the primary protein of the bacterial Z ring guiding cell division, has been recently shown to engage in intriguing treadmilling dynamics along the circumference of the division plane. When co-reconstituted *in vitro* with FtsA, one of its natural membrane anchors, on flat supported membranes, these proteins assemble into dynamic chiral vortices, compatible with treadmilling of curved polar filaments. Replacing FtsA by a membrane targeting sequence to FtsZ, we have discovered conditions for the formation of dynamic rings, showing that the phenomenon is intrinsic to FtsZ. Ring formation is only observed for a narrow range of protein concentrations at the bilayer which is highly modulated by free magnesium and depends upon GTP hydrolysis. Interestingly, the direction of rotation can be reversed by switching the membrane targeting sequence from the C-terminus to the N-terminus of the protein, implying that the filament attachment must have a perpendicular component to both, curvature and polarity. Remarkably, this chirality switch concurs with previously shown inward or outward membrane deformations by the respective FtsZ mutants. Our results lead us to suggest an intrinsic helicity of FtsZ filaments with more than one direction of curvature, supporting earlier hypotheses and experimental evidence.

This section corresponds to the published article:

Authors: Diego Ramirez*[1,2], Daniela A. García-Soriano*[1,2], Ana Raso*[1,3], Jonas Mücksch[1], Mario Feingold[4], Germán Rivas[3] and Petra Schwille#[1]

[1]Department of Cellular and Molecular Biophysics, Max Planck Institute for Biochemistry, Martinsried, Germany, [2]Graduate School for Quantitative Biosciences (QBM), Ludwig-Maximillians-University, Munich, Germany, [3]Centro de Investigaciones Biológicas, Consejo Superior de Investigaciones Científicas (CSIC), Madrid, Spain, [4]Department of Physics, Ben Gurion University, Beer Sheva, Israel.

* Contributed equally

Journal: PLoS Biol. 2018,16(5): e2004845.

4.1. RESULTS

4.1.1. Membrane-targeted FtsZ assembly is controlled by GDP/GTP and Mg^{2+}

The minimal molecular system that we have used (FtsZ-YFP-mts) is a chimera consisting on an FtsZ construct fused to a yellow fluorescence protein, which can reversibly bind to the membrane through an engineered amphipathic segment in the absence of the natural tethering elements ZipA or FtsA. To study the effect of nucleotides and Mg^{2+} on the state of self-association and polymerization of FtsZ-YFP-mts in solution, sedimentation velocity (SV) and dynamic light scattering (DLS) assays were performed. SV allows to quantitatively determining the degree of homogeneity and distribution of macromolecular species in reversible associating systems (Gonzalez *et al.*, 2005). In our case, the sedimentation coefficient distributions of FtsZ-YFP-mts under different experimental conditions, generated from the analysis of the sedimenting boundaries using SEDFIT (see Materials and Methods), have revealed that the association properties of the membrane-targeted FtsZ in solution were controlled by GDP/GTP and Mg^{2+} (**Figure 4.1**), similarly to the natural FtsZ protein (Rivas *et al.*, 2013). These assays showed that only in the presence of millimolar amounts of GTP and Mg^{2+} to promote protein polymerization, the chimeric FtsZ formed high molecular weight species in solution with s-values ranging from 6 and 20 S, while in the absence of both physiological ligands, the protein exists predominantly as a unique molecular specie with s-value 5.5 S, compatible with the hetero-dimer of the chimeric FtsZ protein.

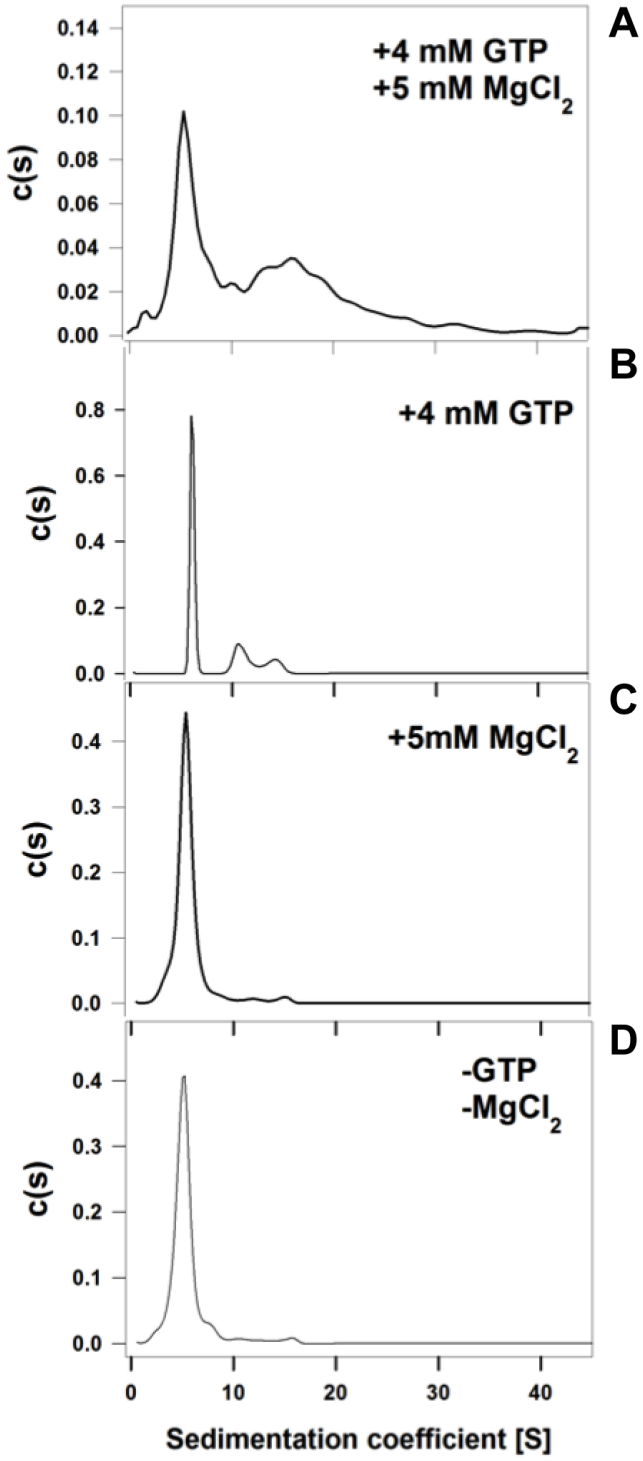

Figure 4.1. FtsZ-YFP-mts sedimentation velocity analysis. c(s) sedimentation coefficient distributions obtained for the chimeric FtsZ variant (7 μM) in working buffer at the following conditions: 4 mM GTP and 5 mM Mg^{2+} **(A)**, 4 mM GTP but no Mg^{2+} added **(B)**, 0.05 mM GDP and 5 mM Mg^{2+} **(C)**, and 0.05 mM GDP and no Mg^{2+} added **(D)**. These experiments show that FtsZ-YFP-mts is a well-behaved self-associating protein: In the absence of GTP and/or Mg^{2+} (B-D) the protein exists mainly as a slowly sedimenting species with s-value of around 6 S (C-D), compatible with the heterodimeric FtsZ-YFP form. In the presence of both GTP and Mg^{2+} (A) most of the protein (70%) sediments as a polydisperse mixture of higher orders species with an average s-value of 20 +/- 5 S.

The DLS autocorrelation curve of GDP-bound FtsZ-YFP-mts in the absence of magnesium overlapped with that obtained in the presence of 5 mM concentration of the cation. Analysis according to Equation 3.1 rendered similar values for the average apparent diffusion coefficients (D_{app}), suggesting that the effects on association properties derived from Mg^{2+} binding, if any, are minor (**Figure 4.2.**). The shift of diffusion towards longer diffusion times in the presence of GTP and magnesium was indicative of nucleotide triggered FtsZ-YFP-mts polymerization. Accordingly, GTP-FtsZ polymers showed a significant decrease of the translational diffusion coefficient regarding the unassembled FtsZ form, as in the case of the natural FtsZ protein in which the apparent diffusion coefficients for the assembled and unassembled forms were $4x10^{-8}$ and $5x10^{-7}$ cm^2/s, respectively (Monterroso *et al.*, 2012). Moreover, our findings using DLS were in good agreement with the sedimentation velocity results reported above (**Figure 4.1**).

A.

Experimental conditions	Dapp (cm^2/s)
1 µM FtsZ	(1.6 ± 0.1) 10^{-7}
1 µM FtsZ, 5mM Mg^{2+}	(1.5 ± 0.2) 10^{-7}
1 µM FtsZ, 5mM Mg^{2+}, 4mM GTP	(5.6 ± 0.9) 10^{-8}

B.

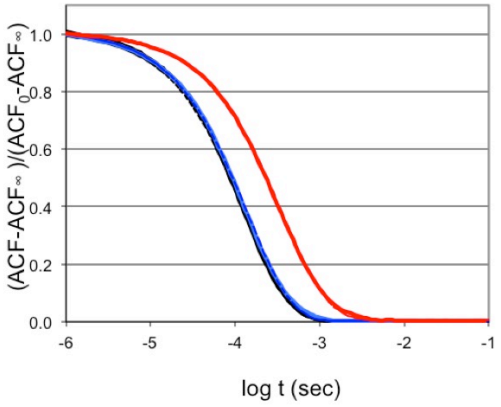

Figure 4.2. Translational diffusion properties of FtsZ-YFP-mts. (A) Apparent diffusion coefficients (Dapp) of FtsZ-YFP-mts under the indicated experimental conditions. **(B)** Normalized DLS autocorrelation curves of FtsZ-YFP-mts (0.07 g/L, 1 µM) in its assembled and disassembled forms. FtsZ-YFP-mts in the absence and presence of 5 mM Mg^{2+} (blue lines) and in the presence of 5 mM Mg^{2+} and GTP (red line). Dashed lines are the fits to the model indicated in Material and Methods (**Equation 3.1**).

As previously described (Rivas *et al.*, 2013), wild-type FtsZ is able to bind and hydrolyse GTP. The assembly of FtsZ into polymers is dependent on GTP hydrolysis, which controls the dynamics of FtsZ filaments. Here we have found that the presence of the yellow fluorescence protein (YFP) and a membrane target sequence (mts) did not alter the GTPase activity of FtsZ when compared to the native protein, both in solution and in presence of liposomes (SUVs at 0.5 g/L) (**Figure 4.3**).

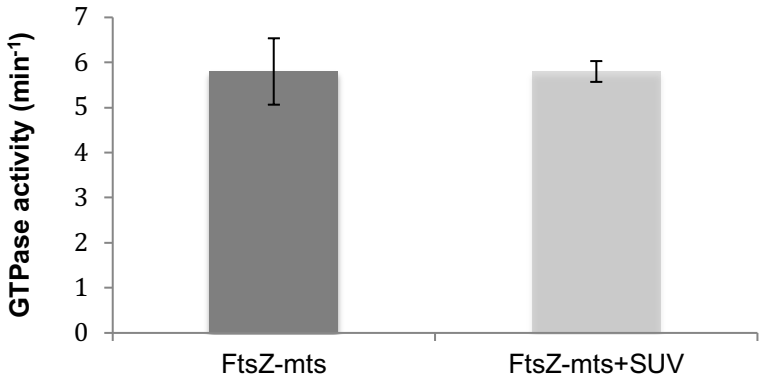

Figure 4.3. GTPase activity of 5 μM FtsZ in solution or in presence of small unilamellar vesicles (SUVs). The data show the average of five experiments.

4.1.2. Assembled and unassembled FtsZ-YFP-mts interact differently with *E. coli* lipids

To extend our understanding of the influence of GTP and magnesium in the chimeric FtsZ assembly, the binding of polymeric and unassembled FtsZ-YFP-mts to *E. coli* lipid bilayers was quantitatively analysed using microbeads coated with this lipid mixture. To study membrane-tethered FtsZ binding under polymeric conditions, increasing concentrations of the coated beads were incubated with FtsZ-YFP-mts (1 μM) in the presence of GTP (4 mM) and Mg^{2+} (5 mM) (**Figure 4.4**). In order to test the differences between the oligomeric and monomeric form of this protein regarding its interaction with the bilayers, we also did the same experiments without GTP and Mg^{2+}. Analysis of the binding curves using an empirical function compatible with the experimental data rendered apparent affinity constants, corresponding to the inverse of the concentration of lipid at which 50% of the protein is bound to the lipids.

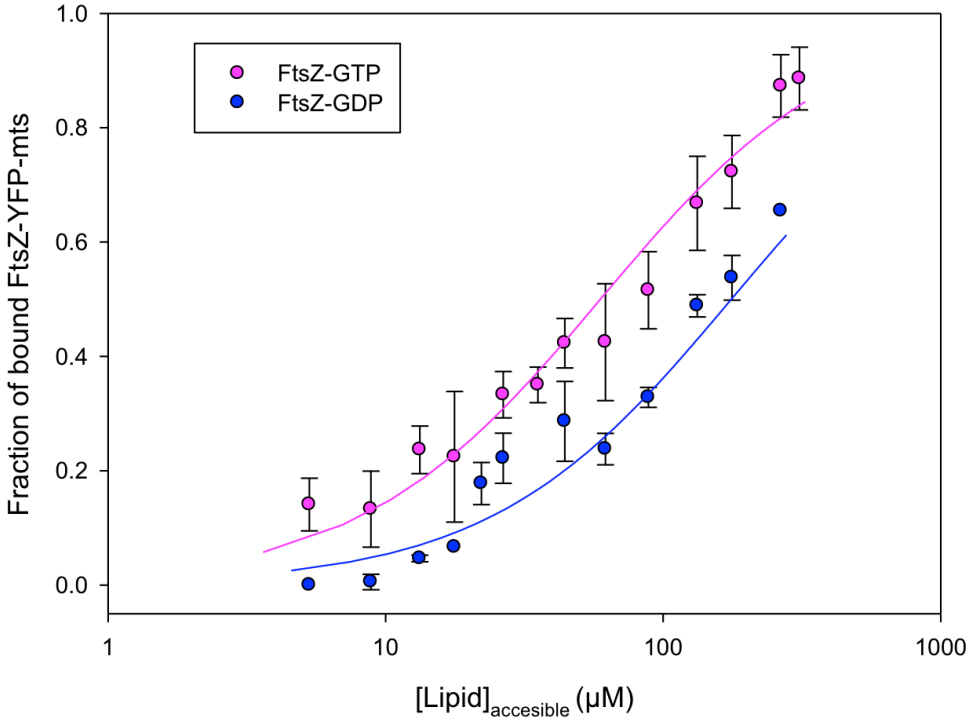

Figure 4.4. FtsZ-YFP-mts binding to *E. coli* lipids coated microbeads. FtsZ-YFP-mts (1 μM) binding to lipids was studied under two different conditions: 4 mM GTP and 5 mM Mg^{2+} (pink circles) or in the unassembled form of FtsZ-YFP-mts (neither GTP, nor Mg^{2+}) (blue circles). Solid lines correspond to the fit of Equation 3.4 (see Materials and Methods) to the experimental data. Data correspond to the average of 5 experiments ± SD.

These results suggest that chimeric FtsZ binds to *E. coli* lipids with moderate affinity, higher in the presence of GTP, as evidenced by the values of apparent affinity constant from the titration curves: K_{app}= (1.7 ± 0.3) · 10^4 M^{-1} in the presence of GTP and K_{app}= (5.7 ± 0.3) · 10^3 M^{-1} when GTP was absent. In addition, FtsZ-GDP binding isotherm does not seem to reach a saturation plateau in contrast to FtsZ-GTP data. These results indicated that FtsZ filaments and unassembled protein show differences in the interaction with the lipids.

4.1.3. Chiral vortex dynamics on membranes is an intrinsic property of FtsZ

The protein chimera FtsZ-YFP-mts (0.5 μM) in its GDP-bound form (corresponding to a non-assembled state, according to sedimentation velocity, **Figure 4.1**) did not form visible structures on a supported lipid membrane, as revealed by TIRFM. We have found that FtsZ-YFP-mts under assembly-promoting conditions (4 mM GTP, 5 mM Mg^{2+}) formed filaments on supported lipid bilayers, which self-organize with time into dynamic ring-like structures (**Figure 4.5A and Movie 4.S1**). These structures that apparently rotated actually did not reflect a total movement since the observed dynamic behaviour was due to the fact that FtsZ curved fibbers were gradually growing on one end and dissolving at the other end. The

assembly of the dynamic rings is a time-dependent phenomenon. After several minutes upon GTP addition, in which highly dynamic short filaments were observed to attach, detach and diffuse on the surface, longer curved filaments appeared to grow directionally (**Figure 4.5.B panel 5:00**). At this stage, intrinsic motion drives filament-filament interactions to create small and dim closed circular structures (**Figure 4.5.B panel 15:00**). These structures tend to be highly unstable: closed filaments were able to open, fuse with adjacent filaments or to close back**.** At later times, closed circular strands turned into thicker ring-like structures (**Figure 4.5.B panel 30:00**).

To understand the formation of circular structures and how they evolve into stable and thicker rings, we resolved and tracked individual filaments (consisting of several protofilaments) before stable ring formation. Here, we identified nucleation sites where clockwise chiral growth leads to the formation of circular structures (**Figure 4.5.C and Movie 4.S2**). Despite the fact that growth seems to be a discontinuous phenomenon limited by the accessibility of soluble protein, we can estimate a mean growth rate (slope p in the kymograph) which was found to be around 60 nm/s. Strikingly, these images also showed filament flexibility (panels 7-12) and breakage (panels 15-18) resulting in the formation of short free fragments. Such fragments were found to glide and “explore” the surface via a mechanism compatible with treadmilling (**Figure 4.5.D and Movie 4.S3**) indicating that this process fuels filament-filament interactions and therefore ulterior formation of closed circular structures. The kymograph in **Figure 4.5.D** showed a representative example of one filament growing in the leading edge (p-line) and shrinking in the trailing edge (d-line). A coarse estimation of the velocity of displacement of this filament was about 55 nm/s.

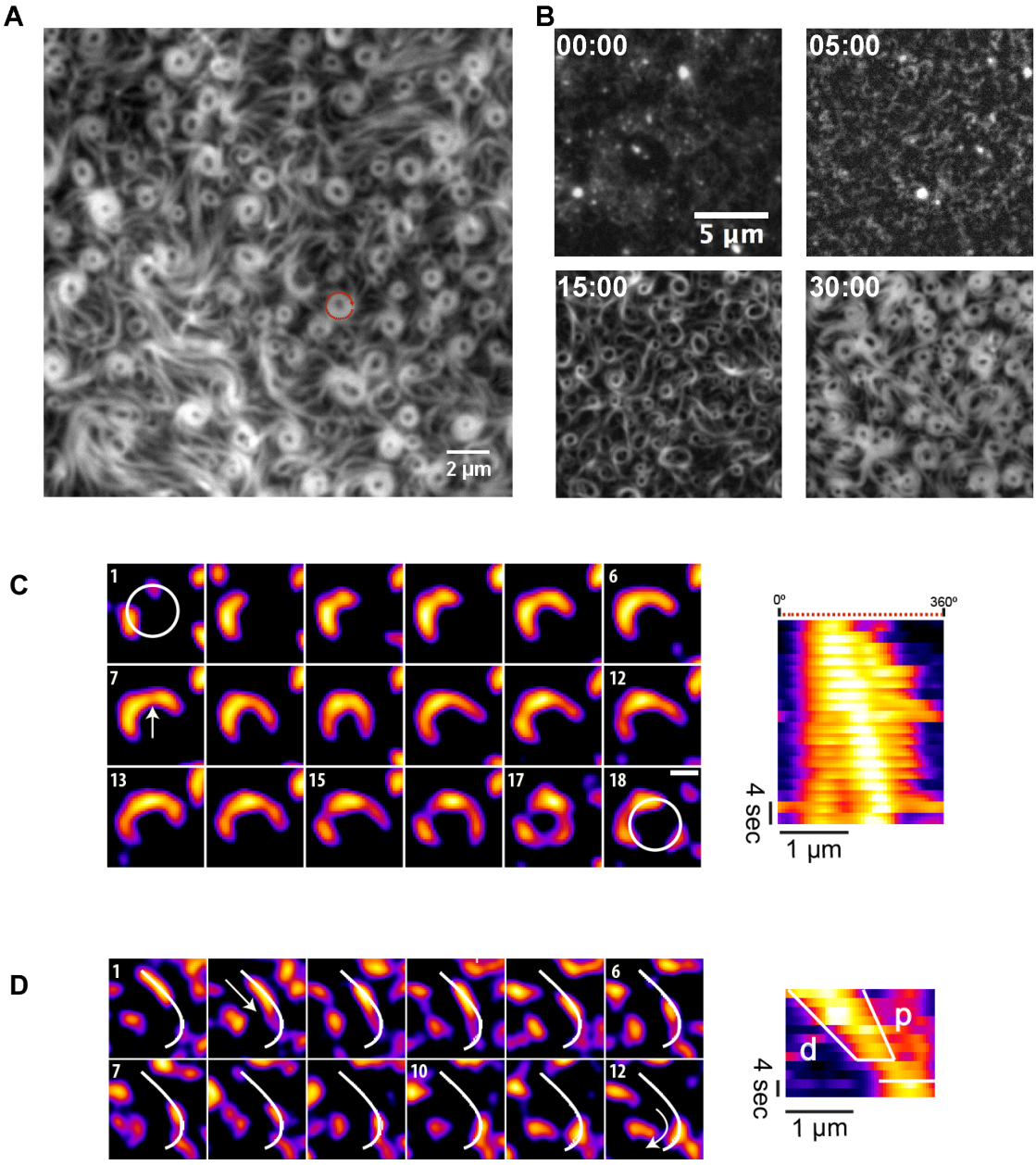

Figure 4.5. Nucleation and growth of FtsZ filaments into rings on supported lipid bilayers. (A) Membrane-targeted FtsZ assembles into dynamic cytoskeletal patterns on SLBs. TIRFM image (YFP channel) of 0.5 µM FtsZ-YFP-mts in the presence of 4 mM GTP and 5 mM Mg^{2+}. **(B)** Representative snapshots from a time-lapse experiment displaying different stages of ring formation. Frames correspond to the times (min) indicated after the addition of GTP and Mg^{2+}. **(C)** Polar clockwise growth of a single FtsZ from a nucleation point. Growth seems to occur stepwise and depend on the accessibility of small filaments nearby (panel 1). Lower local protein density (white arrow) correlates with a higher flexibility of the polymer (panels 7-12). Breakage occurs primarily in trailing regions (15). After ca. 3 min, a primitive ring made of three distinct short filaments is exhibited (17). **(D)** Directional filament gliding via treadmilling. Fragmentation or depolymerization destabilizes the trailing ("older") edge as shown in the kymograph (d-labelled white line). Images in (C) and (D) were taken every 2 s and the scale bar represents 500 nm. Movies reconstructed from the whole collection of images can be found in supplemental movies **4.S2** and **4.S3.**

4.1.4 Surface FtsZ concentration critically modulates the emergence of dynamic chiral ring-like structures

We further investigated the impact of protein concentration on the stability and dynamics of FtsZ vortex formation, in the presence of GTP (4 mM) and Mg^{2+} (5 mM). Below 0.2 μM, no FtsZ filaments could be detected (**Figure 4.6**). Interestingly, increasing the protein concentration to around 1.0 μM resulted in the formation of abundant three-dimensional polymer networks on the membrane, and no dynamic FtsZ rings were observed (**Figure 4.6**) and as previously described (Loose and Mitchison, 2014). These results showed that the self-organization behaviour of membrane-targeted FtsZ polymers was critically dependent on total protein concentration.

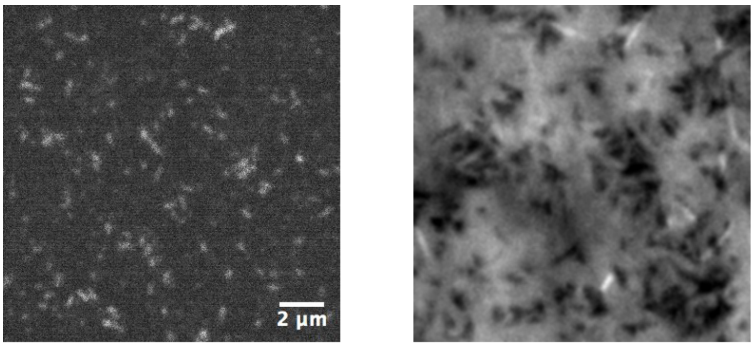

Figure 4.6. Representative images of FtsZ-YFP-mts at low (left panel) and high (right panel) protein concentrations. Only short filaments could be detected at 0.1 μM, no further structures were later observed. On the contrary, when 1.0 μM of FtsZ-YFP-mts is added, polymer networks were observed almost instantly at the vicinity of the membrane. Dynamic rings were only noticed at intermediated protein concentrations.

Next, we compared the kinetics of protein binding to the membrane at 0.2 μM and 0.5 μM of protein (**Figure 4.7**), under conditions previously used to detect the swirling rings (**see Figure 4.5**). Upon the addition of GTP (4 mM) and Mg^{2+} (5 mM) a similar membrane adsorption rate (**Figure 4.7.A**) and the parallel appearance of short and highly dynamic filaments (**Figure 4.7.B**) were initially found for the two protein concentrations. Remarkably, the transition from short filaments to rudimentary circular structures (grey area in **Figure 4.7.A**) also occurred at similar times in both cases. After a lag time of around 10 min, the adsorption rate was found to be significantly slower at 0.2 μM than at 0.5 μM, suggesting that the kinetics of ring stabilization and widening of the structures was concentration-dependent (**Figure 4.7.A**). These differences, found at elapsed times greater than 10 min, also correlated with the fact that the morphology of the rings observed at a protein

concentration of 0.2 μM after 45 min incubation (**Figure 4.7.B, bottom right panel**) were similar to the ones obtained after a lag time of 20 min when 0.5 μM protein was used (**Figure 4.7.B, upper mid panel**). The morphological similarity found at these two-time points (denoted as 2 and 3 in **Figure 4.7.A**) occurred at a similar protein coverage of the membrane, suggesting that protein surface density, rather than bulk concentration, is the key parameter determining the nature of the network that assembles on the membrane. The correlation between the morphologies at time points 2 and 3 of **Figure 4.7.A** was further established by determining the average diameter of the formed rings to be about 1 μm at both protein concentrations (**Figure 4.7.B**). This suggests that although the adsorption rates were different at these time points, the proteins condensed into similar structures.

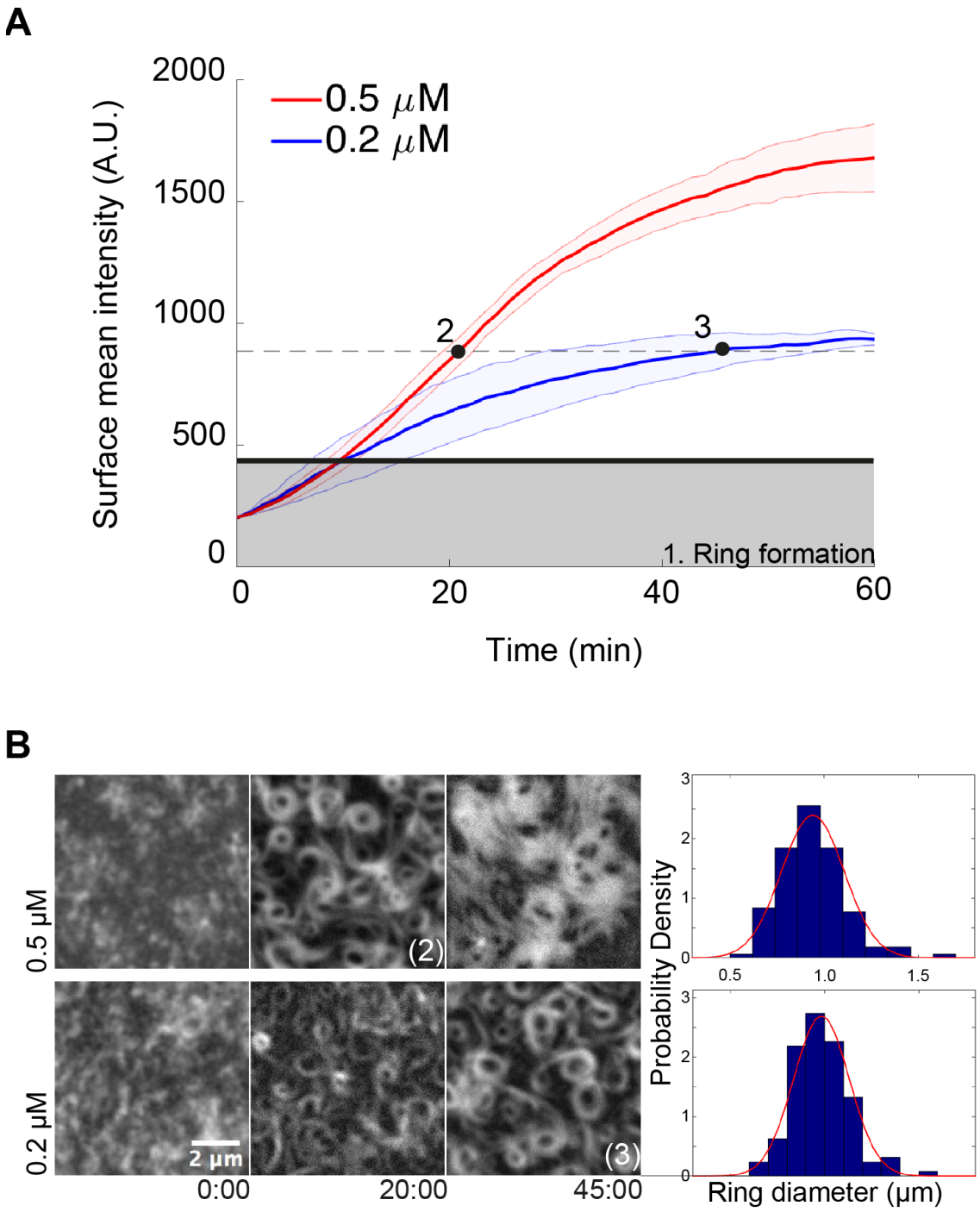

Figure 4.7. Dependence of FtsZ-YFP-mts vortex formation on protein surface concentration. (A) Time-dependence of the average fluorescence intensity of FtsZ-YFP-mts on the bilayer upon 4 mM GTP and 5 mM Mg^{2+} addition, as measured by TIRFM, at 0.2 (blue line) and 0.5 (red line) μM protein concentration. The grey area marks the intensity when first closed rings are observed, which is approximately the same for both protein concentrations. After closed rings have formed, the further accumulation of protein at the surface is strongly concentration dependent. The dashed line represents the phase in which clearly discernible, locally stable dynamic vortices are observed. While at 0.2 μM the system reaches this regime after an elapsed time of 45 min (time point 3), at 0.5 μM it only takes ~20 min (time point 2). **(B)** Representative images of the experiment shown in panel (A). Frames were taken at elapsed times in minutes. Right: Ring size distributions at time points 2 and 3, indicated in panel (A), with average diameters of 0.94 +/- 0.16 μm, N = 140 and 0.98 +/- 0.14 μm, N = 128 respectively. Size distributions of rings are similar, since both correspond to the same protein surface density (~880 A.U.)

Then, we monitored the impact of GTP concentration (0.04, 0.4, and 4 mM) on the formation of swirling vortices at fixed protein (0.2 μM) and Mg^{2+} (5 mM) concentration. Surprisingly, at the lowest GTP assayed (0.04 mM), a highly ordered mesh of static filaments was found at *t=0*. These filaments retained a certain degree of curvature and behaved as a nematic phase that entirely covered the membrane area (**Figure 4.8.A right panel and 4.9 left panel**). A similar behaviour was also observed at intermediate GTP concentration (0.4 mM) (**Figure 4.8.A left panel**). Notably, the surface mean intensity is 3-fold (~1500) increased, compared to the minimal density to form rings (**Figure 4.7.A**), suggesting that the parallel arrangement of filaments correlates with a high-density regime of protein. Furthermore, aligned filaments showed no significant change after 10 minutes, in contrast to dynamic rings (**Figure 4.8**).

It is known that Mg^{2+} favours self-association and assembly of FtsZ both in solution and at membranes (Monterroso *et al.*, 2013) (Rivas *et al.*, 2013). Therefore, one possibility could be that the free Mg^{2+} controls the surface protein density, rather than the total GTP concentration, since GTP is known to bind Mg^{2+} with affinity in the millimolar range (Menendez *et al.*, 1998). To examine this alternative, we repeated the self-organization assays at 0.04 mM GTP in the presence of 1 mM free Mg^{2+}, which resulted in the formation of chiral vortices (**Figure 4.9, right panel**). Interestingly, the emergence of chiral vortices was found to correlate with a significantly lower mean surface protein density than the one measured at 0.04 mM GTP and 5 mM Mg^{2+} which resulted in the dense packing of static polymers (**Figure 4.9, left panel**). These findings show that free Mg^{2+} controls the concentration of GTP FtsZ-YFP-mts polymers at the membrane and then the self-assembly of the FtsZ filaments in the membrane.

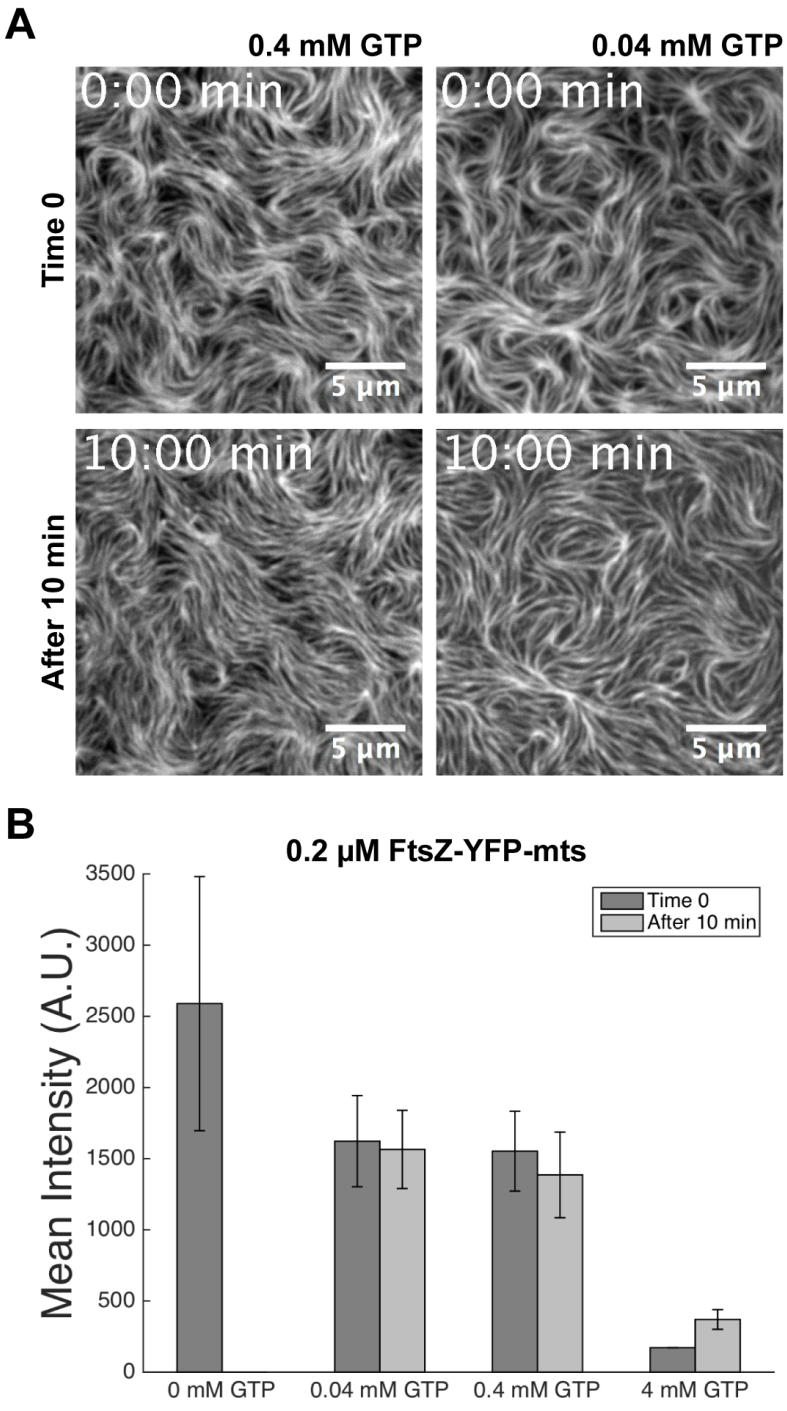

Figure 4.8. Effect of GTP concentration on the FtsZ-YFP-mts rings formation. (A) Images of 0.2 µM FtsZ-YFP-mts bundles after the addition of 0.4 mM GTP and 0.04 mM GTP showing long filaments with a parallel arrangement. Images of upper panels were taken 1-2 minutes (initial acquisition) after GTP addition. Lower panels represent images after 10 minutes. **(B)** Bar plot of the mean fluorescence intensity of the different GTP concentrations at initial time of triggering and 10 minutes later.

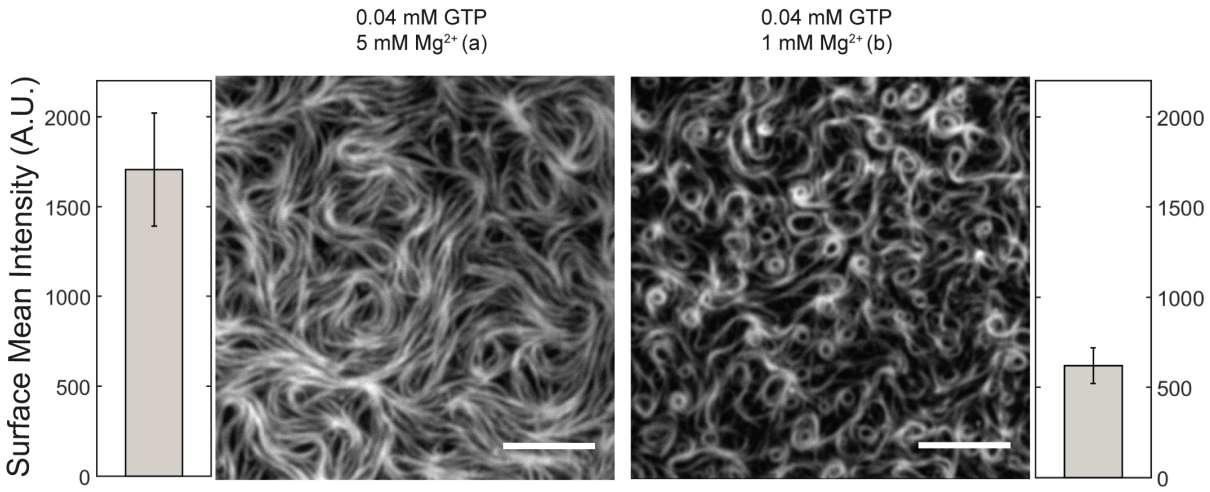

Figure 4.9. Free Mg^{2+} regulates protein surface concentration and thus, self-organization of membrane-targeted GTP-FtsZ. Representative snapshots showing TIRFM images of FtsZ-YFP-mts (0.2 μM) polymers on the bilayer taken 2-3 minutes after the addition of 0.04 mM GTP in the presence of 1 mM and 5 mM free Mg^{2+} concentrations, respectively. Next to each image, the mean fluorescence intensity, proportional to the FtsZ-YFP-mts density on the membrane, is shown (average of 3 experiments). The protein network observed at 5 mM free Mg^{2+} correlates with a high FtsZ-YFP-mts density regime, at least 3-fold larger (~1500 A.U.) than required for ring formation (~500 A.U.).

4.1.5. Directionality of vortices and destabilization of the trailing edge

After formation, single rings reach a quasi-steady-state as rotating vortices, meaning that the light intensity along their perimeter shows a nearly periodic time dependence. These rotating structures formed by the membrane-targeted FtsZ-YFP-mts (mts C-terminal) consistently showed a chiral clockwise rotation (**Figure 4.10.A and Movie 4.S4**). The directional ring dynamics was confirmed by the positive slope of kymographs generated along the ring circumference. Quantifying the slope of the kymograph (see Materials and Methods) of N=60 rings, we calculated the velocity distribution with a mean velocity of 34 nm/s or 3.9° s^{-1} for rings of about 500 nm radius (**Figure 4.10.D**). Interestingly, the rotational velocities measured here are in good agreement with those reported *in vivo* (30 nm/s) in spite of the significantly reduced complexity of the reconstituted system (Yang *et al.*, 2017) (Bisson-Filho *et al.*, 2017).

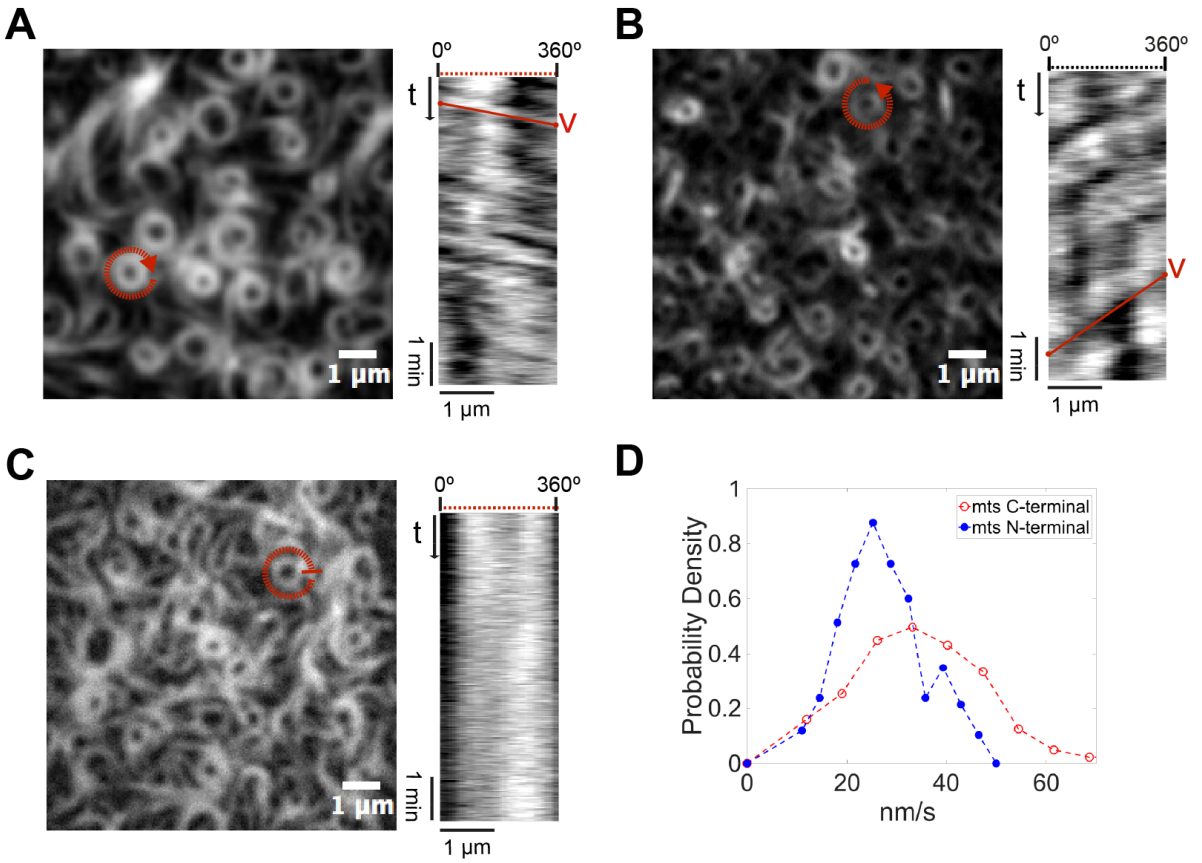

Figure 4.10. Steady-state treadmilling and chirality of FtsZ vortices: dependence on GTPase activity and location of the membrane targeting sequence (mts). (A-C) Left panels: Representative snapshots of the rings formed upon addition of GTP (4 mM) and Mg^{2+} (5 mM) by **(A)** FtsZ-YFP-mts, whose membrane-targeting sequence is located at the C-terminus of FtsZ, **(B)** mts-H-FtsZ-YFP, with mts located at the N-terminus of FtsZ, and **(C)** FtsZ*[T108A]-YFP-mts, a variant of FtsZ-mts with diminished GTPase activity. Right panels: Kymograph analysis showing **(A)** a positive slope that corresponds to the apparent clockwise rotation time of the selected ring (red circle), **(B)** a negative slope that corresponds to an apparent anti-clockwise rotation, indicating that the position of the membrane targeting sequence determines the chirality of the apparent rotation, **(C)** no apparent slope corresponding to static rings, suggesting that the apparent rotation in (A) and (B) is mediated by GTP hydrolysis. **(D)** Velocity distributions for FtsZ-YFP-mts (red) and mts-H-FtsZ-YFP (blue) with mean rotational speed values of 34 nm/s and 25 nm/s respectively.

We next sought to understand whether there was any relationship between the structural features of the protein and the obviously chiral dynamics of our FtsZ mutants. Hence, we made use of previously established chimera variants that were shown to have opposite effects on deformable membranes (Osawa *et al.*, 2009) (Arumugam *et al.*, 2012). In the presence of GTP, FtsZ-YFP-mts is able to induce inwards (concave) deformations on lipid vesicles. Strikingly, when the mts sequence is switched to the N-terminus, an outwards (convex) deformation is observed (Osawa *et al.*, 2009). To study the role of the position of the mts in our dynamic vortices, we carried out similar self-organization assays using an FtsZ chimera in which the membrane attachment was located at the opposite, N-terminal, end (mts-H-FtsZ-YFP). Upon addition of GTP and Mg^{2+}, defined dynamic rings were

observed (**Figure 4.10.B**). Strikingly, now the FtsZ swirls appeared to rotate anti-clockwise (**Movie 4.S4**), a feature that was confirmed by the negative slope of the kymographs (**Figure 4.10.B**). As before, we measured the slope of kymographs for N=50 different rings to calculate the velocity distribution with a mean of about 25 nm/s or 2.8° s^{-1} for a ring of 500 nm radius. This velocity is slower than that of the FtsZ-YFP-mts vortices (34 nm/s) (**Figure 4.10.D**). These observations show that the positioning of the membrane targeting sequence determines the direction of polymerization as it does for membrane binding and transformation. The fact that the N-terminal mts mutant, without a protein spacer between the FtsZ and the membrane attachment, results in the same qualitative dynamic behaviour, although being inverted in chirality, also refutes potential speculations that YFP may take over a necessary (sterical) role of FtsA (Loose and Mitchison, 2014).

To further investigative how exactly GTP hydrolysis influences the formation of collective streams, we carried out similar self-organization assays using a variant of the FtsZ chimera with no GTPase activity (**Figure 4.11**), in which the Threonine at position 108 was replaced by an Alanine (FtsZ*[T108A]-YFP-mts). As shown in **Figure 4.11**, GTPase activity reported for these variant polymers was almost zero.

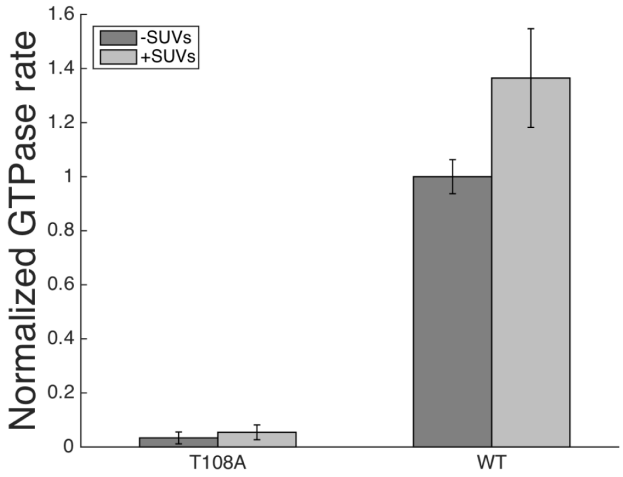

Figure 4.11. GTPase activity of FtsZ-YFP-mts (5 µM) or FtsZ*[T108A]-YFP-mts (5 µM) in the absence or presence of phospholipids (4 mg/ml). The corresponding rates where normalized to the GTP activity of FtsZ-YFP-mts in the absence of phospholipids. Error bars correspond to S.D. from three different experiments.

Using FtsZ chimera with no GTPase activity, well-defined rings similar in size to the ones found with FtsZ-YFP-mts could be observed upon the addition of GTP and Mg^{2+} (**Figure 4.10.C**). Interestingly, these rings did not seem to treadmill and rotate (**Movie 4.S4**), as evidenced by the lack of clear patterns in the kymographs generated to track polymer dynamics (**Figure 4.10.C**). Interestingly, FtsZ*[T108A]-YFP-mts rings grow from nucleation

points in a less dynamic manner compared to FtsZ-YFP-mts (**Movie 4.S5**). From these results, we conclude that GTPase activity is not required for the formation, but for the quasi-steady-state rotational dynamics of the ring patterns, suggesting that GTPase activity particularly promotes filament destabilization in the trailing edge.

Treadmilling can be explained by an imbalance between growth and shrinkage at the two opposite ends of the polar filament. Since treadmilling is obviously GTP turnover-dependent, and the growth into ring-like structures by capturing preformed diffusing filaments is not, the critical requirement for treadmilling seems to be the destabilization and shrinkage at the trailing edge. In order to directly visualize the destabilization dependent on nucleotide state, we developed a single molecule assay using FtsZ-YFP-mts incubated with fluorescently labelled nanobodies (GFP-Booster-Atto647N, see Materials and Methods) (**Figure 4.12**) to investigate the protein turnover at the membrane, implying that faster disassembly suggests higher destabilization. By measuring the probability of protein detachment as a function of time (see **4.3. Annex**), we could calculate the mean residence time of single FtsZ subunits within the filaments on the membrane. Using this analysis, we found that the mean residence time of FtsZ-YFP-mts in fragments forming dynamic rings was $t_r = 11.5\ s$ (**Figure 4.12.B**) in good agreement with previous FRAP studies with native FtsZ (Anderson *et al.*, 2004) (Chen and Erickson, 2005). These residence time turns out to be significantly faster than for the GTP hydrolysis-deficient mutant FtsZ*[T108A]-YFP-mts, (see **4.3. Annex Figure 4.3. Annex.B**, similar to the photobleaching time scale contribution $\sim 32\ s$). Interestingly, by considering the rotational speed as measured in **Figure 4.10.D** and this residence time, we reason that rings are assembled by multiple filaments with a mean length of $\langle l \rangle = \bar{v} * t_{res} = 390\ nm$ (78 monomers). In comparison, *in vitro* assembly of natural FtsZ showed shorter filaments, that were on average 120 to 200 nm long (30-50 monomers) (Erickson and Osawa, 2017). In addition, we measured the residence time without GTP (GDP form) with 1 mM free Mg^{2+} (**Figure 4.12.A(c) and B**). Assuming that the residence time of a polymer of n-monomers scales to the power of n ($t_r^{pol} \sim (t_r^{mon})^n$), one can estimate that the residence time associated to one monomer is ~1 s, which agrees with our results (~ 0.8 s) in GDP form at 1 mM free Mg^{2+}.

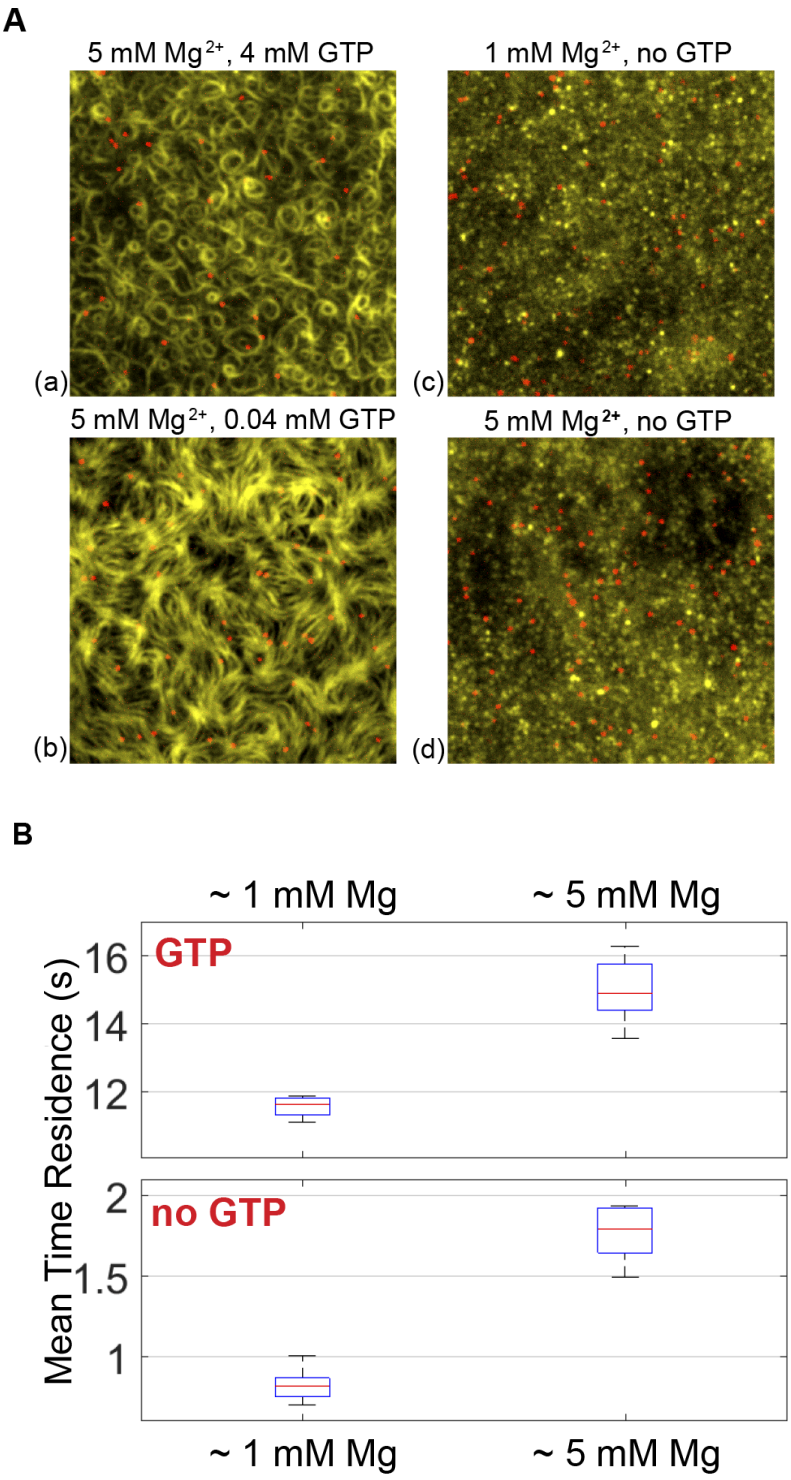

Figure 4.12. Residence times of single membrane-targeted FtsZ molecules at the bilayer, dependent on nucleotide and free Mg^{2+}. (A) Overlaid images of FtsZ-YFP-mts structures (yellow channel) incubated with GFP-Booster-Atto647N (nanobody) (single molecules: red channel) in the presence of GTP (a, b), in the absence of GTP (c, d) and indicated free Mg^{2+} concentration. The protein concentration in all cases was around 0.2 µM. **(B)** Mean residence times of FtsZ-YFP-mts were calculated using an exponential fit of the cumulative residence time distribution. Mean residence times were measured for different GTP and Mg^{2+} conditions.

Our single molecule experiments also allowed to directly elucidate the impact of free Mg^{2+} and in particular, its obvious role in the formation of the high density FtsZ mesh. It was found that the protein release from the membrane upon GTP addition was slower at 5 mM ($t_r = 15.1\ s$) than at 1 mM free Mg^{2+} (**Figure 4.12.B**). These findings represent compelling evidence that the formation of a high density mesh of filaments is linked to the slow detachment of protein, at least when compared to the dynamic rings at lower free Mg^{2+} (1 mM). Also, the residence time of FtsZ in GDP form at 5 mM free Mg^{2+} was increased ($t_r = 1.72\ s$) compared to 1 mM. This general increase in the residence time implies that lateral interactions (bundling), favoured by free Mg^{2+}, promote larger and more crosslinked polymeric species with higher membrane affinity and less susceptibility to destabilization.

4.2. DISCUSSION

The assembly of the artificially membrane-targeted variant of FtsZ (mts-FtsZ) in the presence of GTP and Mg^{2+} has been studied in solution and in membrane systems. The sedimentation velocity data clearly demonstrated that FtsZ-YFP-mts is a well-behaved protein from a self-association point of view: it exists as a heterodimer (FtsZ + YFP) in solution in the absence of GTP and Mg^{2+} (GDP-bound form of the protein; (Rivas *et al.*, 2000) and it only forms higher-order oligomers in the presence of both GTP and Mg^{2+} (**Figure 4.1**). This is consistent with the apparent diffusion coefficients of the protein under similar experimental conditions, as measured by DLS (**Figure 4.2**). These findings are relevant, as they allow controlling the association state of the membrane-targeted FtsZ variant by physiological ligands (GTP and Mg^{2+}), which is crucial to get the reproducible ring formation on bilayers as it is demonstrated in this section.

The broad distribution of higher order species shown in **Figure 4.1.A** contrast to the sharp s-values observed in previous studies from the Rivas lab under specific experimental conditions of protein and buffer composition (Rivas *et al.*, 2013). These differences in sedimentation coefficient distributions of FtsZ under assembly promoting conditions could in part be related to the presence of the mts-tag. However, they are also compatible with the behaviour of self-assembling systems as plastic as FtsZ, in which it would take only a very small free energy perturbation to produce large changes in the relative abundance of the species present as higher order oligomers (Rivas *et al.*, 2013).

To extend our understanding of the influence of GTP and Mg^{2+} in FtsZ polymerization, we examined the effect of nucleotides and magnesium on the apparent affinity of the binding of FtsZ-YFP-mts to *E. coli* lipids coated microbeads. Our results show that FtsZ-YFP-mts polymers interact strongly with *E. coli* lipids than the unassembled form of the protein (**Figure 4.4**). Interestingly, these findings are in good agreement with the lipid-binding properties of the wild-type FtsZ measured using the same membrane system (Sobrinos-Sanguino *et al.*, 2017).

Once the membrane-targeted FtsZ protein was biochemically characterised, in our minimalistic *in vitro* reconstitution study we found that polymers of membrane-tethered FtsZ protein autonomously and without the presence of FtsA self-organize on a supported bilayer upon addition of GTP and Mg^{2+}, to form chiral ring-like dynamic patterns (**Figure 4.5**), displaying a clockwise or anti-clockwise protein movement, dependent on whether the membrane attachment was enforced through the C-terminal or N-terminal end of the protein, respectively (**Figure 4. 10.A-B and Figure 4.13**). The membrane targeting sequence in both cases was taken from MinD, one of the elements of the site-selection MinCDE complex. We thus showed that the ability of FtsZ to create dynamic patterns is an intrinsic property (**Figure 4.5.A**) rather than a specific interaction with a specific protein anchor. Instead, the formation of dynamic FtsZ ring structures *in vitro* is highly linked to (i) the surface protein density and (ii) GTPase activity, destabilizing surface-bound filaments und thus being key for treadmilling (Yang *et al.*, 2017).

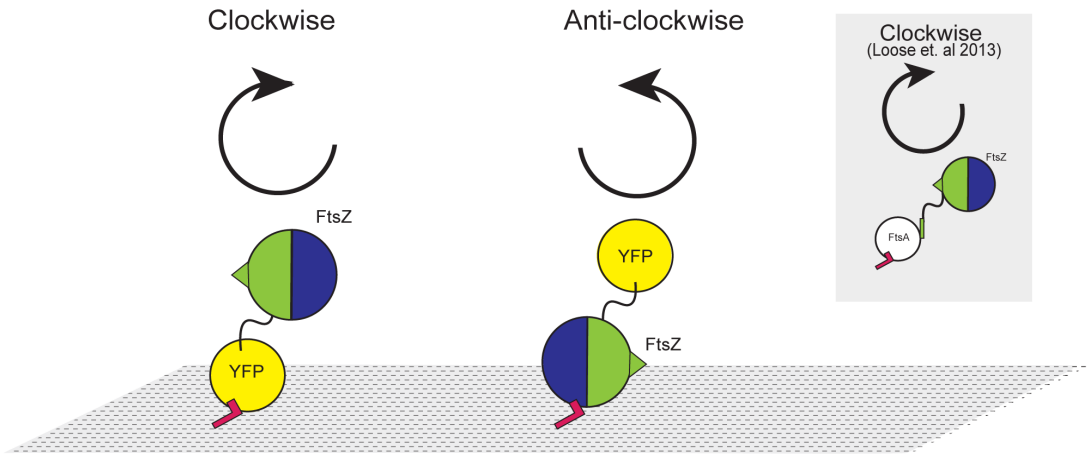

Figure 4.13. Model of FtsZ membrane binding. Wild-type FtsZ is tethered to the membrane through FtsA (right diagram); the C-terminal peptide of FtsZ (central hub) works as binding peptide for FtsA, and the latter anchors the membrane via its amphipathic helix (red polygon). The C and N domains of FtsZ are represented as blue and green hemispheres, respectively. In the case of FtsZ-YFP-mts, the FtsZ binding peptide is replaced with YFP and an amphipathic helix (left diagram). In mts-H-FtsZ-YFP, this amphipathic segment is incorporated at the N-terminal of FtsZ, while the YFP remains at the C-terminal (mid diagram).

We found that the most decisive factor for the emergence of dynamic vortices of FtsZ on membranes is the overall surface coverage by protein monomers and filaments (**Figure 4.14.A**), which varies over time upon protein adsorption to the membrane (**Figure 4.7**) and can be greatly affected by free Mg^{2+} concentration (**Figure 4.9**). Dynamic vortices appear primarily in an intermediate density regime (surface mean intensity: 450-1000 A.U.) and isotropic bundles in a high-density regime (surface mean intensity > 1000 A.U.). Transitions from highly dynamic vortices to isotropic bundles occur upon an increase in lateral contacts that arrest treadmilling filaments, increasing their mean effective length (as in the case of ZipA) (Loose and Mitchison, 2014). This was clearly observed in our single molecule assay (**Figure 4.12**) that shows a slower turnover in the situation of dense isotropic bundles, i.e., longer filaments. Along these lines, the increase in lateral interactions at high free Mg^{2+} also explains the rapid formation of filaments at 5 mM free Mg^{2+} (**Figure 4.9**), since larger FtsZ assemblies bind to the membrane and interact with each other more frequently (**Figure 4.12B**). Presumably, the main reason why Loose and Mitchison failed to observe dynamic vortices in the case of the FtsZ-YFP-mts (Loose and Mitchison, 2014), is because of the high protein concentration used in their experiments (1.5 μM).

Our results are compatible with previous atomic force microscopy analysis of static structures formed by FtsZ polymers on mica as a function of protein concentration at the surface (Mingorance *et al.*, 2005). The protein concentration-dependent formation of dynamic FtsZ patterns also nicely correlates with a recent theoretical study suggesting that protein density at the membrane controls the formation of vortex patterns on membranes in a phase-like behaviour. According to this, independent curved polar filaments showing chiral motion and repulsion can self-assemble into vortex or ring-like structures in an intermediate density regime. While at low protein densities, filaments travel independently, at the high-density regime they form isotropic networks and jammed bundles (Denk *et al.*, 2016).

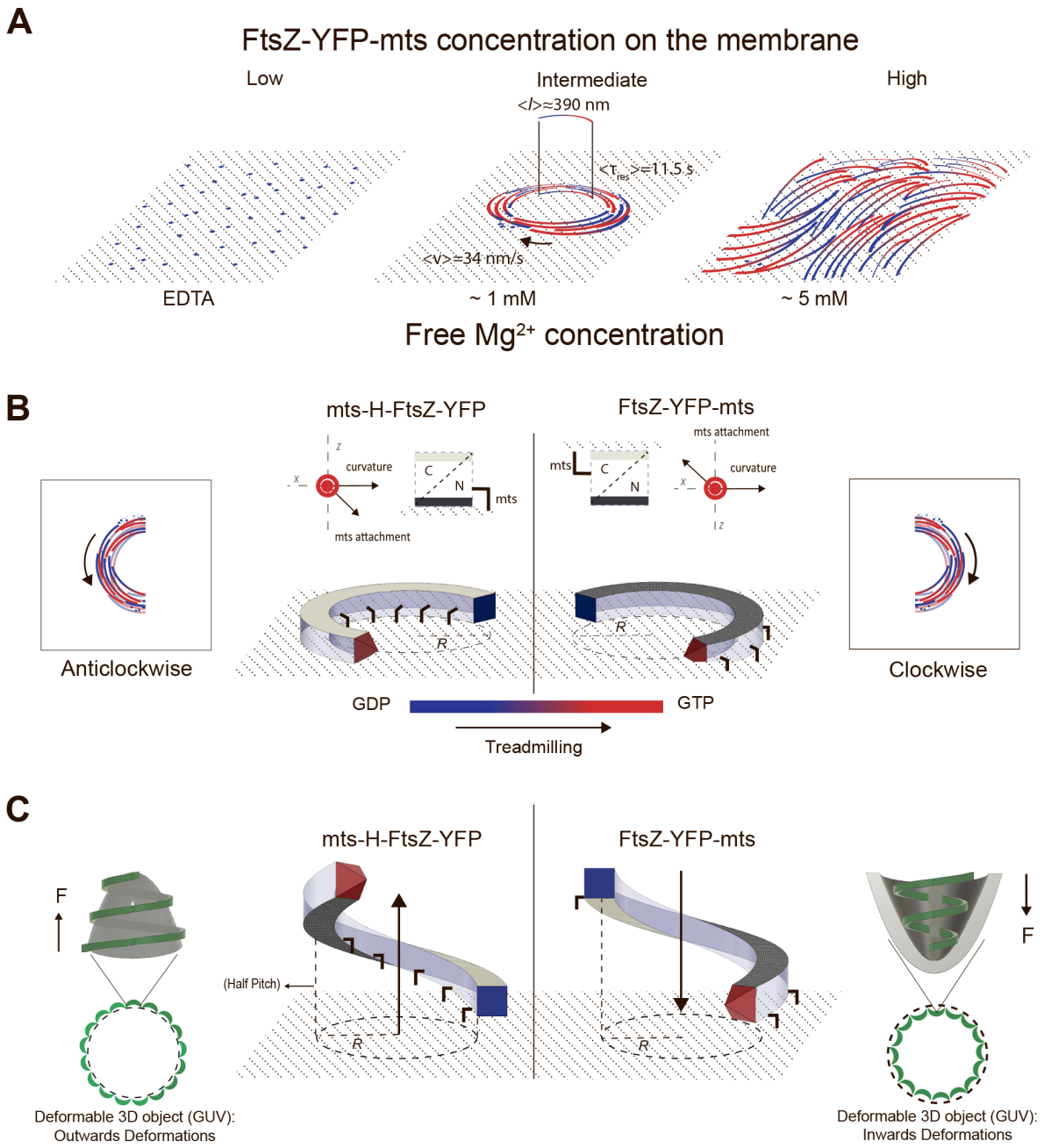

Figure 4.14. (A) FtsZ-YFP-mts ring formation is dependent on GTP and protein surface concentration. At low protein concentration and no GTP and Mg^{2+}, FtsZ transiently binds to the membrane without forming visible structures. With GTP, dynamic chiral rings are formed as a function of time. Once stable swirls are built, they exhibit a mean velocity of 34 nm/s and a turnover time of short fragments of 11.5 s. From the velocity and the turnover time, the average length of the protofilaments can be estimated to 390 nm. However, ring formation is only observed at intermediate protein density regimes. At high protein density, a parallel network of filaments (nematic phase) is observed. **(B)** To guarantee chirality, attachment needs to have a perpendicular component to both, the ring curvature and filament polarity to have a preferential binding face. In this case, the mts interacts with the flat surface on opposite sides of the FtsZ filament, so curvature is also in the opposite direction. **(C)** We here suggest that an intrinsic helical FtsZ shape, characterised by a radius and a pitch, can alternatively explain previous FtsZ induced inwards/outwards deformations in the following way: due to the intrinsic pitch, the growing filament would either pull up (left) or push down (right) the surface. On the contrary, if the surface is not deformable (SLB), the filament would experience a strain, get destabilized, and eventually break upon growth.

With gradually increasing protein concentration on the membrane, we were able to investigate the initial formation phase of dynamic rings. At low density (surface mean intensity < 450 A.U), curved and polar filaments initially emerge from nucleation points, which presumably are small attached filaments above a critical length. Intriguingly, the overall adsorption rates to the membrane at this stage are similar for protein concentrations of 0.2 μM and 0.5 μM (**Figure 4.7.A**). Upon sufficiently high membrane coverage of nucleating filaments after the initial phase, protein binding from solution begins to scale with total (i.e., bulk) protein concentration. Whether nucleators are directly formed on the membrane after GTP addition or whether short polymers are formed in solution and an increase in affinity with growth brings them to the membrane cannot be determined based on our data, and will be the topic of further investigation.

We found that filaments growing from nucleators are prone to fragmentation, resulting in free fragments, which may stay connected to the membrane. There, they assemble with other attached filaments by diffusion and directional treadmilling, which ultimately results in closed rings, in which the treadmilling continues. Our experiments demonstrate that treadmilling, particularly via destabilization of the trailing edge, is highly regulated by GTPase activity. When GTPase activity is switched off (FtsZ*[T108A]-YFP-mts), rings seemed to grow only from nucleation points and do not treadmill, at least on time scales found for FtsZ-YFP-mts (**Figure 4.10.C**). Moreover, the residence time of single FtsZ*[T108A]-YFP-mts subunits in the filaments is comparable with the photobleaching control, implying that protein turnover is almost non-existent (see **4.3. Annex Figure 4.3. Annex.B**). It has been suggested that a kinetic and structural polarity, at monomeric level, and a GTP/GDP gradient are requirements for robust treadmilling (Wagstaff *et al.*, 2017). As seen from our experiments of the initial vortex growth phase, a GTP/GDP gradient along the treadmilling direction is likely to result from the preferential addition of GTP subunits to the existing filaments at the polar front, and a more likely GTP turnover towards the “older” tail.

In light of the role of GTPase activity for the formation of dynamic vortices, the measured velocity of the FtsZ + FtsA vortices reported by Loose and Mitchison is about three-fold faster (108 nm/s) compared to our FtsZ-YFP-mts rings (34 nm/s). In addition, these authors reported a higher GTPase activity of the FtsZ + FtsA compared the FtsZ-YFP-mts (Loose and Mitchison, 2014). Nonetheless, it is not clear how variables such as GTPase activity and attachment strength influence the speed of rotation. For instance, our mutant mts-H-FtsZ-YFP has shown a considerable decrease in rotation speed compared to the FtsZ-YFP-mts. Remarkably, to observe mts-H-FtsZ-YFP dynamic rings, we had to increase the bulk

concentration to 1.25 µM. This may be due to a reduced affinity for membranes, affecting the overall dynamics.

The most remarkable outcome of this study is the clear dependence of vortex chirality on the positioning of the membrane anchor, which in turn has severe effects on the topology of membrane deformation by FtsZ. Chirality is inverted by switching the membrane anchor from the C-terminus (clockwise) to the N-terminus (anticlockwise). Intriguingly, these two different mutants cause concave (C-terminal) or convex (N-terminal) deformations when bound to deformable liposomes (Osawa *et al.*, 2009). To explain these different deformations, Erickson and colleagues have previously depicted FtsZ filaments as arc segments with a direction of membrane attachment either parallel or antiparallel to the vector of curvature. In order to support the here observed chiral treadmilling of curved rings on planar membranes, however, attachment through the preferential binding face of the filaments needs to have a perpendicular component to both, the ring curvature and filament polarity. **Figure 4.14.B** shows a curved filament with a C-terminal (clear grey) and N-terminal (dark grey) face perpendicular to the curvature of the filament. Note that the mts is represented here with one parallel component to the curvature, as suggested by Erickson, and one perpendicular component to accommodate flat membrane binding. In this flat representation of a curved FtsZ filament, treadmilling is explained by a polar growth at the leading edge and a destabilization mechanism, driven by GTP hydrolysis, towards the GDP enriched region at the trailing edge (Wagstaff *et al.*, 2017).

Nevertheless, the fact that curved structures can be either attached along their axis of apparent curvature (*in vivo*, Osawa & Erickson (Osawa *et al.*, 2009) or perpendicular to their axis of primary curvature (as reported here), we have to conclude that either the membrane attachment of the filament is immensely flexible, or – and this is more likely based on previous structural investigations – that the filament does not have a single, but rather more than one direction of curvature, like a helix or a twisted arc (Arumugam *et al.*, 2012) (Gonzalez de Prado Salas *et al.*, 2014). Indeed, a very similar geometry with more than one curvature direction has recently been reported for ESCRTIII filaments (nicely reviewed by Chiaruttini and Roux (Chiaruttini and Roux, 2017). This is particularly intriguing, as among many other roles in eukaryotic and prokaryotic cells connected with membrane abscission, ESCRT is the alternative system to FtsZ with respect to cell division in Archaea (Samson *et al.*, 2008) (Lindas *et al.*, 2008).

Therefore, in the light of evidence showing that FtsZ forms helical structures *in vivo* (Thanedar and Margolin, 2004) (Holden S. J. *et al.*, 2014) and *in vitro* (Arumugam *et al.*,

2012), we here suggest an alternative structural model to the one depicted in **4.14.B** (**Figure 4.14.C**). We propose that an FtsZ filament with more than one main direction of curvature, such as a helix, would much more elegantly accommodate the combination of inwards/outwards deformations and chiral treadmilling for the opposite mts mutants. Such a cork-screw like FtsZ filament can be simply described by an intrinsic radius and a pitch, where the latter would reflect on the attachment direction (**Figure 4.14.C**). On a deformable surface (deflated liposome), the growing filament would either pull up (left) or push down (right) the surface due to the respective pitch. The interplay between the elastic response of the membrane (increased membrane tension) and local changes in the helix radius, due to GTP hydrolysis , (Huecas and Andreu, 2004) (Lu *et al.*, 2000) could explain the stabilization of higher curvature or smaller radii regions (**Figure 4.14.C**). On a non-deformable surface (SLB), however, since the surface is not resilient, the filament would experience a strain, get destabilized, and eventually break upon growth.

Thus, together with the very recent studies showing the linkage between treadmilling of FtsZ polymers and peptidoglycan synthesis in *E. coli* (Yang *et al.*, 2017) and *B. subtilis* (Bisson-Filho *et al.*, 2017) cells, our findings shed new light on the interplay between FtsZ structure and treadmilling dynamics, but may also hint to a direct mechanical link of these to bacterial division. The minimal system we used unambiguously shows that the observed chiral vortices are the result of intrinsic GTP-linked FtsZ polymerization dynamics on the membrane without the need of additional complex interactions with FtsA and ATP, pointing to a fascinating archetypal feature of this important structural protein. The reduced number of components allowed us to selectively determine the influence of key factors, e.g. the surface density of FtsZ, on the self-organization behaviour, thus contributing to a much better mechanistic understanding of FtsZ's dynamic architecture and its potential physiological implications.

4.3. ANNEX: Cumulative residence time distributions

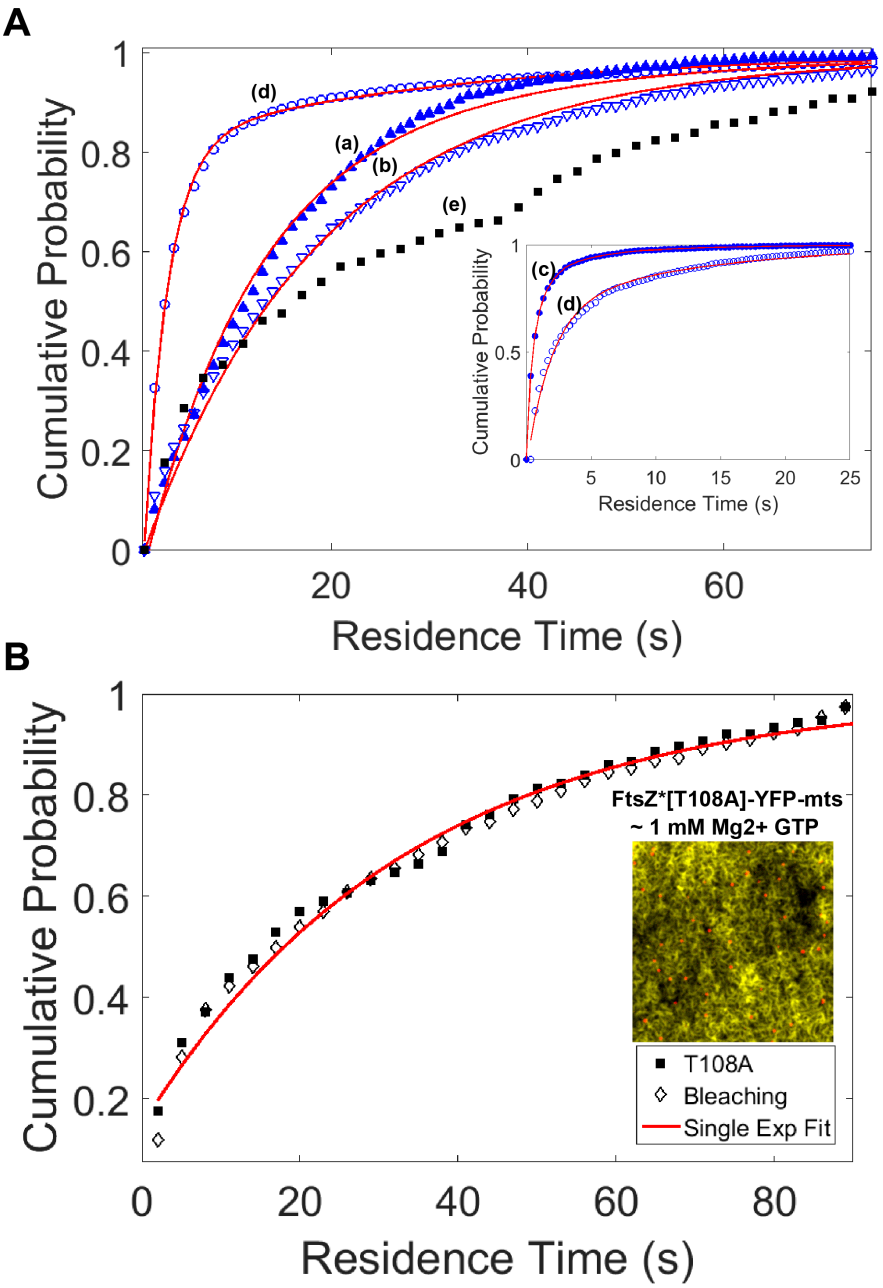

Figure 4.3. Annex: (A) Cumulative probability of the residence time distributions for (a) 4mM GTP, 1mM free Mg^{2+} and (b) 0.04 mM GTP, 5 mM free Mg^{2+} having an acquisition rate (1 fps). Inset: Cumulative residence time distribution for GDP forms with a faster acquisition rate (3 fps) at (c) 1 mM free Mg^{2+} and (d) 5 mM free Mg^{2+}. Note that the residence time distributions for GDP - 5 mM Mg^{2+} (blue circles) are equivalent at 1 fps or 3 fps. (e) represents photobleaching decay. Curves were fitted to a double exponential function to calculate the mean residence time having a constant photo-bleaching contribution (see Materials and Methods, section 3.5.2.2). **(B)** Cumulative probability of the residence time distribution for FtsZ*[T108A]-YFP-mts (closed squares). In the same plot the photobleaching timescale of fixed nanobodies is shown (empty inverted triangles). TIRF micrograph: Overlaid image of FtsZ*[T108A]-YFP-mts doped with 0.1% of FtsZ*[T108A]-YFP-mts incubated with GFP-Booster-Atto647N (nanobody) (single molecules: red channel) in the presence of GTP.

ACKNOWLEDGEMENTS

This chapter includes the results obtain in collaboration with: Diego Ramirez*[1,2], Daniela A. García-Soriano*[1,2], Mario Feingold[4], Germán Rivas[3] and Petra Schwille[1]. Diego A. Ramirez made a major contribution in Single Molecule experiments and Daniela García in the designs of the mutant FtsZ*[T108A]-YFP-mts.

[1]Department of Cellular and Molecular Biophysics, Max Planck Institute for Biochemistry, Martinsried, Germany, [2]Graduate School for Quantitative Biosciences (QBM), Ludwig-Maximillians-University, Munich, Germany, [3]Centro de Investigaciones Biológicas, Consejo Superior de Investigaciones Científicas (CSIC), Madrid, Spain, [4]Department of Physics, Ben Gurion University, Beer Sheva, Israel.

5. FtsZ polymers tethered to the membrane by ZipA are susceptible to spatial regulation by Min Waves

Bacterial cell division is driven by an FtsZ ring in which the FtsZ protein localizes at midcell and recruits other proteins, forming a divisome. In *Escherichia coli*, the first molecular assembly of the divisome, the proto-ring, is formed by the association of FtsZ polymers to the cytoplasmic membrane through the membrane-tethering FtsA and ZipA proteins. The MinCDE system plays a major role in the site selection of the division ring because these proteins oscillate from pole to pole in such a way that the concentration of the FtsZ ring inhibitor, MinC, is minimal at the cell centre, thus favouring FtsZ assembly in this region. We show that MinCDE drives the formation of waves of FtsZ polymers associated to bilayers by ZipA, which propagate as antiphase patterns with respect to those of Min as revealed by confocal fluorescence microscopy. The emergence of these FtsZ waves results from the displacement of FtsZ polymers from the vicinity of the membrane by MinCD, which efficiently competes with ZipA for the C-terminal region of FtsZ, a central hub for multiple interactions that are essential for division. The coupling between FtsZ polymers and Min is enhanced at higher surface densities of ZipA or in the presence of crowding agents that favour the accumulation of FtsZ polymers near the membrane. The association of FtsZ polymers to the membrane modifies the response of FtsZ to Min, and comigrating Min-FtsZ waves are observed when FtsZ is free in solution and not attached to the membrane by ZipA. Taken together, our findings show that the dynamic Min patterns modulate the spatial distribution of FtsZ polymers in controlled minimal membranes. We propose that ZipA plays an important role in midcell recruitment of FtsZ orchestrated by MinCDE.

This section corresponds to the published article:

Authors: Ariadna Martos[1], Ana Raso[1,2], Mercedes Jiménez[2], Zdeněk Petrášek[3], Germán Rivas[2], Petra Schwille[1]

[1]Max Planck Institute of Biochemistry. Am Klopferspitz 18. D-82152 Martinsried, Germany.
[2]Centro de Investigaciones Biológicas, CSIC. Ramiro de Maeztu 9, 28040 Madrid, Spain.
[3]Institut für Biotechnologie und Bioprozesstechnik, TU-Graz. Petersgasse 10-12/I, 8010 Graz, Austria.

Journal: *Biophysical Journal* 2015, 108 (9), p2371–2383

5.1. RESULTS

5.1.1. FtsZ polymers associated to lipid bilayers through ZipA form dynamic networks

The full-length ZipA protein, which provides membrane tethering to FtsZ, was incorporated in supported *E. coli* lipid bilayers to reproduce the lipid composition found in the bacterial inner membrane. The surface density of ZipA (ρ_{ZipA}) in these bilayers (ZipA-SLBs) was controlled as they were formed by vesicle fusion of previously prepared proteoliposomes containing a known amount of ZipA (see Materials and Methods, section 3.4).

To determine if ZipA is able to diffuse in supported lipid bilayers, fluorescence recovery after photobleaching (FRAP) experiments on SLBs containing ZipA-Alexa 488 were conducted. FRAP analysis revealed that the reconstituted ZipA remained immobile and evenly distributed in the SLBs. The fluorescence intensity of ZipA in the bilayers did not recover completely after photobleaching (data not shown), most probably due to interactions of the ZipA molecules with the glass support underneath hindering diffusion. Furthermore, the half-time turnover ($\tau_{1/2}$) of FtsZ subunits attached *to* ZipA-SLBs were obtained from FRAP measurements on the surface of the bilayer for the different samples. Since ZipA remains immobile in those bilayers *(*ZipA-SLBs*),* fluorescence recovery after bleaching in these samples was just due to exchange of FtsZ monomers with the solution (**Figure. 5.1**).

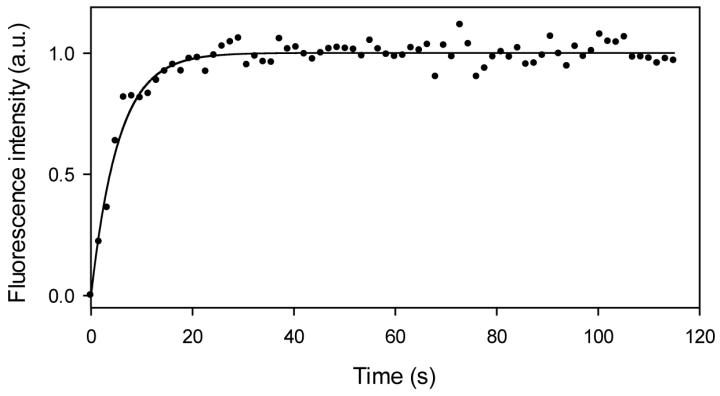

Figure 5.1. FRAP experiment of a 2 µM GTP-FtsZ network on ZipA-SLBs. The plot shows the intensity fluorescence of the photobleached region over time (corrected and normalized for bleaching caused by imaging). The data points (●) were fitted by a simple exponential curve (–) to calculate the half-time turnover value ($\tau_{1/2}$). The $\tau_{1/2}$ in this particular example was 3.7 s. The $\tau_{1/2}$ values presented correspond to the mean values of at least 3 independent experiments.

The specificity of the ZipA-FtsZ interaction was proved when no recruitment of FtsZ was observed in the absence of ZipA. However, when ZipA was in the bilayer, was able to recruit GDP-FtsZ, as revealed by fluorescence confocal microscopy. Then, upon addition of GTP, an immediate recruitment (within seconds) of FtsZ polymers to ZipA-SLBs was observed, resulting in a 10-fold increase of the relative fluorescence intensity in the vicinity of the membrane when compared with the signal of GDP-FtsZ (**Figure 5.2., A and B**). Furthermore, it was observed that the concentration of GTP-FtsZ at the membrane increased less than linearly with the ZipA concentration (**Figure 5.2.C**). The turnover time of FtsZ subunits within the polymer network assembled (~3.6 s), as measured by FRAP, was found to be similar to the value determined for FtsZ protofilaments in solution (Gonzalez *et al.*, 2003) and much faster than that measured for pronounced polymer bundles (Arumugam *et al.*, 2014). Thus, it can be assumed that the FtsZ network on the membrane in these reconstitution assays is essentially assembled by protofilaments tethered to the membrane via ZipA.

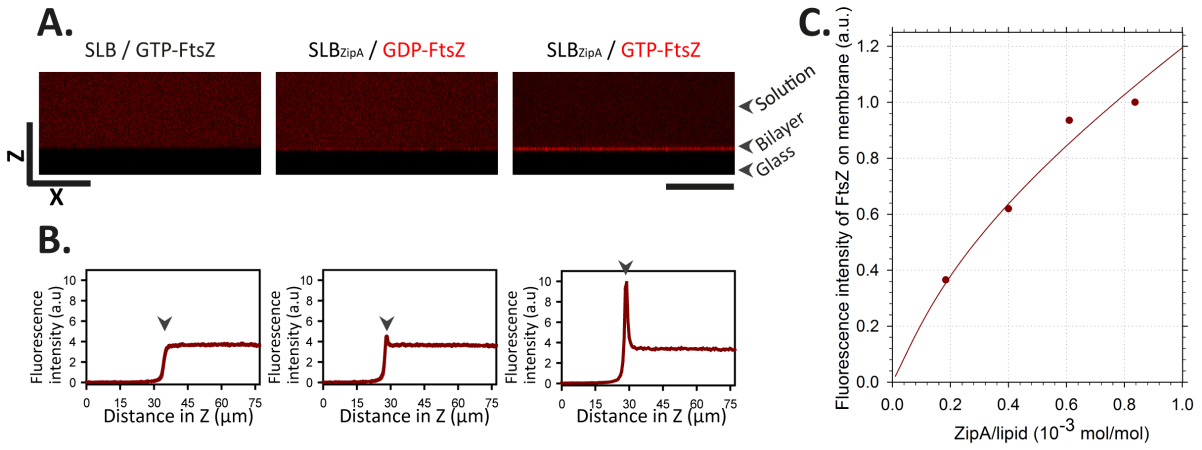

Figure 5.2. Recruitment of FtsZ polymers to lipid bilayers by the action of ZipA. (A) Vertical confocal image (XZ) showing the distribution of GDP- and GTP-FtsZ on SLBs with and without ZipA. No FtsZ is recruited in the absence of ZipA. Scale bars are 50 µm. **(B)** FtsZ fluorescence intensity profiles corresponding to the cross sections shown in (A). The arrows indicate the position of the bilayer. **(C)** Fluorescence intensity of FtsZ on the membrane depending on the surface densities of ZipA.

Dynamic and plastic polymer networks compatible with the ones reported here were previously observed in experimental conditions similar to those used in this work (Mateos-Gil *et al.*, 2012). Thicker and less dynamic FtsZ polymer bundles were found at greater ZipA surface densities (1–8 molar % of a soluble variant of ZipA (lacking the transmembrane region) attached to the bilayers) and under milder salt conditions (Loose and Mitchison, 2014), which are known to favour interactions between FtsZ polymers. This is consistent

with the well-known plasticity and polymorphic nature of FtsZ polymers. These previous studies used high concentrations of membrane associated FtsZ, lower salt concentrations, and an oxygens scavenging system. These experimental conditions, which are known to favour the formation of higher-order polymer structures, may explain the discrepancies between those studies and ours. Indeed, we confirmed the formation of FtsZ polymer bundles in low-salt buffers using the soluble form of ZipA attached to the bilayer at high surface density (results not shown).

5.1.2. FtsZ polymer networks anchored to the membrane via ZipA reorganize into propagating waves by the action of the Min system

The dynamic behaviour of the Min proteins was successfully reconstructed on ZipA-SLBs containing 0.083 molar % of ZipA (equivalent to an average distance of 30 nm between two ZipA molecules). The dynamic behaviour of the Min system observed in these experiments, as characterised by velocity, wave period, and wavelength, was similar in the absence or presence of ZipA (data not shown). At the same time, neither the FtsZ binding to ZipA nor the dynamics of the Min system affected the spatial distribution of ZipA in our assays, as it remained evenly distributed and immobile in the bilayers (see Materials and Methods).

Upon reconstitution of the MinCDE complex on the ZipA-SLBs, FtsZ and GTP were added to allow the formation of ZipA-anchored FtsZ polymer networks as described in the previous section. Time-lapse fluorescence confocal microscopy revealed the formation of FtsZ dynamic wave-like patterns (**Figure 5.3**). Those propagating FtsZ waves resulted from the exclusion of FtsZ polymers on the membrane by the Min traveling waves. In particular, it is expected that MinC disrupt interactions between FtsZ subunits, as well as ZipA-FtsZ interactions to a lesser extent.

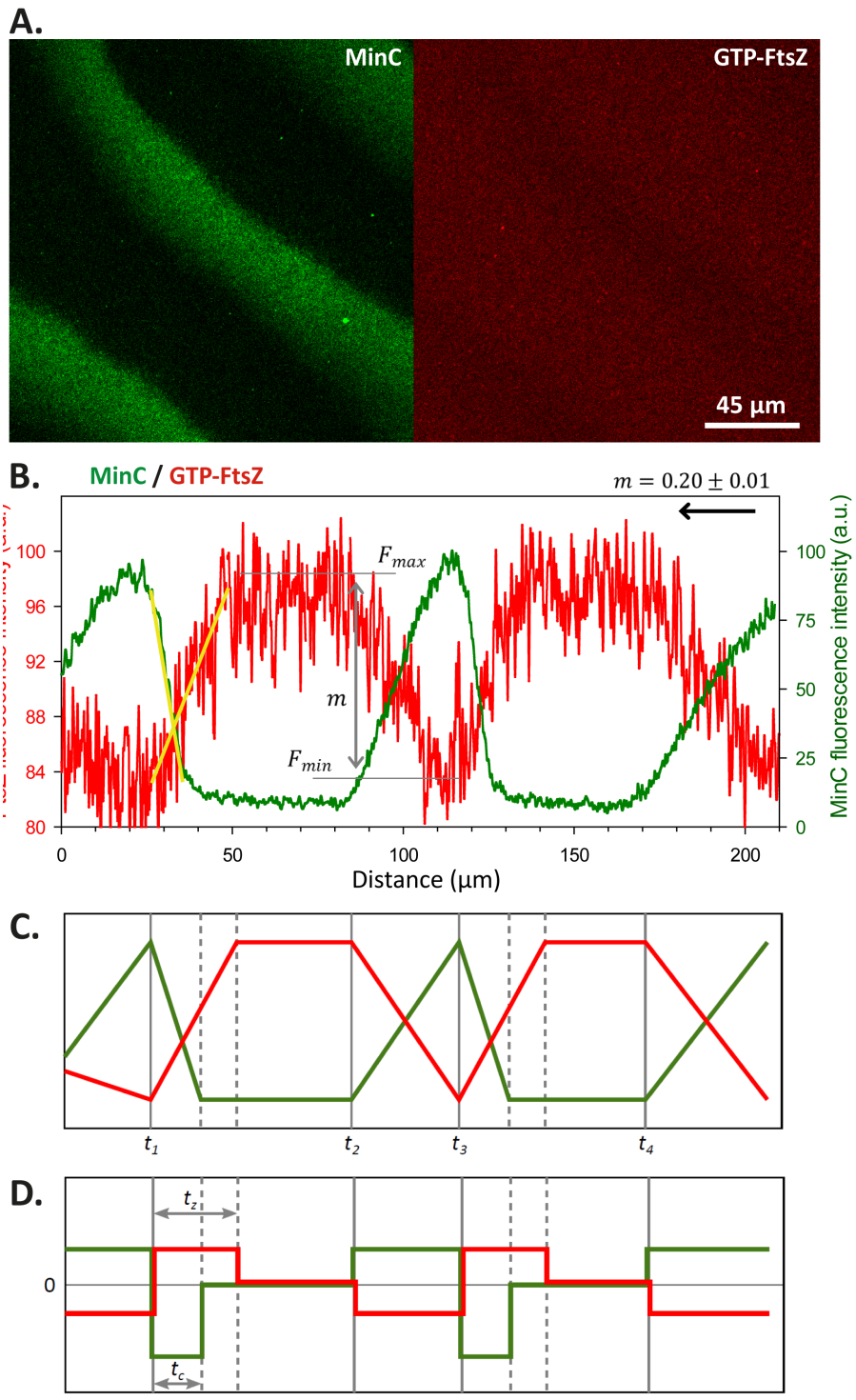

Figure 5.3. Dynamic coupling of MinCDE and FtsZ propagating waves on ZipA-SLBs. (A) Confocal fluorescence micrographs showing MinCDE (labelled protein: eGFP-MinC) and FtsZ (labelled protein: FtsZ-Alexa 647) waves, observed upon joint reconstruction on ZipA-SLBs. **(B)** Fluorescence intensity profiles of MinC and FtsZ acquired from the image shown in (A). MinC displaces FtsZ in such a way that the maximal intensity of FtsZ correlates with the minimal signal of MinC. While MinC has a sharp concentration maximum towards the rear of the wave, the maximum of FtsZ is relatively broad. The FtsZ wave observed in these conditions was characterised by a modulation value, *m*, of 0.20 ± 0.01. The arrow indicates the direction of the propagating wave. The slopes of the FtsZ and MinC profiles are highlighted with yellow lines. The wavelength of this wave is 95 µm, the period is 130 s, and the velocity is 0.73 µm/s. **(C)** Scheme of the MinC and FtsZ profiles. FtsZ reacts almost immediately to the decrease (times t_1 and t_3) and

increase (times t_2 and t_4) of MinC concentration on the membrane. **(D)** Scheme of the derivatives of the MinC and FtsZ profiles. The response of FtsZ to MinC during the membrane attachment phase is somewhat slower than that observed during detachment: MinC reaches its steady state after time t_c after the time point t_1, whereas FtsZ requires a longer time t_z.

The fluorescence intensity of the propagating wave-like pattern of FtsZ, which is proportional to the protein concentration at the membrane, reaches its maximum when the fluorescence signal of MinC is minimal, showing that oscillations of FtsZ and Min are in antiphase (**Figure 5.3.B**). Although MinC, like MinE (Loose *et al.*, 2008),(Loose *et al.*, 2011), has a sharp concentration maximum toward the rear of the wave, the maximum of FtsZ is relatively broad, coinciding with the broad minimum of the MinC wave (**Figure 5.3.B**). The temporal sequence of protein detachment and the shapes of the concentration profiles of Min proteins along the wave in these experiments did not significantly differ from the distributions previously obtained in the absence of FtsZ *in vitro* (Loose *et al.*, 2008). The ability of the MinCDE system to dynamically modulate the dislodgement (and subsequent recruitment) of FtsZ from (to) the membrane, i.e., the degree of coupling between the MinC and FtsZ waves *in vitro*, can be described by a modulation parameter (*m*). It is defined as the relative difference between the maximum and minimum fluorescence intensity of the FtsZ wave: $m = (F_{max} - F_{\min})/F_{max}$ (**Figure 5.3** and see Materials and Methods, section 3.5.1.1.). If the two systems were not coupled, FtsZ waves would not be observed in the presence of MinC, resulting in a value of *m* equal to zero. On the other hand, complete depletion of FtsZ in the wave minima would correspond to an *m* value equal to one. Under the conditions used in our assays (0.083 molar % of ZipA in the bilayer), the modulation value of the FtsZ waves was found to be 0.20 ± 0.01, suggesting a moderate regulation of FtsZ distribution by the Min system. The MinC and FtsZ waves are tightly coupled in time by the inhibitory interaction. Whenever the concentration of MinC starts to change, either by decreasing (times t_1 and t_3 in **Figure 5.3.C**) or increasing (times t_2 and t_4), FtsZ reacts almost immediately with a change in the opposite direction. However, the increase of FtsZ is somewhat slower than the change in MinC concentration: after the time t_1 (**Figure 5.3. C and D**) MinC reaches a steady state within t_c ~10 s, whereas FtsZ requires a longer time, t_z ~20 s. This slower response of FtsZ is consistent with the response of the FtsZ network to MinC occurring on a timescale on the order of 10 s (Arumugam *et al.*, 2014). In contrast, the opposite process—the decline of FtsZ with an increase of MinC—is tightly coupled in duration.

The presence of MinC, the element of the Min system that impairs FtsZ assembly, was essential in these experiments, as FtsZ waves were not observed on ZipA-SLBs with only MinD and MinE present (**Figure 5.4.**) The concentration of MinC in solution did not

significantly affect the modulation value m within the range of 0.06–0.3 μM (data not shown). Since the recruitment of MinC to the membrane by MinD results in a great increase in the concentration at the membrane (Hu *et al.*, 1999), small changes in the bulk concentration of MinC are not expected to have a big impact on the dynamics of the system. We consistently obtained these results using different combinations of fluorescently labelled proteins as tracers (data not shown).

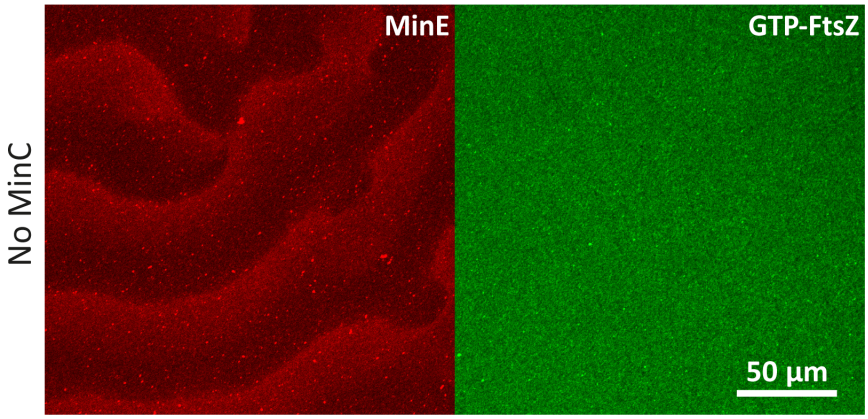

Figure 5.4. MinC is absolutely required for the coupling of MinCDE and FtsZ polymers. MinDE proteins (traced by MinE-Alexa 647) and FtsZ (traced by FtsZ-Alexa 488) were co-reconstituted on the ZipA-SLBs. FtsZ dynamic waves were not detected in absence of MinC.

5.1.3. The modulation of FtsZ-waves by MinC depends on ZipA concentration

We tested the recruitment of FtsZ to the bilayer in our system by reconstituting ZipA at different surface densities, from 0.018 to 0.083 molar % of ZipA in the bilayer, covering the estimated range of ZipA concentrations in the bacterial membrane (see Materials and Methods, section 3.4.4.2 Table 3.1). Preparations containing higher ZipA concentrations resulted in the formation of nonhomogeneous bilayers due to their high protein content, thus precluding their use. We observed that ZipA density modulates the above-mentioned coupling, as evidenced by the direct correlation observed between the modulation of the FtsZ waves and the amount of ZipA incorporated in the bilayer (**Figures 5.2.C and 5.5**). The wave modulation is stronger at higher ZipA densities, suggesting that the interaction of FtsZ with the membrane is modified in such a way that makes it more susceptible to the action of MinC.

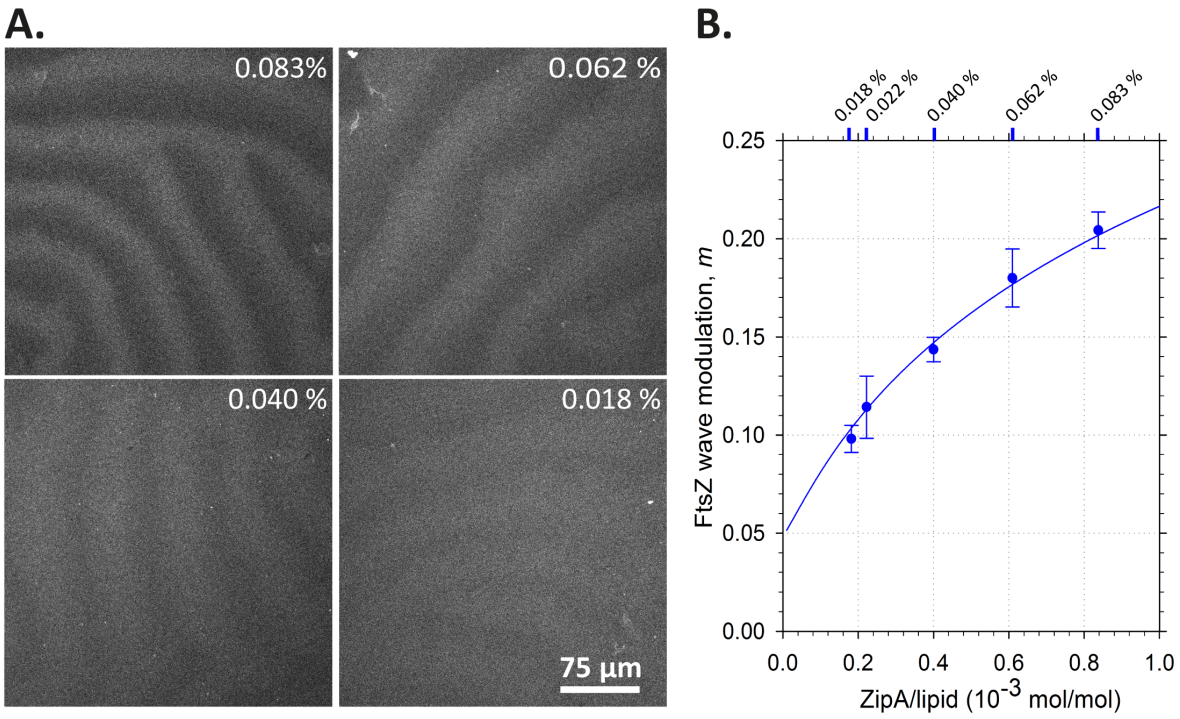

Figure 5.5. Effect of ZipA surface density on the modulation of the FtsZ waves driven by Min. (A) Confocal fluorescence micrographs showing FtsZ waves (traced by FtsZ-Alexa 647) on bilayers with different surface densities of ZipA (ZipA content as molar %). **(B)** Modulation of the FtsZ waves, *m*, depending on the surface density of ZipA on the membrane (●). The data shown correspond to the mean values of at least four independent experiments plotted with the corresponding standard error. The line shows the fitting of the proposed model (**5.3. Annex**) to the experimental data. The fit parameters were k_2/k_{-2} = 10.1 X 10^3 lipid, k_{-1}/k_1 = 1.89. **Figure 5.3. Annex.B** shows the concentrations b_i of FtsZ filaments anchored with *i* ZipA molecules for this fit.

The increase in wave modulation with the ZipA concentration observed in our experiments suggests that the structural organization of membrane-tethered FtsZ and/or its interaction with ZipA is modified at higher concentrations of ZipA. This leads to an increased susceptibility of FtsZ to MinC at the membrane. In addition, the experiments show that the FtsZ concentration at the membrane increases less than linearly with the ZipA concentration (**Figure 5.2.C**). One plausible explanation is that at higher ZipA densities, single FtsZ filaments are anchored to the membrane by several ZipA molecules, bringing them closer to the membrane and therefore increasing their rate of encounters with membrane-bound MinC (**Figure 5.3. Annex.A**). This idea leads to a model described in 5.3. Annex. Fitting this model to our data, the dependencies of FtsZ intensity on the membrane (**Figure 5.2.C**) and FtsZ wave modulation (**Figure 5.3.B**), shows that this model can describe our main experimental observations, i.e., the FtsZ concentration increases less than linearly with ZipA (**Figure 5.2.C**), and the FtsZ wave modulation increases with ZipA (**Figure 5.5.B**). In

addition, **Figure 5.3. Annex.B** shows the concentrations b_i of FtsZ filaments anchored with i ZipA molecules for this fit.

Notably, we found that alternative schemes to explain the Min-FtsZ coupling did not describe our experimental observations. One of them assumes that MinC could have a maximum capacity of FtsZ that it can remove from the membrane during the pass of the wave. This would mean that always the same amount of FtsZ would be removed, regardless of the total amount of FtsZ on the membrane. This would lead to decreasing modulation *m,* with higher ZipA, which is the opposite of what was observed in this work. Another possibility is that MinC is able to remove FtsZ from the membrane with an effective rate proportional to the concentrations of both MinC and FtsZ. In this case, always the same fraction of FtsZ would be removed independently of the ZipA concentration, resulting in a constant wave modulation *m,* which again does not describe the experimental observations.

The anchoring of FtsZ to the membrane through ZipA was required for the formation of anticorrelated FtsZ and MinCDE patterns. In the absence of ZipA, a small fraction of FtsZ was found to be transported within the MinCDE wave, giving rise to distinct correlated MinCDE and FtsZ patterns (referred to as MinCDE-FtsZ waves; **Figure 5.6**). In contrast to the FtsZ waves in the presence of ZipA (**Figure 5.3**), in its absence the FtsZ profile is correlated with the MinC profile (**Figure 5.6**). Although the MinC and MinD profiles are similar, when compared with the FtsZ profile without ZipA, FtsZ is closer to the MinC wave than to the MinD wave (**Figure 5.6.B and D**). The maxima of the FtsZ profile on these MinCDE-FtsZ waves are ~4-fold less intense than the maxima reached by FtsZ waves on ZipA-SLBs. In this situation, where ZipA is not present in the bilayer to tether FtsZ, the colocalization of MinC and FtsZ might indicate a weak transient interaction between MinC and GTP-FtsZ.

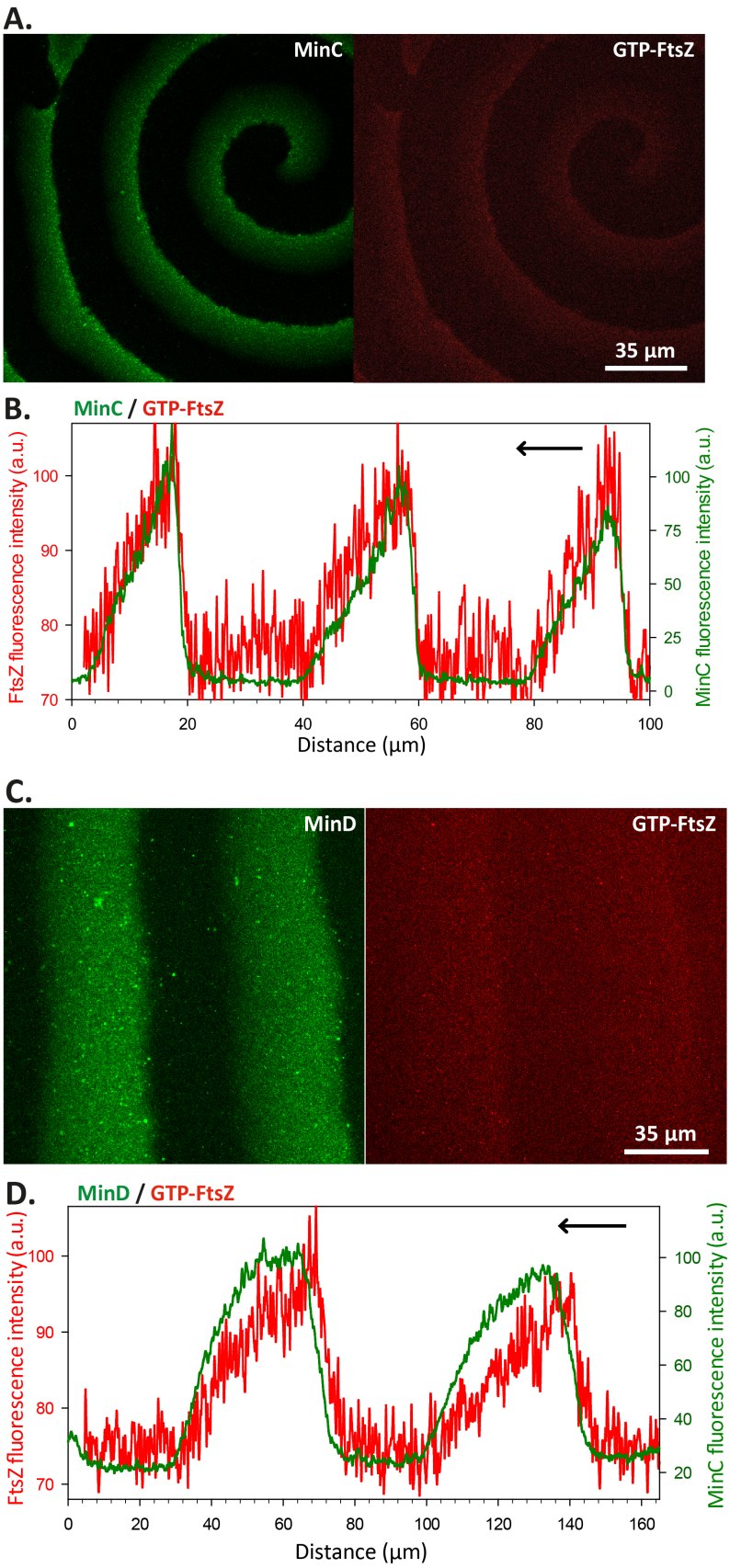

Figure 5.6. ZipA is required for the anticorrelated coupling of MinCDE and FtsZ. (A) Confocal fluorescence micrographs showing MinCDE-FtsZ waves (labelled proteins: eGFP-MinC and FtsZ-Alexa 647) observed upon joint reconstruction on bilayers without ZipA. **(B)** Fluorescence intensity profiles of MinC and FtsZ acquired from the image shown in A. **(C)** Confocal fluorescence micrographs showing MinCDE-FtsZ waves (labelled proteins: eGFP-MinD and

FtsZ-Alexa 647), observed upon joint reconstruction on bilayers without ZipA. **(D)** Fluorescence intensity profiles of MinD and FtsZ acquired from the image shown in C. In the absence of ZipA, a small fraction of FtsZ was found to be transported with the MinCDE wave by binding to MinC. In contrast to the situation described for ZipA-SLBs, where anticorrelated FtsZ and MinCDE patterns were observed, here FtsZ colocalizes with MinC, matching its profile.

5.1.4. Crowding enhances the coupling of membrane-tethered FtsZ polymers to Min waves

High concentrations of biochemically inert macromolecules, such as Ficoll 70, have commonly been used to simulate the natural crowding conditions found on the cytoplasm of *E. coli*. In the case of FtsZ, Ficoll 70 is known to promote the formation of dynamic, FtsZ polymer networks resulting from lateral interactions between protofibrils, which are thermodynamically favoured in crowded environments because they occupy less of the total volume (Gonzalez *et al.*, 2003) (Rivas *et al.*, 2013). As expected, bundles of FtsZ fibrils on ZipA-SLBs were found in the presence of high concentrations of Ficoll 70 (**Figure 5.7**).

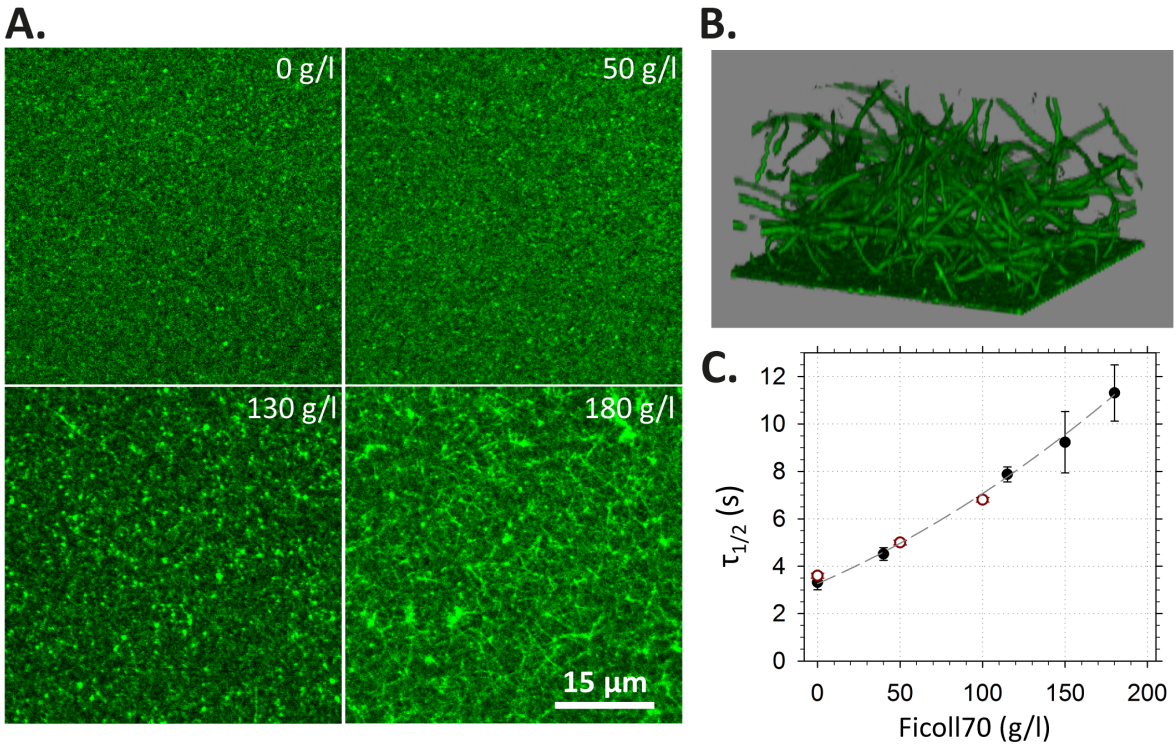

Figure 5.7. Confocal microscopy analysis of crowding-induced FtsZ assembly in ZipA-SLBs. (A) Confocal fluorescence images showing FtsZ networks formed on ZipA-SLBs in the presence of 0, 50, 130, and 180 g/L of Ficoll 70. **(B)** 3D reconstruction of confocal fluorescence images showing Ficoll-induced FtsZ bundles on ZipA-SLBs. The image was taken at 190 g/L Ficoll 70. These dense and dynamic 3D networks localize in solution and are connected to the bilayer by some fibbers. Frame size: 45 µm X 45 µm (4.4 nm per pixel). **(C)** Half-time turnover ($\tau_{1/2}$) of FtsZ subunits on the membrane depending on the Ficoll 70 concentration, as determined by FRAP (●) and image

correlation (○) (see Materials and Methods; section 3.5.1.2 Figure 3.3). Ficoll 70 significantly retards the subunit exchange within the polymer. The dashed line is an arbitrary curve drawn to guide the eye. The data shown correspond to the mean values of at least three independent measurements plotted with the corresponding standard error.

The addition of this crowding agent retarded the exchange of FtsZ subunits within the membrane-tethered polymer by up to 3-fold when compared with the exchange measured in the absence of Ficoll 70 (see above), as revealed by FRAP and correlation measurements (**Figure 5.7.C** and see Materials and Methods). The slowdown of the subunit turnover within the network by the increase of Ficoll 70 illustrates the formation of higher-order structures in a Ficoll-dependent manner, being compatible with the values previously measured in solution (Gonzalez *et al.*, 2003) (Anderson *et al.*, 2004).

At the same time, the effect of Ficoll 70 on the Min wave propagation was addressed. In the presence of increasing amounts of this crowder, both the wavelength (λ) and velocity (v) of the Min waves decreased, whereas the period (*T*, *T*= *λ*/*v*) remained practically independent of Ficoll 70 (~100 s; **Figure 5.8**). This effect can be tentatively linked to the lower diffusion coefficient of the Min proteins at higher Ficoll 70 concentrations.

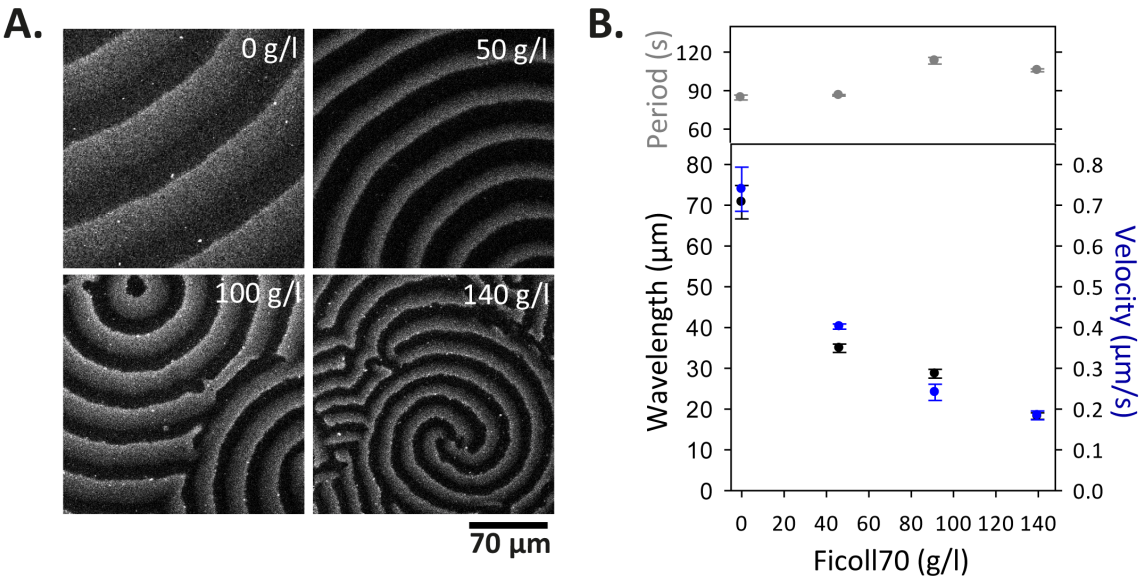

Figure 5.8. Effect of Ficoll 70 on Min wave propagation. (A) Confocal fluorescence micrographs showing MinCDE waves obtained in the presence of different Ficoll 70 concentrations (labelled protein: eGFP-MinD). **(B)** Both the wavelength (λ) and velocity (v) of the Min waves decrease with higher crowder concentration, while the period (T, T= λ/v) remains practically constant.

Above the threshold concentration of Ficoll 70 (at ~135 g/L), high-order FtsZ dynamic polymer filaments and networks were thick enough to be resolved by fluorescence confocal microscopy (**Figure 5.7.A and B**). Under these conditions, the turnover rate of FtsZ Ficoll 70 was found to be ~9 s, which is similar to the half-time of recovery of the bleached FtsZ region at the Z ring measured *in vivo* (Anderson *et al.*, 2004). In this situation, the lateral interactions between FtsZ fibbers are maximized and the modulation of the membrane-tethered FtsZ waves by MinC was substantially enhanced (m= 0.55 ± 0.01) (**Figure 5.9 and Movie 5.S1**), when compared with the coupling between the two systems measured in the absence of crowders (m= 0.20 ± 0.01). As noted above, the presence of crowders enhances the lateral interactions between FtsZ protofilaments, thus increasing the effective concentration of FtsZ on the membrane. This FtsZ network would contain more stretches of FtsZ not directly anchored to the membrane by ZipA. Thus, the substantial increase in wave modulation could be explained as follows: if MinC broke the network at these nonanchored parts, larger fragments of FtsZ could be released upon breakage, effectively enhancing the action of MinC, meaning that more FtsZ would be released after the same number of breakage events.

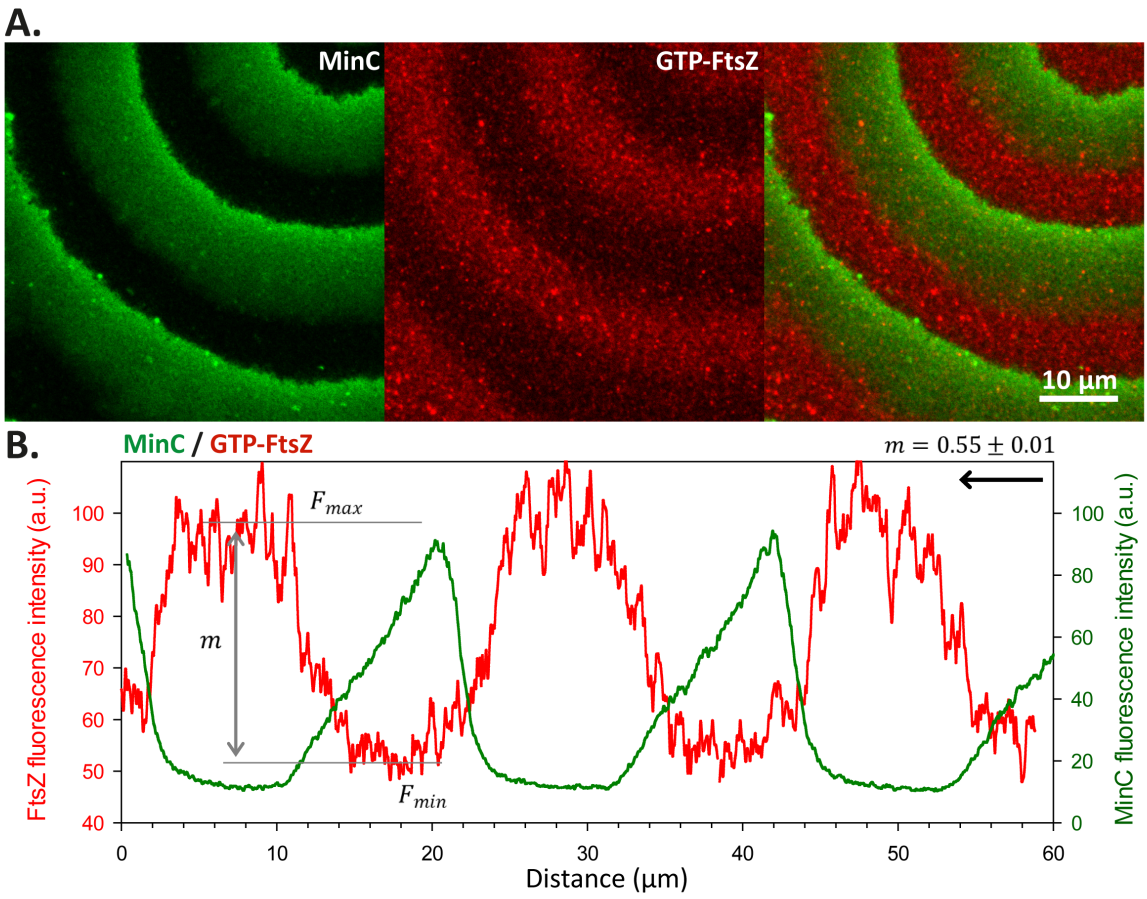

Figure 5.9. Dynamic coupling of crowding-induced FtsZ polymers in ZipA-SLBs to Min propagating waves. (A) Confocal fluorescence micrographs showing MinCDE waves (traced by eGFP-MinC) and the FtsZ network (traced by FtsZ-Alexa 647) to ZipA-SLBs in the presence of 130 g/L Ficoll 70. **(B)** Fluorescence intensity profiles of MinC and FtsZ acquired from the image shown in (A). The modulation value, *m*, of the FtsZ observed in these conditions was 0.55 ± 0.01. The arrow indicates the direction of the propagating wave. See also **Movie 5.S1**.

5.2. DISCUSSION

In this work, we investigated the interaction between the site-selection MinCDE system and two proteins that assemble in the *E. coli* proto-ring (the soluble FtsZ and the membrane-bound ZipA) in lipid bilayers as minimal membrane systems. We found that the Min system drives the dynamic distribution of FtsZ polymers when they are tethered to the membrane by ZipA, as revealed by confocal microscopy analysis, resulting in the dislodgment of FtsZ from the membrane and the subsequent generation of FtsZ wave-like patterns (**Figure. 5.10.A**). These rearrangements are mediated by MinC, the element of the Min system that acts as an inhibitor of FtsZ assembly. The dynamic coupling between the Min proteins and membrane-

associated FtsZ polymers is facilitated by experimental conditions that promote the accumulation of more FtsZ molecules in the vicinity of the membrane, as an increase in the ZipA surface concentration or crowding induces the formation of dynamic FtsZ polymer networks, leading to a relatively stronger exclusion of FtsZ from regions in which MinC waves reaches a maximum (**Figures 5.5 and 5.9**).

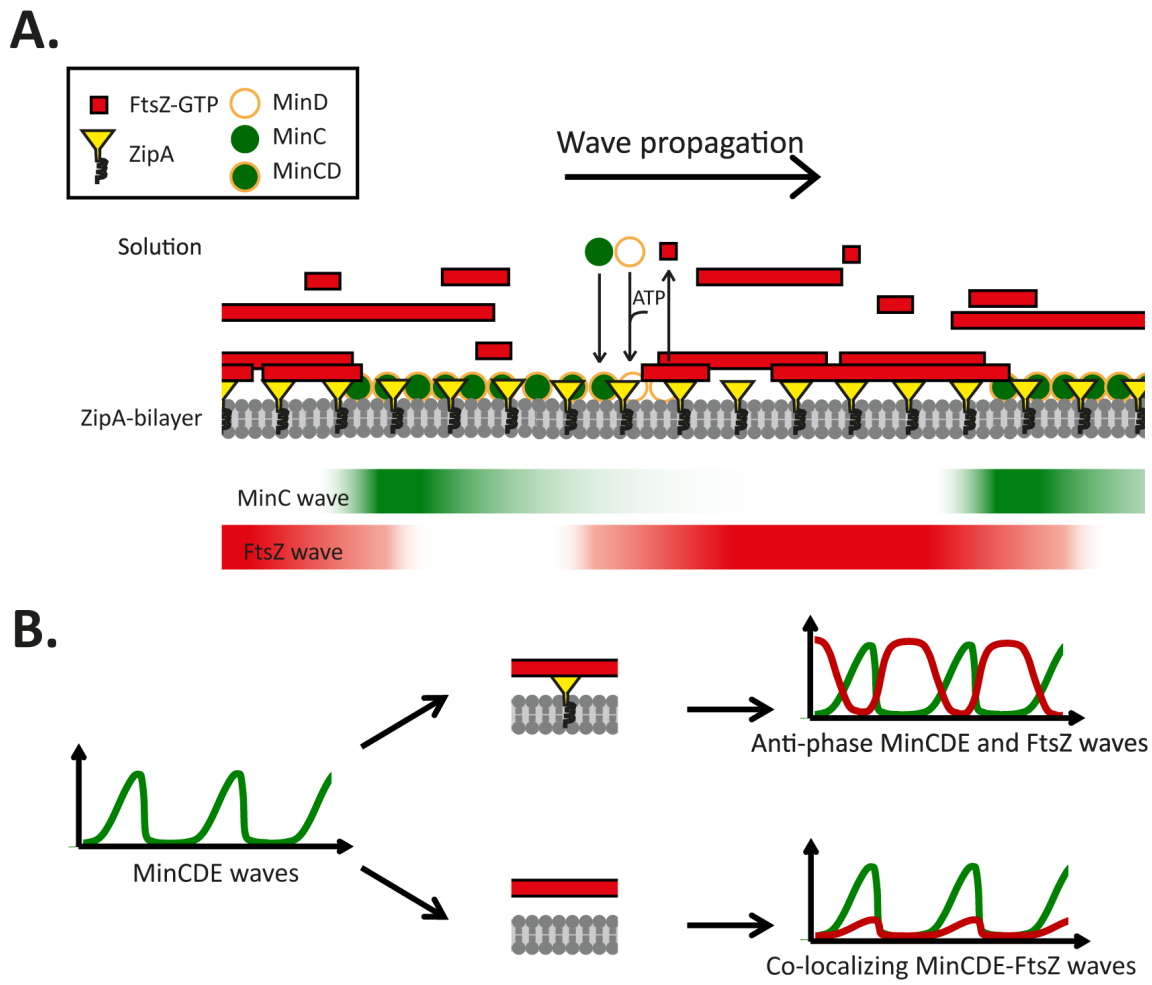

Figure 5.10. (A) Model showing the dynamic distribution of FtsZ polymers coupled to Min oscillations in membranes containing ZipA. In the Min system, MinD and MinE govern this oscillation behaviour. MinC is a weak inhibitor of FtsZ polymerization that together with the membrane-bound MinD forms an inhibitory complex, preventing FtsZ polymers from accumulating in its vicinity. MinE (omitted in this figure for simplicity) acts on the membrane-bound MinCD complex and induces its dissociation. In this work, the MinCDE waves were observed by time-resolved confocal imaging as they displaced the fluorescent signal of FtsZ from the membrane. Thus, a maximal concentration of MinC correlates with a minimal concentration of FtsZ on the membrane. The Min-FtsZ coupling is facilitated at high surface densities of ZipA and enhanced by crowding-induced lateral interactions of FtsZ polymers (for simplicity, crowders are not represented here). **(B)** Effect of membrane recruitment of FtsZ polymers by ZipA: FtsZ waves in antiphase with the MinCDE waves are formed when FtsZ is anchored to the membrane through ZipA, resulting in an efficient dislodgment

of FtsZ from the membrane regions where MinC is present. Correlated MinCDE and FtsZ waves are found when FtsZ is not anchored to the membrane by ZipA.

The reconstruction strategy we used allowed us to investigate the influence of membrane tethering on the response of FtsZ polymers to the action of the oscillating Min system (**Figure 5.10**). In this way, we found that although Min-mediated FtsZ waves are formed when FtsZ is associated to the membrane through ZipA, they are not observed in the absence of ZipA, when FtsZ is free in solution. Interestingly, in this case, correlated MinCDE and FtsZ waves emerged in the presence of GTP to trigger FtsZ polymerization, as further elaborated below (**Figure 5.10.B**).

From our results, we can conclude that the association of FtsZ to the membrane by ZipA plays an important role in the counter-oscillations of FtsZ polymers promoted by the Min system. This is consistent with the Min-driven FtsZ waves observed using the variant of FtsZ (FtsZ-YFP-mts) (Zieske and Schwille, 2014) (Arumugam *et al.*, 2014) (Bisicchia *et al.*, 2013). The interaction of FtsZ with ZipA takes place through the C-terminal end of FtsZ (Mosyak *et al.*, 2000), which also interacts with the C-terminal domain of MinC (Shen and Lutkenhaus, 2009) and other division-related proteins (Haney *et al.*, 2001) (Ma and Margolin, 1999), acting as a central hub to integrate multiple interactions that modulate the assembly of the division machinery. Our findings suggest that the affinity of MinC (in complex with MinD at the membrane) for FtsZ is higher than the association of FtsZ with ZipA, thus resulting in the displacement of FtsZ polymers from the membrane. The latter is compatible with the well-established role of the interaction between the C-terminal regions of MinC and FtsZ in disrupting the lateral associations of FtsZ molecules in the polymer (Shen and Lutkenhaus, 2009). A significant fraction of the FtsZ subunits in the membrane-bound polymer network will have C-terminal regions accessible for interactions with MinC, allowing them to respond also to MinC and leading to a strong FtsZ coupling to the Min waves, as occurs in the case of multistranded polymers formed in macromolecularly crowded solutions.

The experiments showing that a fraction of soluble FtsZ polymers comigrated with Min waves in the absence of ZipA provide additional clues as to the mechanisms of interaction between MinC and FtsZ. These correlated MinCDE and FtsZ waves were not found in the presence of GDP, suggesting that GTP-containing FtsZ polymers, but not GDP forms, bind to MinCD at the membrane. This behaviour may indicate that the interaction between MinCD and GTP-FtsZ polymers at the membrane is stronger than the interaction between MinCD and GDP-FtsZ species. Structural changes in MinC as it interacts with MinD at the

membrane may explain why MinC alone, in contrast, preferentially binds to GDP-bound FtsZ (Arumugam *et al.*, 2014) (Hernandez-Rocamora *et al.*, 2013).

The observations reported here strongly suggest that ZipA may play an important regulatory role in Z ring placement guided by the Min system in *E. coli* cells. It is known that the recruitment of ZipA and FtsA to the division ring at midcell depends on FtsZ (Addinall and Lutkenhaus, 1996) (Hale and de Boer, 1999). Consistent with our findings, one of the functions of the Min proteins may be to couple their dynamic oscillating behaviour to guide the attachment of FtsZ to the membrane by the action of ZipA and, to a lesser extent by FtsA, given the rapidly reorganizing FtsZ polymers driven by FtsA (Loose and Mitchison, 2014).

Our results may also help to clarify some of the puzzling features of the proposed stages in the assembly of the *E. coli* proto-ring. FtsA may provide a link between FtsZ and the membrane weaker than that conferred by ZipA, as both the interactions between FtsA and the membrane, and between FtsZ and FtsA are thought to be weaker than the equivalent interactions provided by ZipA. Additionally, FtsA is displaced from the Z ring *in vivo* more readily than ZipA (Shen and Lutkenhaus, 2009). However, the initial stage of proto-ring assembly may still be orchestrated by the association of FtsZ to the membrane through FtsA if, for example, soluble FtsZ-FtsA hetero-complexes are the ones that preferentially bind to the membrane. In the absence of ZipA, these FtsZ polymers, once associated to the membrane, would be very dynamic, in agreement with the coordinated streams of FtsZ polymers and chirally rotating rings observed upon the co-reconstitution of FtsZ and FtsA in lipid bilayers (Loose and Mitchison, 2014). This observation can be reconciled with the role of ZipA in proto-ring stabilization if after the first stage of assembly, driven by FtsA, a second stage involving a competition between ZipA and FtsA for the C-terminus of FtsZ (given the relatively stronger binding affinity for FtsZ of ZipA) occurs, as a result of which FtsA is replaced by ZipA in the attachment of FtsZ to the membrane. In this way, FtsA is then free to recruit late division proteins, such as FtsN and FtsI (Rico *et al.*, 2004), to assemble the molecular machinery for cytokinesis.

In line with the results described here, dynamic FtsZ oscillations have also been observed in *E. coli* cells, showing a period of oscillation similar to that of the Min proteins (Bisicchia *et al.*, 2013) (Thanedar and Margolin, 2004) (Tonthat *et al.*, 2013). Interestingly, in these in vivo studies it was found that MinCDE drives the counter-oscillation of early division proteins, such as ZipA, along with FtsZ (Bisicchia *et al.*, 2013), suggesting that a fraction of ZipA moves along the membrane with FtsZ. Our observations of anticorrelated waves of FtsZ

driven by the Min system in minimal membranes, obtained under defined conditions, complement the *in vivo* counter-oscillation of FtsZ along with ZipA reported by Bisicchia et al. (Bisicchia *et al.*, 2013). The high complexity of the cellular environment precludes us from proposing a simple molecular description of the observed co-oscillation of FtsZ and ZipA. Therefore, it remains to be determined whether the observed mobility is conferred by, for example, the interaction between ZipA and FtsZ-GDP or even the interaction of ZipA with other division proteins.

In summary, the data presented here show that the bacterial division protein FtsZ, when associated to the membrane through ZipA, assembles into antiphase dynamic patterns by the action of the site-selection Min system. The presence of MinC is required for the formation of the FtsZ propagating waves, suggesting that this FtsZ ring inhibitor, when complexed to MinD, has a higher affinity for the central hub of FtsZ than ZipA, resulting in the displacement of FtsZ polymers from the membrane. The reconstruction approach adopted here, using ZipA as a natural membrane tether of FtsZ, is uniquely suited for exploring the impact of FtsZ membrane attachment on Min-FtsZ coupling. In this way, we have shown that when FtsZ is free in solution, a fraction of FtsZ polymers comigrate with the Min waves instead of forming the Min-mediated antiphase FtsZ waves observed in ZipA-containing membranes. This evidence suggests that ZipA, in addition to its role in proto-ring stability, is of central importance for the dynamic coupling between the self-oscillating Min system and the remodelling of FtsZ polymers at the early stages of division in *E. coli*, contributing to the efficient selection of the division site. This study may help to elucidate the conditions needed to generate Min-FtsZ dynamic patterns inside cell-like compartments, eventually leading to a controlled division of these containers.

5.3. ANNEX: Model of FtsZ·ZipA complex at membranes

The model to describe the hypothesis that single FtsZ filaments are anchored to the membrane by several ZipA molecules was developed by Dr. Zdeněk Petrášek. In this model it is assumed that free ZipA (= A) binds FtsZ (= Z) from the solution with a rate constant k_1 to form FtsZ complexes anchored to the membrane with one ZipA molecule (= ZA_1, with concentration b_1) (Equation 5.3.1). FtsZ can also dissociate from ZipA (with a rate constant k_{-1}) resulting in its dislodgment from the membrane. Additionally, FtsZ anchored to the membrane with i ZipA molecules (= ZA_i, with concentration b_i) can either bind one more ZipA (with a rate constant k_2) to form FtsZ complexes anchored with $i+1$ molecules, or dissociate one ZipA (with a rate constant k_{-2}) to form FtsZ anchored with $i-1$ molecules (Equation 5.3.2).

$$\mathrm{Z} + \mathrm{A} \underset{k_{-1}}{\overset{k_1}{\leftrightarrow}} \mathrm{ZA}_1 \tag{5.3.1}$$

$$\mathrm{ZA}_i + A \underset{k_{-2}}{\overset{k_2}{\leftrightarrow}} \mathrm{ZA}_{i+1} \tag{5.3.2}$$

The total concentration of ZipA on the membrane is a_0, the concentration of free (not bound to FtsZ) ZipA is a, with the rest of ZipA being bound to FtsZ. The following rate equations then describe the system:

$$db_1/dt = k_1 a - k_{-1} b_1 - k_2 b_1 a + k_{-2} b_2 \tag{5.3.3}$$

$$\mathrm{d}b_i/\mathrm{dt} = k_2 b_{i-1} a - k_{-2} b_i - k_2 b_i a + k_{-2} b_{i+1} \tag{5.3.4}$$

$$\mathrm{d}b_N/\mathrm{dt} = k_2 b_{N-1} a - k_{-2} b_N \tag{5.3.5}$$

$$a_o = a + \textstyle\sum_{j=1}^{N} j b_j \tag{5.3.6}$$

where N is the maximum number of ZipA molecules bound to one FtsZ filament (limited by the filament length). We assume steady state, with all time derivatives on the left side set to zero. The total concentration of membrane-bound Z b is then:

$$b = \textstyle\sum_{j=1}^{N} b_j \tag{5.3.7}$$

and the FtsZ fluorescence on the membrane is proportional to b: $F = \alpha b$ (**Figure 5.2.C**). The FtsZ filaments with more ZipA anchors will be more susceptible to MinC; we can assume that the susceptibility of a filament will be directly proportional to the number of its ZipA anchors. The susceptibility of all the bound FtsZ will then be proportional to $\sum_{j=1}^{N} jb_j$, and the wave modulation *m* will be proportional to the fraction of susceptible FtsZ relative to the total FtsZ:

$$m = m_0 \frac{\sum_{j=1}^{N} jb_j}{b} \tag{5.3.8}$$

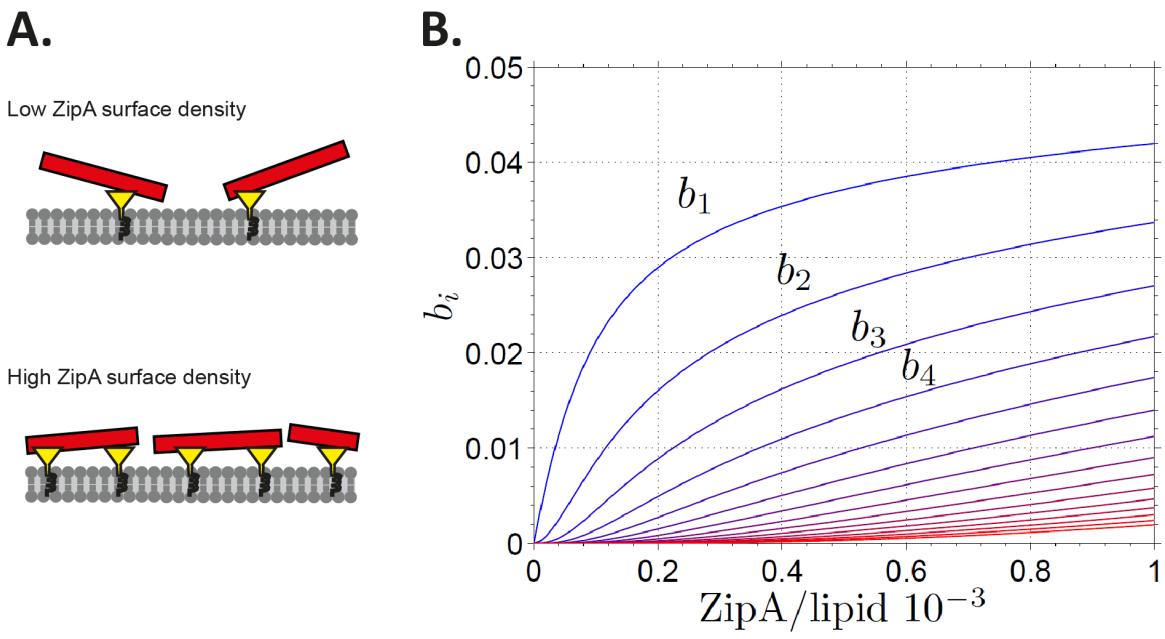

Figure 5.3. Annex: (A) At low ZipA concentration most FtsZ filaments are anchored by one ZipA and parts of filaments are out of reach of the MinCD complex. At high ZipA concentration FtsZ filaments are attached by more ZipA molecules, bringing the filament closer to the membrane and making them more susceptible to MinCD. **(B)** Membrane concentrations b_i of FtsZ protofilaments with i ZipA anchors as obtained from the model described above (Equations 5.3.1-8). While at low ZipA concentration there are mainly FtsZ filaments with one or two anchors, filaments with more anchors are abundant at high ZipA densities.

ACKNOWLEDGEMENTS

This work was done in collaboration with Ariadna Martos[1], Mercedes Jiménez[2], Zdeněk Petrášek[3], Germán Rivas[2], Petra Schwille[1]

[1]Max Planck Institute of Biochemistry. Am Klopferspitz 18. D-82152 Martinsried, Germany.
[2]Centro de Investigaciones Biológicas, CSIC. Ramiro de Maeztu 9, 28040 Madrid, Spain.
[3]Institut für Biotechnologie und Bioprozesstechnik, TU-Graz. Petersgasse 10-12/I, 8010 Graz, Austria.

6. Co-reconstitution of the FtsA-FtsZ-MinCDE system in bilayers: Min-FtsZ coupling is controlled by MinC and the FtsZ membrane tethering element

The FtsA protein interacts with FtsZ at early stages of cell division in most bacteria forming part of the first molecular assembly of the divisome at the membrane (the proto-ring), which acts as a scaffold to recruit the remaining elements of the division ring driving cytokinesis. The assembly of the ring is highly regulated in time and space by several mechanisms, one of them involving the self-oscillating MinCDE protein complex. In this work, we have optimized the protocol of FtsA purification allowing us to obtain a soluble and active protein, which exists as a mixture of monomers and oligomeric species, and binds membrane lipids with moderate affinity. FtsA-FtsZ self-organization assays on flat supported membranes showed that these proteins assemble into dynamic chiral vortices mediated by the GTPase activity of FtsZ whose diameters resemble the cell circumference. The presence of propagating waves of MinCDE in the FtsA-FtsZ system resulted in the formation of Min-FtsZ co-migrating waves, as revealed by confocal microscopy, which are similar to the ones previously observed when FtsZ was free in solution, in the absence of membrane tethering elements. This behaviour contrasts with the waves of FtsZ polymers driven by MinCDE when FtsZ is associated to the membrane by ZipA. These findings suggest that the susceptibility of FtsZ polymers to spatial regulation by MinCDE – driven by MinC - depends on the nature of the FtsZ tethering element, being FtsA or ZipA.

6.1. RESULTS

6.1.1. FtsA purified by the SUMO-fusion-system forms monomers and oligomers, interacts with *E. coli* lipids and recruits FtsZ to the membrane

In section 5, the dynamic reorganization of FtsZ polymers in ZipA-containing membranes by the action of the MinCDE system resulting in the formation of FtsZ waves was described. In this section, we have examined the effect of FtsA in the coupling between FtsZ polymers and MinCDE complex. This requires the production of a soluble functional FtsA, which it is a challenge because FtsA is a recalcitrant protein with high tendency to aggregate. Previously, in our laboratory, FtsA was purified from inclusion bodies by His_6-FtsA over-expression and a subsequent refolding step (Martos *et al.*, 2012). More recently, a new FtsA purification protocol has been reported using a SUMO construct which allows to obtain the untagged protein in a soluble form (Loose and Mitchison, 2014). Here, FtsA was purified following this protocol, using the same pML29 plasmid, with some modifications, the principal one being the addition of CHAPs detergent, which was removed in a final step by size exclusion chromatography, to enhance FtsA solubility (see Materials and Methods, section 3.2.4.).

The yield of the FtsA purification process was around 0.35 mg of protein/L of culture. SDS-PAGE allowed determining that FtsA was 95% pure (**Figure 6.1.A**) and the electrophoretic migration of purified FtsA was compatible with that expected for a protein with a molecular weight of around 45 kDa. The highest concentration of soluble FtsA that we obtained was 0.7 g/L (15 μM), which was around 3 times lower that the one reported by Loose and Mitchison (Loose and Mitchison, 2014).

After evaluation of the purity of FtsA, analytical ultracentrifugation was used to characterise the association state of the protein in solution. Distributions of sedimentation coefficients, obtained from SEDFIT analysis of the sedimenting boundaries in presence of ATP or ADP, showed some polydispersity, with a mayor (40%) slow species at s= 2.7 $\pm$ 0.1 S and a frictional relation 1.4, compatible with monomeric FtsA (**Figure 6.1.B**). Therefore, the sedimentation velocity data allowed determining that the association state of FtsA was not affected by ATP or ADP. These sedimentation coefficient values were in good agreement with the experimental findings described previously using refolded His_6-FtsA purified from inclusion bodies (Martos *et al.*, 2012). Martos and co-workers reported a theoretical s-value (2.8 S) for monomeric FtsA and also stated that ATP or ADP did not influence the sedimentation behaviour of FtsA.

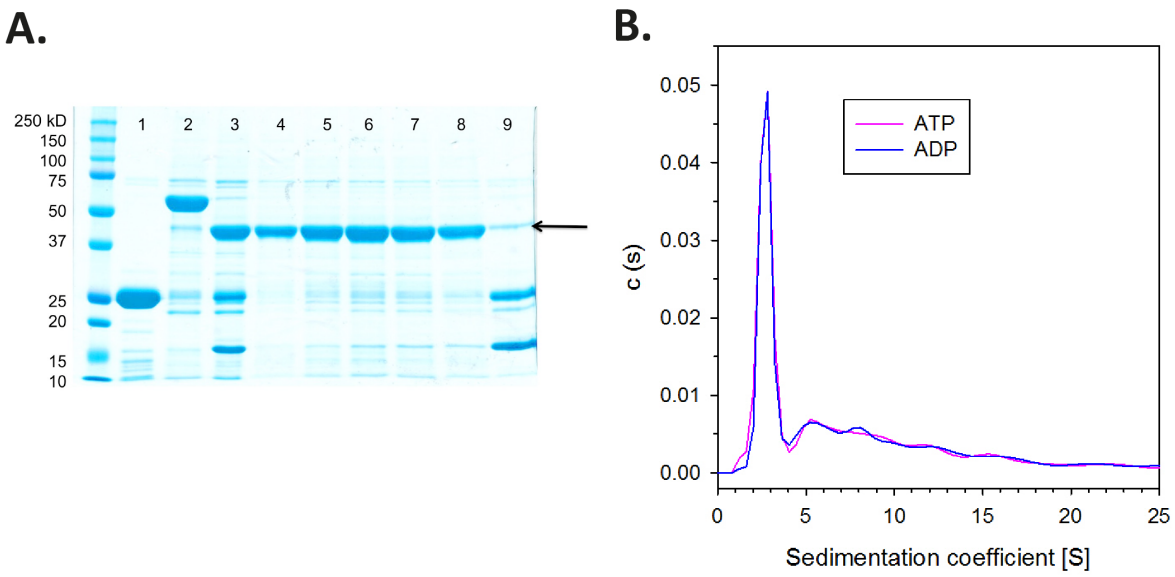

Figure 6.1. Purification and molecular characterization of FtsA. (A) SDS-PAGE (12%) analysis of FtsA purification (1: SUMO Protesase, 2: FtsA-SUMO before enzymatic digestion, 3: FtsA, SUMO Protease and SUMO target protein after enzymatic digestion, 4-8: Purified FtsA after chromatography step, 9: SUMO Protease and SUMO target protein). The black arrow points towards FtsA bands. **(B)** Sedimentation coefficient *c(s)* distribution of *E. coli* FtsA (0.2 g/L) in the presence of 1 mM of ATP or 1 mM ADP, generated from sedimentation velocity interference data. The predominant species are compatible with a monomeric protein, with a s-value of 2.7 ± 0.1 S. The rest of the species (60%) correspond to a wide distribution of oligomers.

To further characterise the purified protein, the capacity of FtsA to bind *E. coli* lipids was analysed using two different biomimetic membrane systems: lipid coated silica microbeads and supported lipid bilayers (SLBs). The first approach allows reconstituting different proteins in lipid membranes and measuring the apparent binding affinity of a protein for the membrane. To quantify FtsA binding affinity to *E. coli* lipid membrane, co-sedimentation assays were performed with silica microbeads, coated with the *E. coli* lipids mixture. FtsA labelled with Alexa 488 at 0.5 µM concentration, in the presence of 1 mM ATP (FtsA-ATP) or in the absence of this nucleotide (FtsA-ADP), were essayed. Preliminary binding results showed that the apparent affinity constant determined for FtsA was in the micromolar range, indicating a moderate affinity for the *E. coli* lipids (**Figure 6.2**). In addition, FtsA interaction with *E. coli* lipids was not sensitive to the presence of 1 mM of ATP. These results are compatible with those reported for the His-tagged protein obtained by refolding (Martos *et al.*, 2012). Consequently, untagged FtsA purified from SUMO construct seems to behave very similar to refolded His_6-FtsA that was purified from inclusion bodies.

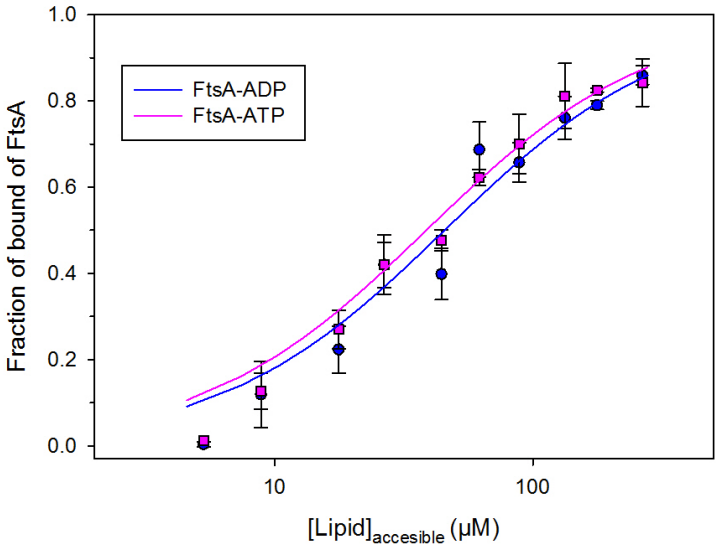

Figure 6.2. FtsA binding to *E. coli* lipids coated microbeads. Assays were done in the presence of ATP (pink squares) and in the absence of ATP (blue circles). Solid lines represent the best fit of Equation 3.4 to the data. The values of the apparent affinity constant were $(2.6 \pm 0.1) \cdot 10^4$ M^{-1} in the presence of ATP and $(2.2 \pm 0.2) \cdot 10^4$ M^{-1} in the absence of the nucleotide.

It was also verified whether soluble FtsA was capable of binding to *E. coli* lipids in supported lipid bilayers. Consistent with our findings with the coated microbeads system, FtsA was also able to interact with *E. coli* lipids in SLBs (data not shown). Then, co-reconstitution assays using FtsA and wild-type FtsZ were conducted in supported membranes to ascertain if the purified FtsA was able to anchor FtsZ to the membrane. TIRF microscopy images confirmed that FtsA recruited FtsZ polymers to the lipid bilayer in the presence of ATP and GTP, and that both proteins self-organize forming dynamic rings on the membrane (**Figure 6.3 and Movie 6.S1**). Therefore, FtsZ filaments tethered by FtsA were highly dynamic in agreement with previous reports (see section 4) (Loose and Mitchison, 2014) (Bisson-Filho *et al.*, 2017) (Yang *et al.*, 2017), where FtsZ filaments apparent rotation was explained by a treadmilling process.

The directional ring dynamics was confirmed by the positive slope tendency of kymographs generated along the ring circumference (**Figure 6.3.B**). Using kymograph analysis, we determined that the rotational speed of these structures was around 30 nm/s (**Figure 6.3.C**) implying that one full rotation takes 1.7 min. Interestingly, the rotational speed values determined for these rings are in the same range as those obtained for membrane-tethered FtsZ dynamic vortices (**Figure 6.3 and Section 4, Figure 4.10**). Morover, *in vivo* treadmilling velocities established in recent studies are in good agreement with our findings (30 nm/s), (Bisson-Filho *et al.*, 2017;Yang *et al.*, 2017), in contrast with the faster FtsA-FtsZ

rings velocities previously reported (108 nm/s), (Loose and Mitchison, 2014) using the same protein concentration ratios and ionic strength in the buffer. One possible explanation for this discordance could be that our experimental studies were performed using only the wild-type proto-ring elements, whereas in this prior study Cys-FtsZ and FtsA mutants were used to label the proteins.

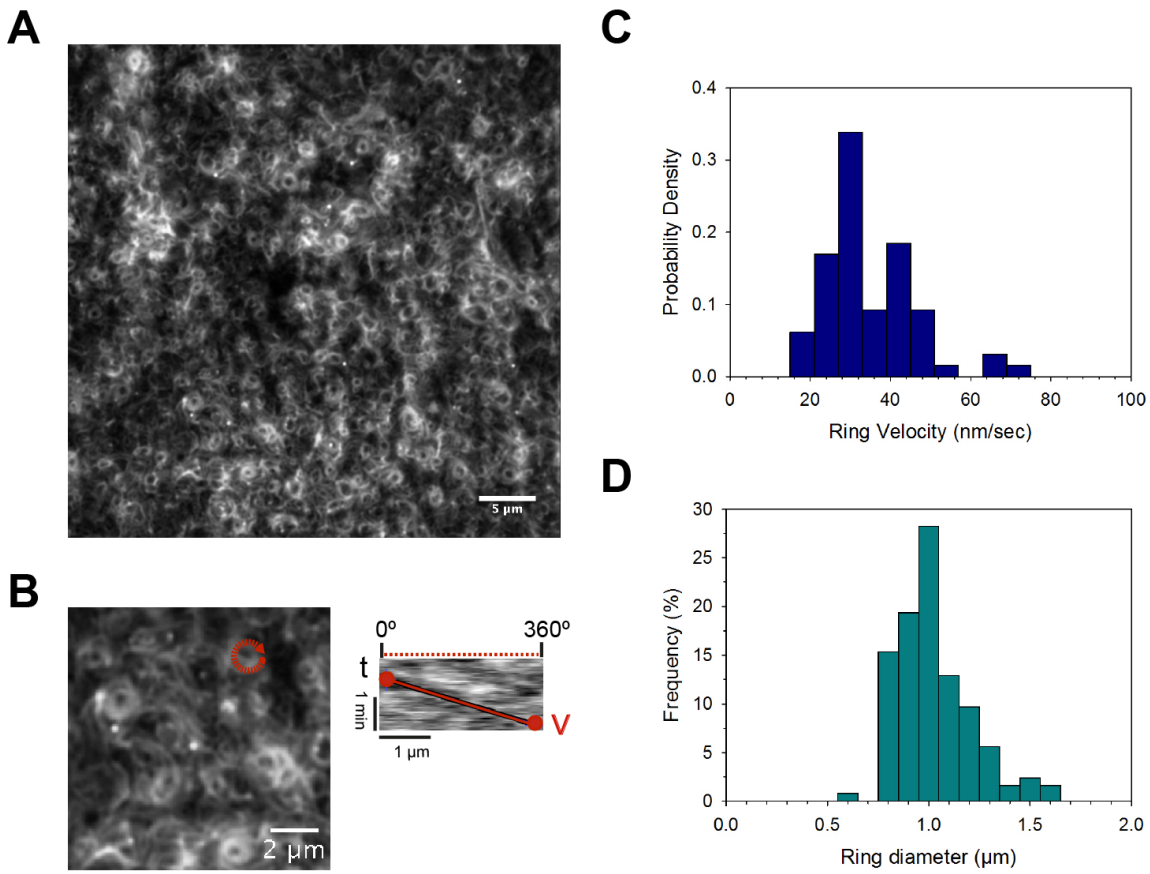

Figure 6.3. FtsA attaches FtsZ polymers to the membrane forming dynamic cytoskeletal patterns. (A) Representative TIRFM image of 1.5 µM FtsZ- (traced by FtsZ-Alexa 488) attached by 0.5 µM FtsA to the *E. coli* lipids bilayer, in the presence of 4 mM GTP and 5 mM Mg^{2+}. **(B)** Left: Representative image of FtsA-FtsZ rings rotating clockwise (see also Movie 6.S1). Right: Kymograph of the vortex computed from the intensity along the red circle showed in the left TIRFM image. **(C)** Velocity distributions for FtsA-FtsZ rings, with a predominant population at rotational speed values around 30 nm/s, N=65 rings. **(D)** Ring size distributions with average diameters of 1.0 ± 0.3 µm, N = 126 rings.

When the diameter of the FtsA-FtsZ vortices was analysed, we obtained a distribution of values from 0.6 to 1.6 µm with a mean ring diameter of around 1 µm (**Figure 6.3.D**). These values are consistent with *E. coli* cell diameter (Moran *et al.*, 2010), and similar to what was

shown for the chimeric FtsZ (see **Section 4, Figure 4.7**) and for FtsA-FtsZ self-organization in a previous work (Loose and Mitchison, 2014).

Taken together, our results evidenced that FtsA-FtsZ dynamic vortices were characterised by a similar pattern than the rings described using FtsZ-YFP-mts (Section 4) or FtsA-FtsZ (Loose and Mitchison, 2014) in preceding self-organization assays. These findings confirm that our FtsA purification protocol optimization produced an active protein that possesses the ability to interact with *E. coli* lipids with a moderate affinity and recruits FtsZ filaments to the membrane allowing a rapid reorganization of the filament network.

6.1.2. FtsZ membrane tethering rules the coupling between the Min system and FtsZ waves

Once we tested that the proto-ring proteins FtsZ and FtsA self-organized in supported lipid membranes, we aimed to reconstitute the MinCDE complex together with FtsA and FtsZ in supported lipid bilayers, similarly to the study performed using the other component of the proto-ring, ZipA (see Section 5). This approach intended to study the effect of the FtsZ membrane anchoring protein in this MinCDE-FtsZ dynamic coupling behaviour. The reconstitution of MinCDE proteins complex and FtsZ using FtsA as the membrane anchor was performed using flat membranes and micro-compartment systems.

- ***6.1.2.1 Reconstitution of FtsA, MinCDE and FtsZ in flat membrane systems***

After proving that purified FtsA was capable of recruiting FtsZ polymers to the membrane (**Figure 6.3 and 6.4.A**), we asked whether MinCDE oscillation waves could be formed when FtsA was attached to the membrane. As shown in **Figure 6.4.B**, FtsA was evenly distributed on the membrane and it was not spatially organized when MinCDE were self-organized into periodic travelling waves on the membrane. The dynamic behaviour of the Min system observed in these experiments, as characterised by velocity, wave period, and wavelength, was similar to that reported previously (see Section 5) (Loose *et al.*, 2008). MinCDE proteins were able to form patterns which did not have an overall preferred orientation, such as spirals and parallel waves, as in the absence of FtsA (data not shown). This indicated that FtsA anchored to the lipid membrane did not disrupt the characteristic MinCDE system oscillation pattern.

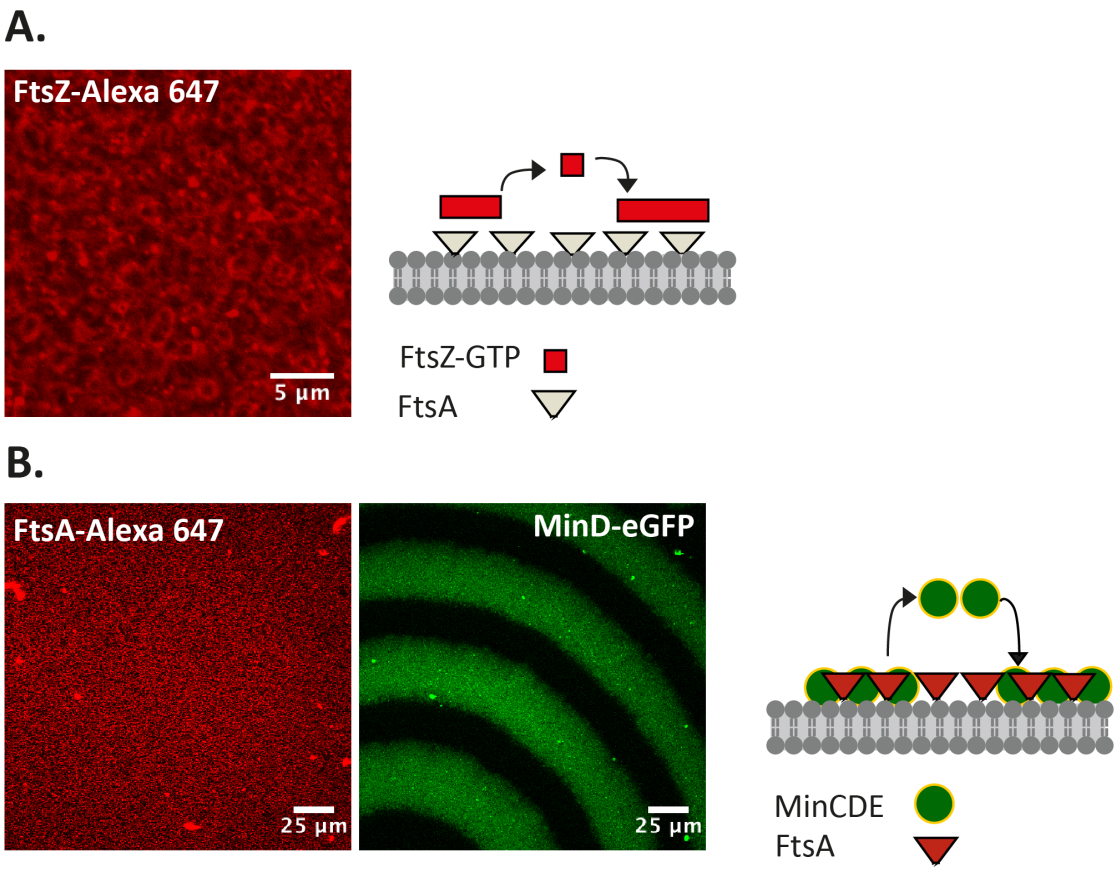

Figure 6.4. **FtsA recruits FtsZ to the membrane and allows a complete MinCDE self-organization on the membrane**. **(A)** Confocal fluorescence micrograph of FtsZ-Alexa 647 (1.5 µM) along with 4 mM GTP, attached by FtsA (unlabelled, 0.5 µM) to an *E. coli* lipid bilayer. FtsA and FtsZ self-organize on the membrane forming dynamic ring patterns (see also **Figure 6.3**). The schematic drawing of the experimental conditions is showed on the right of the confocal image. FtsZ polymers were not observed on the membrane when FtsZ-GTP was added to the lipid bilayer without FtsA or ZipA (data not shown). **(B)** MinCDE dynamic waves were found in the presence of FtsA anchored to the membrane. Confocal fluorescence images showing 0.5 µM FtsA (labelled protein: FtsA-Alexa 647) layer on the membrane along with 2.5 mM ATP and MinCDE dynamic waves (1 µM MinD, 1 µM MinE, 0.06 µM MinC; labelled protein: eGFP-MinD). Schemes illustrating the disposition of the elements are showed on the right of the confocal microscopy images.

Subsequently, we examined the recruitment of FtsZ to the lipid bilayer through FtsA in the presence of the oscillating MinCDE complex. To test this, we used two different approaches, which consisted in adding FtsA protein to the sample before MinCDE protein addition or after observing organized MinCDE propagating waves on the membrane. In both instances, FtsZ along with the GTP-regenerating system were added when oscillatory patterns of Min proteins were detected on the membrane. Under both conditions, and after a suitable incubation time of around 30 min, MinCDE proteins were still able to self-organize on the membrane in the presence of FtsZ-GTP and FtsA. Interestingly, FtsZ wave-like patterns were displayed on the membrane and these dynamic oscillations correlated with the characteristic MinCDE propagating waves (**Figure 6.5.A and Movie 6.S2**). The fluorescence

intensity of these correlated waves was analysed demonstrating that the maximal intensity of FtsZ waves correlates with the maximal signal of eGFP-MinD (**Figure 6.5.C**). Furthermore, the fluorescence intensity in the red channel, corresponding to labelled FtsZ, was appreciably lower than the one observed when only FtsA, but not MinCDE proteins, was present (**Figure 6.4.A**). These findings suggest that FtsZ filaments were either partially detached or more temporally attached to the membrane by FtsA when organized MinCDE travelling waves were detected (see **6.2. Discussion**). In this scenario, FtsZ polymers could remain mainly in solution and only a small fraction of FtsZ might interact with FtsA or/and MinCDE proteins.

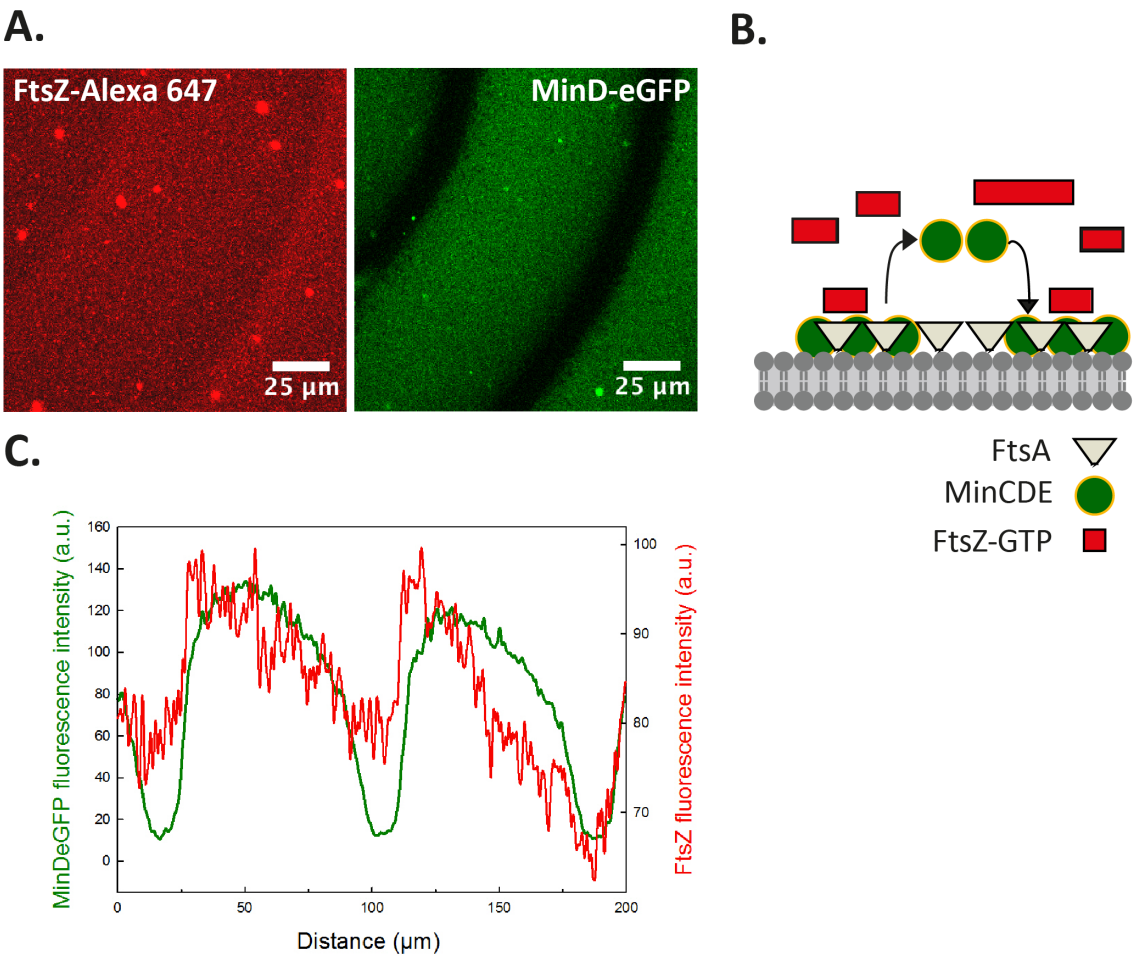

Figure 6.5. Correlated dynamic coupling of FtsZ and MinCDE propagating waves in the presence of FtsA anchor. **(A)** Confocal fluorescence micrographs of organized MinCDE self-organization and FtsZ wave-like patterns on the membrane (FtsA is unlabelled). Dynamic correlated Min-FtsZ waves were noticed in these conditions. For this experiment, ATP (2.5 mM), FtsA (0.5 µM, unlabelled), MinCDE (1 µM MinD, 1 µM MinE, 0.06 µM MinC; labelled protein: eGFP-MinD) and FtsZ-GTP (1.5 µM FtsZ, labelled protein: FtsZ-Alexa 647, 3 mM GTP and Regeneration system) were employed. **(B)** Schematic representation of reconstitution system showed in (A)**.** The black arrows showed the MinCDE self-organization on the membrane. **(C)** Fluorescence intensity profiles of eGFP-MinD (green line) and FtsZ (red line), corresponding to the image shown in (A). See also **Movie 6.S2.**

Then, the same experiment described in **Figure 6.5,** but in the absence of MinC, was performed to analyse the effect of this protein in the coupling Min-FtsZ when FtsA acts as the membrane anchor. As it is shown in **Figure 6.6,** the dynamic MinDE self-organization was detected as was previously reported (Loose and Schwille, 2009). Interestingly, when MinC was not added, FtsA was capable of attaching FtsZ to the membrane and both proteins self-organized into ring-like structures (**Figure 6.6.A right panel and Movie 6.S3**). Moreover, slight anticorrelated MinDE-FtsZ waves were detected on the membrane (**Figure 6.6.C**), in contrast to that observed when MinC is present (**Figure 6.5**). These findings suggest that the low amount of FtsZ in the membrane and the correlated coupling Min-FtsZ observed above (**Figure 6.5**) is mainly due to the MinC effect.

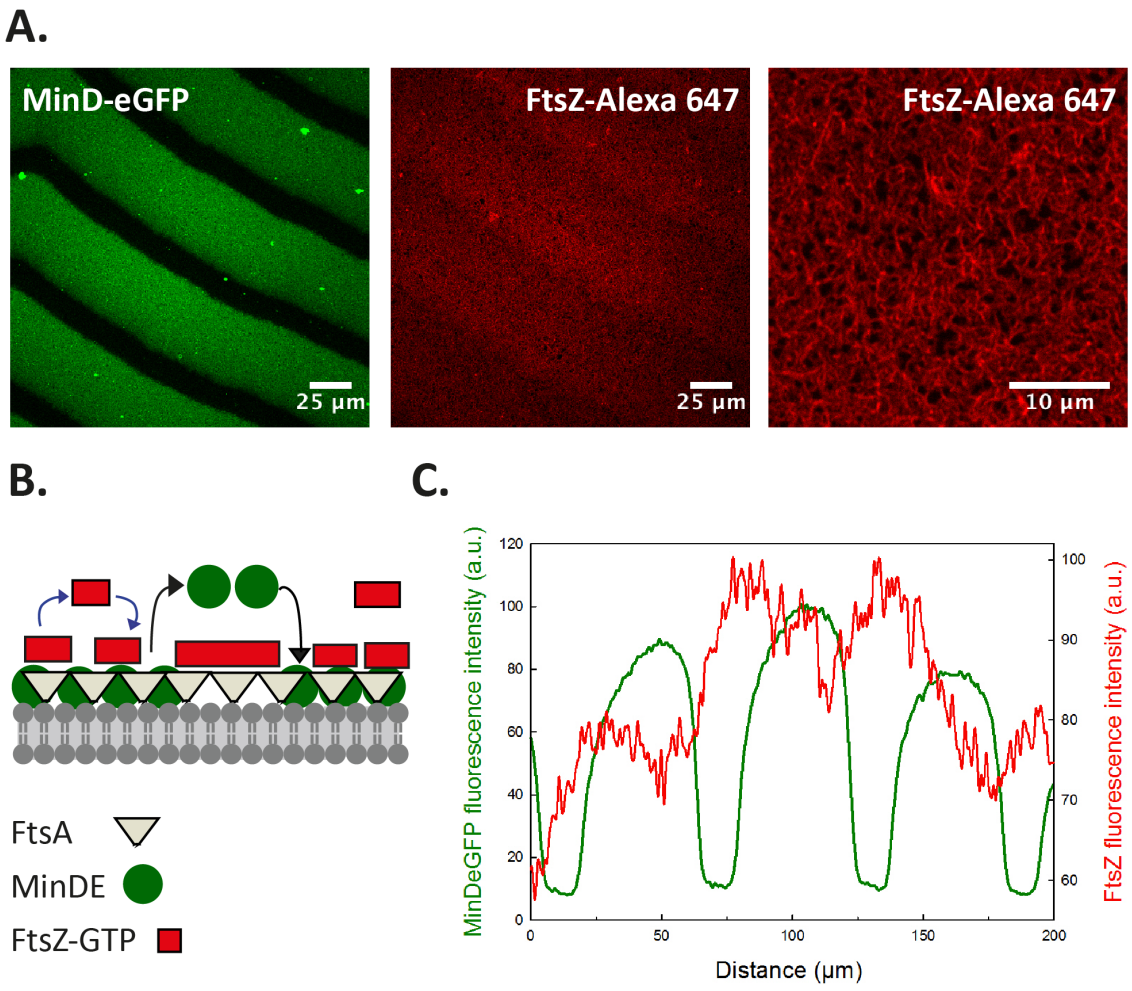

Figure 6.6. FtsA was able to attach FtsZ to the membrane when MinDE self-organization (without MinC) was detected on the bilayer. (A) Confocal fluorescence micrographs showing MinDE (traced by eGFP-MinD) (left) and FtsZ-GTP (labelled protein: FtsZ-Alexa 647) attached to the membrane by FtsA. Under these conditions, FtsA-FtsZ ring patterns were formed on the membrane as it is shown in the right panel (Zoom 6x) **(B)** Schematic representation of reconstitution system showed in (A)**.** The blue arrows show the dynamic self-organization of FtsA-FtsZ. The black arrows show the MinDE self-organization on the membrane. **(C)** Fluorescence intensity profiles of eGFP-MinD (green line) and FtsZ (red line), corresponding to the image shown in (A). The protein concentrations employed in this experiment were the same as in **Figure 6.5**. See also **Movie 6.S3.**

To examine the role of FtsA in the described correlated dynamic coupling of FtsZ polymers and MinCDE complex (**Figure 6.5**), we also analysed the behaviour of these proteins when FtsA was absent in the sample, and therefore FtsZ could not be attached to the membrane by this natural anchor. Under these conditions, correlated Min-FtsZ oscillating waves were also observed (**Figure 6.7.A and Movie 6.S4**), similar to those registered in the presence of FtsA (**Figure 6.5**), as previously found in section 5 where correlated coupling of MinCDE and FtsZ was found in the absence of ZipA (**Figure 5.6**). This finding points out that the presence of a small amount of FtsZ in the membrane, in the absence of the other proto-ring proteins, would be due to the interaction with MinC. This behaviour may be consistent with the known interference of MinC with FtsZ polymerization through preferential interaction with FtsZ-GDP (Hernandez-Rocamora *et al.*, 2013). Therefore, the low amount of FtsZ protein detected traveling on the membrane through MinCDE could correspond to unassembled FtsZ that was not attached to the membrane by FtsA, since MinC hindered the FtsA-FtsZ interaction.

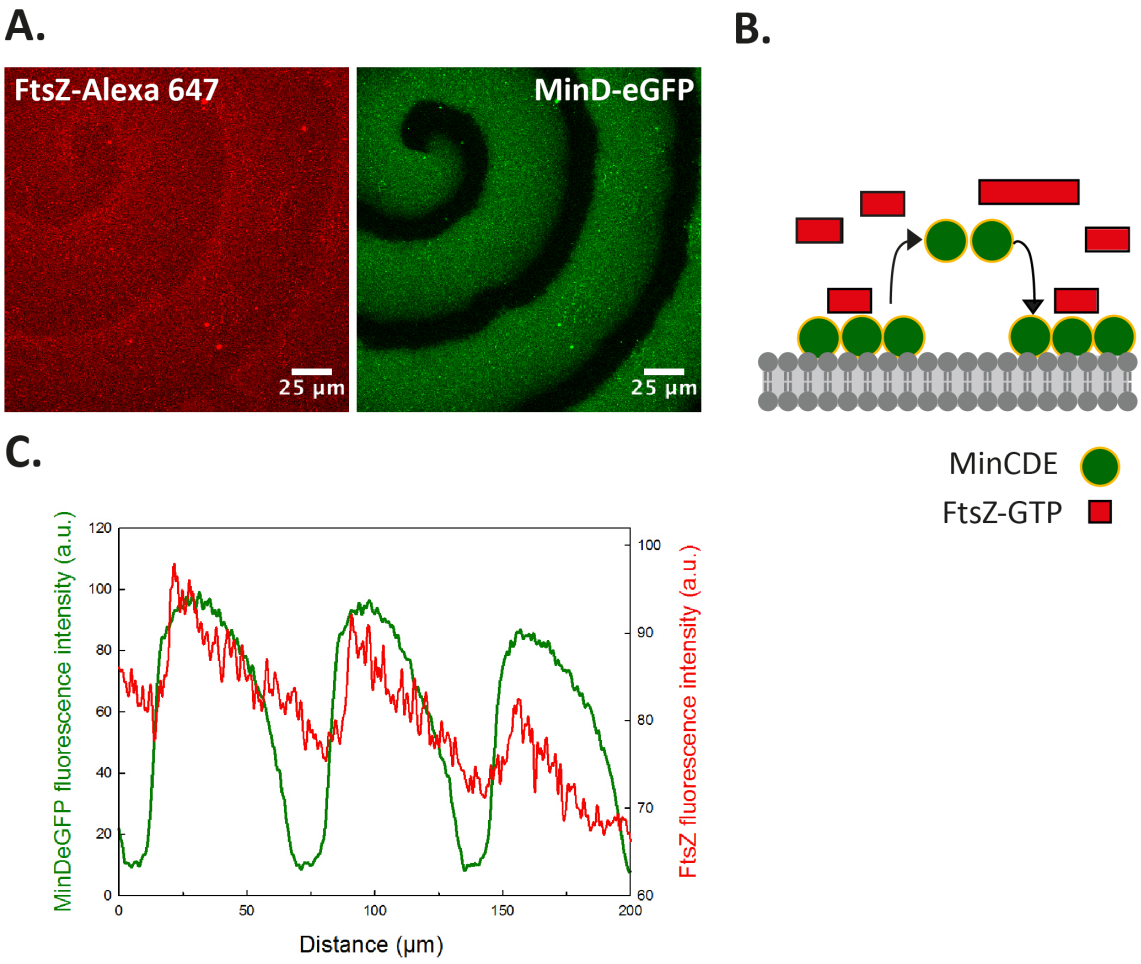

Figure 6.7. Correlated coupling of MinCDE-FtsZ waves in the absence of FtsA anchor. (A) Confocal fluorescence micrographs showing MinCDE (traced by eGFP-MinD) and FtsZ-GTP (labelled protein: FtsZ-Alexa 647) correlated waves in the absence of FtsA. **(B)** Schematic representation of reconstitution system showed in A**. (C)**

Fluorescence intensity profiles of eGFP-MinD (green line) and FtsZ (red line) corresponding to the image shown in A. The protein concentrations employed in this experiment were the same as in **Figure 6.5**. See also **Movie 6.S4.**

Finally, when MinC and FtsA proteins were not added to the sample, MinDE oscillations were observed but FtsZ dynamic waves patterns did not emerge on the membrane (**Figure 6.8 and Movie 6.S5**). In this condition, the FtsZ-GTP fluorescence intensity detected on the membrane and in the bulk solution was similar since the protein was not attached to the lipid bilayer. Therefore, our results again suggest that the observed correlated FtsZ-Min waves are the result of MinC-FtsZ interaction.

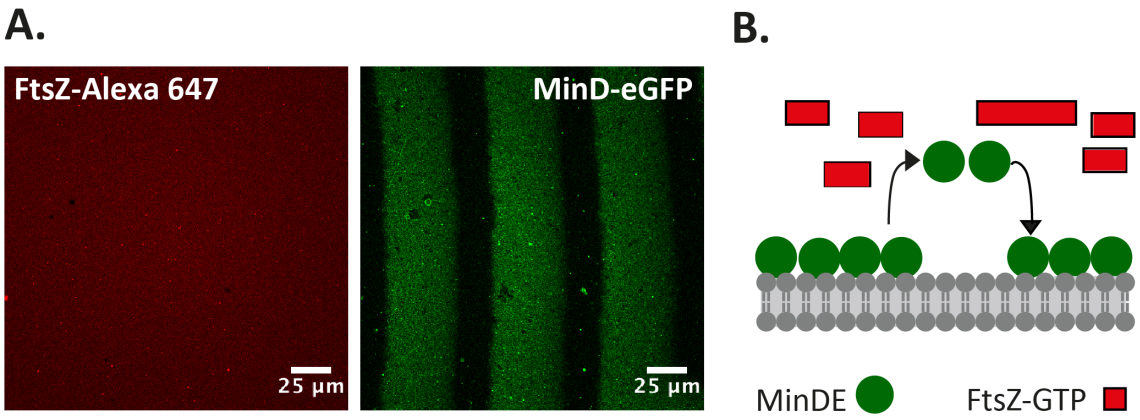

Figure 6.8. Coupling of MinDE-FtsZ was not detected when MinC and FtsA were absent in the sample. **(A)** Confocal fluorescence images showing MinDE oscillation patterns on the bilayer and very low FtsZ fluorescence signal from the FtsZ in the bulk solution. **(B)** Schematic representation of the components showed in A**.** The protein concentrations employed in this experiment were the same as in **Figure 6.5**. See also **Movie 6.S5**.

The findings presented here suggest that a minor fraction of FtsZ, likely unassembled, co-migrated with the MinCDE proteins waves when organized Min proteins oscillations were observed in the presence of FtsA. In this case and contrary to that described in the presence of ZipA (**see section 5**), anticorrelated coupling between MinCDE and FtsZ filaments mediated by MinC inhibition process did not happen probably because FtsZ filaments were only temporarily attached to the membrane by FtsA, since MinC would compete with FtsA for binding of FtsZ as they both interact with the C-terminal central hub of the protein (Ortiz *et al.*, 2016). Furthermore, the soft FtsZ oscillation patterns found without ZipA or FtsA were not displayed in the absence of MinC, indicating that correlated coupling of MinCDE-FtsZ was triggered by MinC.

- ***6.1.2.2 Membrane-clad micro-compartments systems***

The behaviour of the MinCDE-FtsZ-GTP system with FtsA as the membrane anchor was studied in cell-shaped membrane-clad compartments to approach to the bacterial cell confinement (**Figure 6.9**). Preliminary results using these micro-compartments indicated that MinCDE complex and FtsZ filaments oscillated from pole to pole of these chambers due to the space confinement in small sample volumes with cell shaped geometry (**Figure 6.9 and Movie 6.S6**). Interestingly, FtsZ-GTP fluorescence signal recorded in this confined system was higher than when the same proteins were reconstructed on flat membranes (**Figure 6.5 and 6.9**) and, an anti-correlated coupling between the Min system and FtsZ was detected inside the cavities (**Figure 6.9**) in contrast with the correlation observed in flat bilayers. Further experiments using ZipA as the FtsZ membrane anchor could provide significant details about the effect of the space confinement in the Min-FtsZ coupling.

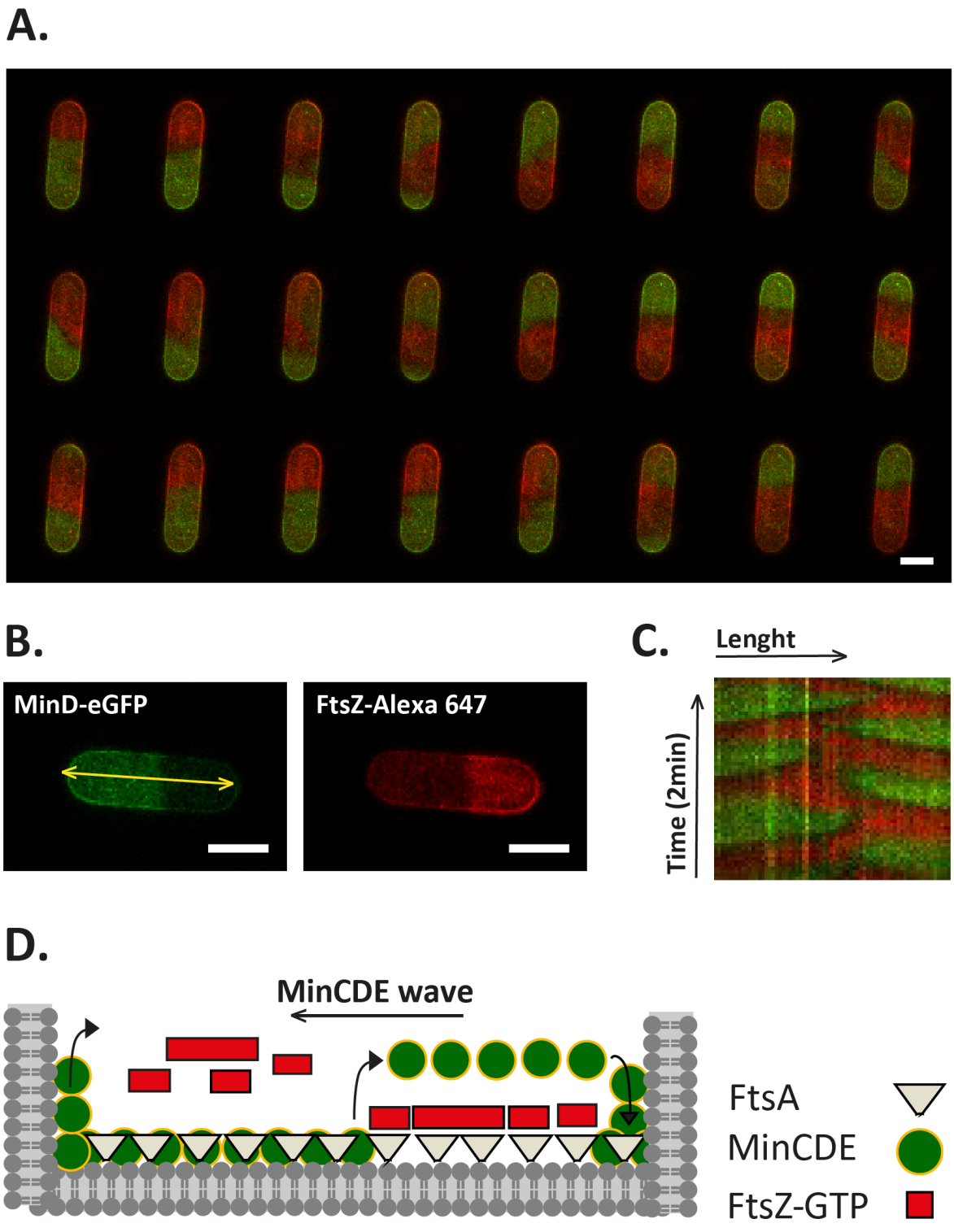

Figure 6.9. Anti-correlated coupling of MinCDE-FtsZ waves in the presence of FtsA in micro-compartments. **(A)** Sequential confocal fluorescence micrographs of MinCDE-FtsZ oscillations inside a micro-compartment (images taken every 5 s). MinCDE dynamic oscillations are traced by eGFP-MinD (green signal) and FtsZ filaments are traced by FtsZ-Alexa 647 (red signal). Unlabelled FtsA was employed in this experiment. **(B)** Confocal fluorescence micrographs of a micro-compartment showing MinCDE proteins (green channel) and FtsZ-GTP (red channel). The yellow arrow points out the pole-to-pole oscillation of MinCDE and FtsZ in the micro-compartments **(C)** The kymograph represents the intensity profile of MinCDE proteins (green channel) and FtsZ-GTP (red channel) along a

selected line (yellow arrow showed in B) along the time. Anti-correlated coupling of MinCDE-FtsZ waves was stated by kymograph analysis. **(D)** Schematic representation of the processes showed in B. The black arrows indicate MinCDE oscillation direction. ATP (2.5 mM), FtsA (0.5 μM, unlabelled), MinCDE (1 μM MinD, 1 μM MinE, 0.06 μM MinC; labelled protein: eGFP-MinD) and FtsZ-GTP (1.5 μM FtsZ, labelled protein: FtsZ-Alexa 647, 3 mM GTP and Regeneration system) were employed. Scale bars (white line in confocal images) correspond to 10 μm. See also **Movie 6.S6.**

6.2. DISCUSSION

The reconstructions of the FtsZ-Min system in the presence of ZipA or FtsA accomplished in this thesis provide new information about the role of these membrane-tethering elements in the FtsZ attachment to the membrane using *in vitro* biomimetic membrane systems. When ZipA attaches FtsZ to the membrane, travelling MinCDE protein patterns drive the propagation of FtsZ anti-correlated waves, since MinC dislodges FtsZ filaments from the membrane (**see Section 5, Figure 5.3**). However, when FtsA is the FtsZ membrane anchor, FtsZ polymers are mainly in the bulk solution and only a small fraction of FtsZ travels with MinCDE complex, giving rise to a correlated coupling of them. Therefore, we found that the dynamic distribution of FtsZ controlled by the MinCDE system is different depending upon which proto-ring protein anchors FtsZ to the membrane (**Figure 6.10**).

To perform this study, the production of the recalcitrant protein FtsA was required. After an optimization of the recently published purification protocol to obtain untagged FtsA (Loose and Mitchison, 2014), the protein characterization in solution and in membrane systems confirmed the functionality of the purified protein. According to our results, FtsA in solution is able to interact with *E. coli* lipids with a moderate affinity and to recruit FtsZ polymers to the membrane allowing the FtsA-FtsZ self-organization into dynamic vortices.

Previous studies evidenced that the membrane targeted sequence (mts) from FtsA can be replaced for the MinD mts without loss of its capacity of attach FtsZ to the membrane (Lutkenhaus, 2007), suggesting that these two domains maybe equivalent for membrane binding. Since the membrane targeted sequence of FtsZ-YFP-mts derives from MinD, the fact that similar apparent affinity constants for the *E. coli* lipids are observed for FtsA and FtsZ-YFP-mts would further support this proposal (**see Figure 4.4 and Figure 6.2**).

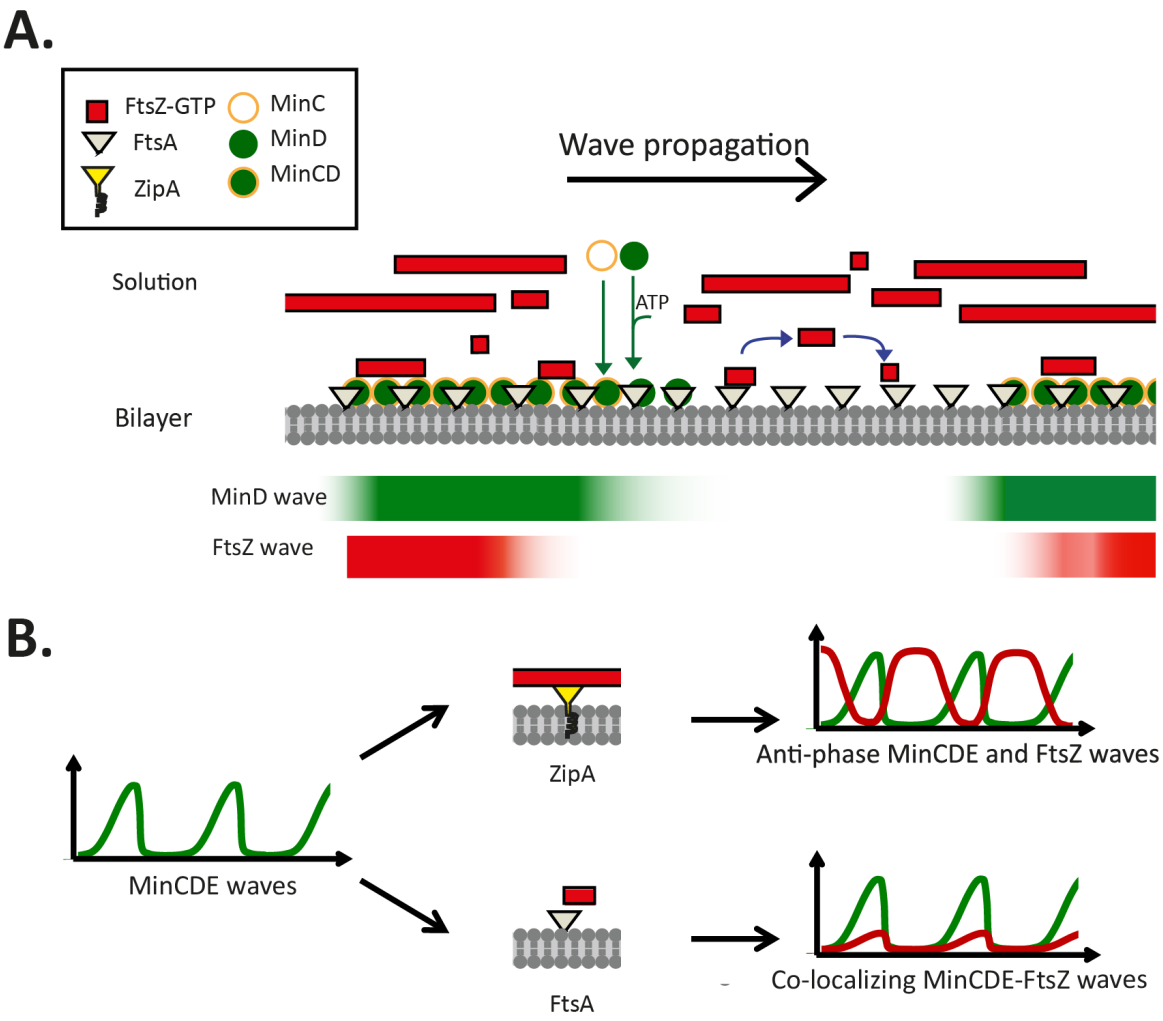

Figure 6.10. **Model showing the effect of the FtsZ membrane anchor in MinCDE-FtsZ coupling. (A)** Model for the dynamic distribution of MinCDE-FtsZ polymers coupling when FtsA acts as the membrane anchor. When complete MinCDE oscillations (MinE was omitted in this figure for simplicity) establish on the membrane, FtsZ filaments interact with Min complex and correlated Min-FtsZ waves are detected. A low FtsZ concentration is weakly attached to the membrane by FtsA as this amphipathic protein co-assembles with FtsZ but also, accomplishes the rapid disassembly of FtsZ filaments (displayed in the figure by the blue arrows). **(B)** Effect of membrane recruitment of FtsZ polymers by a strong anchor (ZipA) or a week anchor (FtsA) in Min-FtsZ coupling: FtsZ waves in antiphase with the MinCDE waves are formed when FtsZ is anchored to the membrane through ZipA, resulting in an efficient dislodgment of FtsZ from the membrane regions where MinC is present. Co-localizing MinCDE-FtsZ waves are found in the presence of FtsA. To simplify the comparison between our findings in the regulation of FtsZ polymers by MinCDE complex when ZipA or FtsA are employed as the membrane-tethering element, an equivalent scheme to the one showed in section 5 has been elaborated.

We have found a dynamic behaviour of FtsZ in the presence of FtsA and the MinCDE system involving correlated coupling between Min waves and FtsZ. Our results strongly suggest that this type of coupling is mainly due to the MinCDE-FtsZ interaction, because it is maintained in samples lacking FtsA. Indeed, it seems that it is the interaction between FtsZ and MinC the one responsible of this behaviour as when both MinC and FtsA are absent in

the sample, MinDE self-organizes forming oscillation waves but dynamic FtsZ waves are not detected on the membrane (**see Figure 6.8**). It is widely known that MinC negatively regulates FtsZ assembly and this inhibition is strongly enhanced by MinD-MinC interaction (Lutkenhaus, 2007). Moreover, FtsZ bundles exclusion by *in vitro* reconstituted MinCDE waves has been detected (Bisicchia *et al.,* 2013). Therefore, when MinCDE proteins oscillations travel on the membrane, MinC/MinD inhibition mechanism would reduce the size of the FtsZ filaments in the vicinity of the membrane. According to this, in our system, most of the FtsZ protein that travels with MinCDE complex could correspond with the unassembled FtsZ that is interacting with MinC.

The results showed in the present section using FtsA as a membrane anchor establish that MinCDE complex drives a different dynamic distribution of FtsZ polymers when ZipA or FtsA are used as natural membrane tethers of FtsZ (**Figure 5.3 and Figure 6.5**). The confocal fluorescence micrographs provide strong evidence pointing out that FtsZ polymers concentration on the membrane is higher when ZipA operates as a membrane anchor and MinCDE proteins self-organize in SLBs. One explanation for the observed differences could be that, as it was mentioned in Section 5.2, FtsZ membrane binding is stronger when ZipA acts as the membrane anchor (Loose and Mitchison, 2014) (Ortiz *et al.*, 2016). This is because FtsA reversibly binds to the membrane, in contrast to ZipA that is a trans-membrane protein. The constant reorganization of the FtsZ-FtsA filament network described above (**see Figure 6.3**) would render a very low FtsZ concentration interacting with the MinCDE system, since most of the FtsZ polymers would be in the bulk solution. In addition, our results demonstrate that FtsA is only able to recruit FtsZ when MinC is not present in the sample (**see Figure 6.6**). This behaviour could be due to the fact that MinC and FtsA compete for FtsZ interaction, since both bind to the FtsZ central hub (Ortiz *et al.*, 2016).

Previous studies stated that FtsA as well as MinC depolymerize FtsZ bundles (Arumugam *et al.*, 2014) (Loose and Mitchison, 2014). Therefore, a synergic effect of both proteins could trigger an enhancement in FtsZ depolymerisation that would lead to a decrease in FtsZ filaments concentration attached on the membrane. Moreover, in contrast to ZipA that has a high binding affinity for FtsZ, recruiting monomers and polymers to the membrane, it has been proposed that FtsA only recruits FtsZ polymers (Loose and Mitchison, 2014). Since MinC counteracts FtsZ polymerization, its presence would significantly reduce the efficiency of FtsZ attachment to the membrane by FtsA. Taken together, our results suggest that the low amount of FtsZ that co-migrates with MinCDE waves in the presence of FtsA might be due to four different factors: dynamic interaction of FtsA-FtsZ, FtsZ filaments

depolymerization by MinC and FtsA, MinC-FtsA competition to bind FtsZ and the preferential binding of FtsZ polymers by FtsA.

As it was predicted in Section 5, the findings reported in the present section demonstrate that ZipA, in addition to its already established function in proto-ring stability (Pazos *et al.*, 2013), may play a central role in *E. coli* Z ring membrane attachment and in its placement driven by the site-selection Min system, that cannot be fully bypassed by FtsA. Our findings support a model proposed previously (Pichoff *et al.*, 2012) (Rico *et al.*, 2013) where the FtsZ recruitment to the proto-ring occurs in two stages: first, FtsA would drive the FtsZ assembly and then it would be replaced by ZipA in the attachment of FtsZ to the membrane.

Cell-shaped membrane-clad micro-compartments represent an excellent biomimetic strategy to reconstruct the Min-FtsZ system, since they allow studying the protein systems in a confined space, more closely resembling the bacterial cell (Kretschmer and Schwille, 2016). Using this approach to reconstruct the MinCDE system together with FtsA-FtsZ filaments, anticorrelated oscillations from pole to pole of the micro-compartments were found, in contrast with that observed in flat membranes with an open and unrestricted geometry (**Figure 6.9 and Figure 6.5**). Based on these preliminary findings, a crucial role of the proteins three-dimensional confinement is proposed since it is the only parameter that was varied with respect to the other experimental setup.

The findings reported here have opened up new pathways of research. In particular, the reconstruction of MinCDE and the complete proto-ring (FtsZ-ZipA-FtsA) in SLBs could represent the next step to clarify the attachment of FtsZ to the membrane by FtsA and ZipA. Furthermore, the addition of crowders (Ficoll 70) or cross-linkers (ZapA-ZapB) to this reconstruction system could provide more information about the effect of the cell environment in Z ring localization and assembly. Importantly, the future incorporation of the complete proto-ring along with the MinCDE complex in micro-compartments will increase our understanding of space confinement effect in bacterial cell division.

7. CONCLUSIONS

The main conclusions that emerge from each subproject of this thesis can be summerize as follows:

I. Self-organization of membrane-tethered FtsZ in flat supported membranes:

1. The self-association and assembly properties of the membrane tethered-FtsZ variant (FtsZ-YFP-mts) are controlled by the same physiological ligands as those regulating the behaviour of natural FtsZ, namely GTP and Mg^{2+}. In addition, the strength of binding of FtsZ-mts polymers to *E. coli* lipids is higher than the one of non-assembled protein.

2. The ability to form rotating rings on lipid bilayers is an intrinsic property of FtsZ. Membrane-targeting of FtsZ is sufficient for the protein to unfold its spatial self-organization behaviour, resulting in dynamic ring-like structures on supported lipid bilayers as a result of treadmilling. These behaviour is regulated by GTPase activity.

3. The formation of dynamic FtsZ swirls only occur within a narrow range of protein concentrations on the membrane, which are modulated by free magnesium and depend upon GTP hydrolysis.

4. The vortex chirality is inverted by switching the membrane anchor from the C-terminus (clockwise) to the N-terminus (anticlockwise).

5. The observed dynamic chiral vortices of FtsZ on planar membranes seem to support the idea that the FtsZ filament does not have a single, but rather more than one direction of curvature, like a helix or a twisted arc.

II. Co-reconstitution of FtsZ-MinCDE complexes in ZipA-containing supported membranes:

1. Dynamic pattern formation of the site-selection Min system is sufficient to modulate the spatial organization of FtsZ polymer networks in membrane-like environments: FtsZ polymer networks anchored to the membrane via ZipA, assembles into antiphase dynamic patterns by the action of the Min system.

2. The presence of MinC is required for the formation of the FtsZ propagating waves, suggesting that this FtsZ ring inhibitor, when complexed to MinD, has a higher affinity for the central hub of FtsZ than ZipA, resulting in the displacement of FtsZ polymers from the membrane.

3. Increased ZipA surface density and crowding-induced FtsZ bundling enhance the coupling between the FtsZ polymer network and the Min system, resulting in a stronger depletion of FtsZ at regions in which the concentration of MinC is maximal.

4. ZipA, in addition to its role in proto-ring stability, is crucial for the dynamic coupling between the self-oscillating Min system and the remodeling of FtsZ polymers at the early stages of division *in E. coli*, contributing to the efficient selection of the division site.

III. Co-reconstitution of FtsZ-FtsA-MinCDE complexes in supported membranes:

1. The optimized protocol to produce FtsA has yielded a soluble and functional FtsA (lipid-binding capability) that recruits FtsZ to the membrane forming dynamic ring patterns.

2. The coupling between FtsZ polymers and MinCDE complex is controlled by MinC and the FtsZ membrane tethering element (ZipA or FtsA).

3. In contrast to the anti-correlated MinCDE-FtsZ patterns observed in ZipA-cointaining bilayers, when FtsA acts as the membrane anchor, FtsZ colocalizes with MinC giving rise to a correlated coupling of MinCDE-FtsZ system.

4. ZipA plays a central role in *E. coli* Z ring membrane attachment and in its placement driven by the site-selection Min system, that cannot be fully bypassed by FtsA.

8. MOVIES APPENDIX

SECTION 4

4.S1 MOVIE. FtsZ-YFP-mts assembles into circular vortices as a time dependent process at a protein concentration of 0.5 μM. After GTP addition, monomers are released into solution where the polymerization is triggered. Then, short protofilaments from solution slowly return to the membrane forming small structures with high lateral diffusion (5 min). After 10 min, those short filaments formed unstable and small circular structures that transiently open and close. At later times, ring-like structures with a defined centre become predominant (15 min). In long time regime, rings become larger and thicker. Images were acquired every 10 seconds using TIRF illumination (YFP channel) and displayed at 15 fps**.** See also **Figure 4.5**.

4.S2 MOVIE. FtsZ-YFP-mts shows a polar clockwise growth from a nucleation point. Right panel corresponds to the square area 1 showed in left panel.

4.S3 MOVIE. FtsZ-YFP-mts forms filaments with a specific direction that can glide by treadmilling.

4.S4 MOVIE. Left panel: Single rings of FtsZ-YFP-mts behave as rotating vortices showing a chiral clockwise rotation as a result of treadmilling at a protein concentration of 0.5 μM. Middle panel: FtsZ chimera with no GTPase activity (FtsZ*[T108A]-YFP-mts) forms defined rings without apparent rotation at a protein concentration of 0.2 μM. This FtsZ chimera shows rings with similar size to the ones found with FtsZ-YFP-mts. Right panel: The protein chimera mts-FtsZ-YFP, which has the membrane targeting sequence (mts) in the N-terminus, creates dynamic rings that strikingly appeared to rotate in the anti-clockwise direction at a protein concentration of 1.25 μM. Images acquired every 3 s and displayed at 16 fps. See also **Figure 4.10**.

4.S5 MOVIE. FtsZ filaments growth from nucleation points with different dynamics. Left panel corresponds to FtsZ-YFP-mts, right panel corresponds to FtsZ*[T108A]-YFP-mts. Both acquisitions have been started right after GTP addition.

SECTION 5

5.S1 MOVIE. Ficoll 70 enhances the MinC-induced modulation of FtsZ polymers anchored to ZipA-SLBs. Sequence of confocal images showing MinCDE waves (traced by eGFP-MinC) and the FtsZ network (traced by FtsZ-Alexa 647) on a ZipA-SLB in the presence of 130 g/L Ficoll 70. The modulation value, m, of the FtsZ observed in these conditions was 0.55 ± 0.01. Images were taken every 20 s. See also **Figure 5.9**.

SECTION 6

6.S1 MOVIE. FtsZ and FtsA self-organize into a chirally rotating rings. Video of FtsZ–FtsA filament pattern formation after addition of GTP. Images were taken every 10 s using TIRF illumination (Alexa 488 channel). Scale bar is 2 μm. See also **Figure 6.3**.

6.S2 MOVIE. Correlated dynamic coupling of FtsZ and MinCDE propagating waves in the presence of FtsA anchor. Images were acquired every 2 s using confocal microscopy and displayed at 30 fps**.** See also **Figure 6.5**.

6.S3 MOVIE. FtsA was able to attach FtsZ to the membrane when MinDE self-organization (without MinC) was detected on the bilayer. Slight anticorrelated coupling of MinCDE-FtsZ waves was detected on the membrane. Images were acquired every 2 s using confocal microscopy and displayed at 30 fps**.** See also **Figure 6.6**.

6.S4 MOVIE. Correlated coupling of MinCDE-FtsZ waves in the absence of FtsA anchor. Images were acquired every 2 s using confocal microscopy and displayed at 30 fps**.** See also **Figure 6.7**.

6.S5 MOVIE. Coupling of MinDE-FtsZ was no detected when MinC and FtsA were absent in the sample. Images were acquired every 2 s using confocal microscopy and displayed at 30 fps**.** See also **Figure 6.8**.

6.S6 MOVIE. Anticorrelated coupling of MinCDE-FtsZ waves in the presence of FtsA in micro-compartments. Confocal time-lapse movie of MinCDE (traced by eGFP-MinD) and FtsZ (traced by FtsZ-Alexa 647) patterns in 10 μm wide compartments. FtsA was untagged. Images were acquired every 2 s using confocal microscopy and displayed at 30 fps**.** Scale bar is 10 μm. See also **Figure 6.9**.

9. REFERENCES

1. Adams D.W. and Errington J. *Bacterial cell division: assembly, maintenance and disassembly of the Z ring.* Nat Rev Microbiol, 2009. 7 (9): 642-53.
2. Addinall S.G. and Lutkenhaus J. *FtsA is localized to the septum in an FtsZ-dependent manner.* J Bacteriol, 1996. 178 (24): 7167-72.
3. Anderson D.E., Gueiros-Filho F.J. and Erickson H.P. *Assembly dynamics of FtsZ rings in Bacillus subtilis and Escherichia coli and effects of FtsZ-regulating proteins.* J Bacteriol, 2004. 186 (17): 5775-81.
4. Arumugam S., Chwastek G., Fischer-Friedrich E., Ehrig C., Monch I. and Schwille P. *Surface topology engineering of membranes for the mechanical investigation of the tubulin homologue FtsZ.* Angew Chem Int Ed Engl, 2012. 51 (47): 11858-62.
5. Arumugam S., Petrasek Z. and Schwille P. *MinCDE exploits the dynamic nature of FtsZ filaments for its spatial regulation.* Proc Natl Acad Sci U S A, 2014. 111 (13): E1192-200.
6. Bailey M.W., Bisicchia P., Warren B.T., Sherratt D.J. and Mannik J. *Evidence for divisome localization mechanisms independent of the Min system and SlmA in Escherichia coli.* PLoS Genet, 2014. 10 (8): e1004504.
7. Beuria T.K., Mullapudi S., Mileykovskaya E., Sadasivam M., Dowhan W. and Margolin W. *Adenine nucleotide-dependent regulation of assembly of bacterial tubulin-like FtsZ by a hypermorph of bacterial actin-like FtsA.* J Biol Chem, 2009. 284 (21): 14079-86.
8. Bisicchia P., Arumugam S., Schwille P. and Sherratt D. *MinC, MinD, and MinE drive counter-oscillation of early-cell-division proteins prior to Escherichia coli septum formation.* MBio, 2013. 4 (6): e00856-13.
9. Bisson-Filho A.W., Hsu Y.P., Squyres G.R., Kuru E., Wu F., Jukes C., Sun Y., Dekker C., Holden S., VanNieuwenhze M.S., Brun Y.V. and Garner E.C. *Treadmilling by FtsZ filaments drives peptidoglycan synthesis and bacterial cell division.* Science, 2017. 355 (6326): 739-743.
10. Brian A.A. and McConnell H.M. *Allogeneic stimulation of cytotoxic T cells by supported planar membranes.* Proc Natl Acad Sci U S A, 1984. 81 (19): 6159-63.
11. Cabré E.J., Sanchez-Gorostiaga A., Carrara P., Ropero N., Casanova M., Palacios P., Stano P., Jimenez M., Rivas G. and Vicente M. *Bacterial division proteins FtsZ and ZipA induce vesicle shrinkage and cell membrane invagination.* J Biol Chem, 2013. 288 (37): 26625-34.
12. Chen Y. and Erickson H.P. *Rapid in vitro assembly dynamics and subunit turnover of FtsZ demonstrated by fluorescence resonance energy transfer.* J Biol Chem, 2005. 280 (23): 22549-54.
13. Chiaruttini N. and Roux A. *Dynamic and elastic shape transitions in curved ESCRT-III filaments.* Curr Opin Cell Biol, 2017. 47 126-135.
14. Coltharp C. and Xiao J. *Beyond force generation: Why is a dynamic ring of FtsZ polymers essential for bacterial cytokinesis?* Bioessays, 2017. 39 (1): 1-11.
15. den Blaauwen T., Hamoen L.W. and Levin P.A. *The divisome at 25: the road ahead.* Curr Opin Microbiol, 2017. 36 85-94.
16. Denk J., Huber L., Reithmann E. and Frey E. *Active Curved Polymers Form Vortex Patterns on Membranes.* Phys Rev Lett, 2016. 116 (17): 178301.

17. Dewachter L., Verstraeten N., Fauvart M. and Michiels J. *An integrative view of cell cycle control in Escherichia coli.* FEMS Microbiol Rev, 2018. 42 (2): 116-136.
18. Erickson H.P., Anderson D.E. and Osawa M. *FtsZ in bacterial cytokinesis: cytoskeleton and force generator all in one.* Microbiol Mol Biol Rev, 2010. 74 (4): 504-28.
19. Erickson H.P. and Osawa M. *FtsZ Constriction Force - Curved Protofilaments Bending Membranes.* Subcell Biochem, 2017. 84 139-160.
20. Garcia-Saez A.J. and Schwille P. *Surface analysis of membrane dynamics.* Biochim Biophys Acta, 2010. 1798 (4): 766-76.
21. Geissler B., Elraheb D. and Margolin W. *A gain-of-function mutation in ftsA bypasses the requirement for the essential cell division gene zipA in Escherichia coli.* Proc Natl Acad Sci U S A, 2003. 100 (7): 4197-202.
22. Geissler B., Shiomi D. and Margolin W. *The ftsA* gain-of-function allele of Escherichia coli and its effects on the stability and dynamics of the Z ring.* Microbiology, 2007. 153 (Pt 3): 814-25.
23. Ghosal D., Trambaiolo D., Amos L.A. and Lowe J. *MinCD cell division proteins form alternating copolymeric cytomotive filaments.* Nat Commun, 2014. 5 5341.
24. Gonzalez de Prado Salas P., Horger I., Martin-Garcia F., Mendieta J., Alonso A., Encinar M., Gomez-Puertas P., Velez M. and Tarazona P. *Torsion and curvature of FtsZ filaments.* Soft Matter, 2014. 10 (12): 1977-86.
25. Gonzalez J.M., Jimenez M., Velez M., Mingorance J., Andreu J.M., Vicente M. and Rivas G. *Essential cell division protein FtsZ assembles into one monomer-thick ribbons under conditions resembling the crowded intracellular environment.* J Biol Chem, 2003. 278 (39): 37664-71.
26. Gonzalez J.M., Velez M., Jimenez M., Alfonso C., Schuck P., Mingorance J., Vicente M., Minton A.P. and Rivas G. *Cooperative behavior of Escherichia coli cell-division protein FtsZ assembly involves the preferential cyclization of long single-stranded fibrils.* Proc Natl Acad Sci U S A, 2005. 102 (6): 1895-900.
27. Haeusser D.P. and Margolin W. *Splitsville: structural and functional insights into the dynamic bacterial Z ring.* Nat Rev Microbiol, 2016. 14 (5): 305-19.
28. Hale C.A. and de Boer P.A. *Recruitment of ZipA to the septal ring of Escherichia coli is dependent on FtsZ and independent of FtsA.* J Bacteriol, 1999. 181 (1): 167-76.
29. Hale C.A., Rhee A.C. and de Boer P.A. *ZipA-induced bundling of FtsZ polymers mediated by an interaction between C-terminal domains.* J Bacteriol, 2000. 182 (18): 5153-66.
30. Haney S.A., Glasfeld E., Hale C., Keeney D., He Z. and de Boer P. *Genetic analysis of the Escherichia coli FtsZ.ZipA interaction in the yeast two-hybrid system. Characterization of FtsZ residues essential for the interactions with ZipA and with FtsA.* J Biol Chem, 2001. 276 (15): 11980-7.
31. Hauser H. *Short-chain phospholipids as detergents.* Biochim Biophys Acta, 2000. 1508 (1-2): 164-81.
32. Hernandez-Rocamora V.M., Garcia-Montanes C., Reija B., Monterroso B., Margolin W., Alfonso C., Zorrilla S. and Rivas G. *MinC protein shortens FtsZ protofilaments by preferentially interacting with GDP-bound subunits.* J Biol Chem, 2013. 288 (34): 24625-35.
33. Holden S. *Probing the mechanistic principles of bacterial cell division with super-resolution microscopy.* Curr Opin Microbiol, 2018. 43 84-91.

34. Holden S.J., Pengo T., Meibom K.L., Fernandez Fernandez C., Collier J. and Manley S. *High throughput 3D super-resolution microscopy reveals Caulobacter crescentus in vivo Z-ring organization.* Proc Natl Acad Sci U S A, 2014. 111 (12): 4566-71.
35. Hu Z. and Lutkenhaus J. *Topological regulation of cell division in E. coli. spatiotemporal oscillation of MinD requires stimulation of its ATPase by MinE and phospholipid.* Mol Cell, 2001. 7 (6): 1337-43.
36. Hu Z. and Lutkenhaus J. *Topological regulation of cell division in Escherichia coli involves rapid pole to pole oscillation of the division inhibitor MinC under the control of MinD and MinE.* Mol Microbiol, 1999. 34 (1): 82-90.
37. Hu Z., Mukherjee A., Pichoff S. and Lutkenhaus J. *The MinC component of the division site selection system in Escherichia coli interacts with FtsZ to prevent polymerization.* Proc Natl Acad Sci U S A, 1999. 96 (26): 14819-24.
38. Huang K.H., Durand-Heredia J. and Janakiraman A. *FtsZ ring stability: of bundles, tubules, crosslinks, and curves.* J Bacteriol, 2013. 195 (9): 1859-68.
39. Huecas S. and Andreu J.M. *Polymerization of nucleotide-free, GDP- and GTP-bound cell division protein FtsZ: GDP makes the difference.* FEBS Lett, 2004. 569 (1-3): 43-8.
40. Hurley K.A., Santos T.M., Nepomuceno G.M., Huynh V., Shaw J.T. and Weibel D.B. *Targeting the Bacterial Division Protein FtsZ.* J Med Chem, 2016. 59 (15): 6975-98.
41. Jimenez M., Martos A., Cabré E.J., Raso A. and Rivas G. *Giant vesicles: a powerful tool to reconstruct bacterial division assemblies in cell-like compartments.* Environ Microbiol, 2013. 15 (12): 3158-68.
42. Jimenez M., Martos A., Vicente M. and Rivas G. *Reconstitution and organization of Escherichia coli proto-ring elements (FtsZ and FtsA) inside giant unilamellar vesicles obtained from bacterial inner membranes.* J Biol Chem, 2011. 286 (13): 11236-41.
43. Kretschmer S. and Schwille P. *Pattern formation on membranes and its role in bacterial cell division.* Curr Opin Cell Biol, 2016. 38 52-9.
44. Lindas A.C., Karlsson E.A., Lindgren M.T., Ettema T.J. and Bernander R. *A unique cell division machinery in the Archaea.* Proc Natl Acad Sci U S A, 2008. 105 (48): 18942-6.
45. Loose M., Fischer-Friedrich E., Herold C., Kruse K. and Schwille P. *Min protein patterns emerge from rapid rebinding and membrane interaction of MinE.* Nat Struct Mol Biol, 2011. 18 (5): 577-83.
46. Loose M., Fischer-Friedrich E., Ries J., Kruse K. and Schwille P. *Spatial regulators for bacterial cell division self-organize into surface waves in vitro.* Science, 2008. 320 (5877): 789-92.
47. Loose M., Kruse K. and Schwille P. *Protein self-organization: lessons from the min system.* Annu Rev Biophys, 2011. 40 315-36.
48. Loose M. and Mitchison T.J. *The bacterial cell division proteins FtsA and FtsZ self-organize into dynamic cytoskeletal patterns.* Nat Cell Biol, 2014. 16 (1): 38-46.
49. Loose M. and Schwille P. *Biomimetic membrane systems to study cellular organization.* J Struct Biol, 2009. 168 (1): 143-51.
50. Lopez-Montero I., Mateos-Gil P., Sferrazza M., Navajas P.L., Rivas G., Velez M. and Monroy F. *Active membrane viscoelasticity by the bacterial FtsZ-division protein.* Langmuir, 2012. 28 (10): 4744-53.
51. Lu C., Reedy M. and Erickson H.P. *Straight and curved conformations of FtsZ are regulated by GTP hydrolysis.* J Bacteriol, 2000. 182 (1): 164-70.

52. Lutkenhaus J. *Assembly dynamics of the bacterial MinCDE system and spatial regulation of the Z ring.* Annu Rev Biochem, 2007. 76 539-62.
53. Lutkenhaus J., Pichoff S. and Du S. *Bacterial cytokinesis: From Z ring to divisome.* Cytoskeleton (Hoboken), 2012. 69 (10): 778-90.
54. Ma X. and Margolin W. *Genetic and functional analyses of the conserved C-terminal core domain of Escherichia coli FtsZ.* J Bacteriol, 1999. 181 (24): 7531-44.
55. Mannik J. and Bailey M.W. *Spatial coordination between chromosomes and cell division proteins in Escherichia coli.* Front Microbiol, 2015. 6 306.
56. Margolin W. *FtsZ and the division of prokaryotic cells and organelles.* Nat Rev Mol Cell Biol, 2005. 6 (11): 862-71.
57. Martos A., Alfonso C., Lopez-Navajas P., Ahijado-Guzmn R., Mingorance J., Minton A.P. and Rivas G. *Characterization of self-association and heteroassociation of bacterial cell division proteins FtsZ and ZipA in solution by composition gradient-static light scattering.* Biochemistry, 2010. 49 (51): 10780-7.
58. Martos A., Jimenez M., Rivas G. and Schwille P. *Towards a bottom-up reconstitution of bacterial cell division.* Trends Cell Biol, 2012. 22 (12): 634-43.
59. Martos A., Monterroso B., Zorrilla S., Reija B., Alfonso C., Mingorance J., Rivas G. and Jimenez M. *Isolation, characterization and lipid-binding properties of the recalcitrant FtsA division protein from Escherichia coli.* PLoS One, 2012. 7 (6): e39829.
60. Martos A., Petrasek Z. and Schwille P. *Propagation of MinCDE waves on free-standing membranes.* Environ Microbiol, 2013. 15 (12): 3319-26.
61. Mateos-Gil P., Marquez I., Lopez-Navajas P., Jimenez M., Vicente M., Mingorance J., Rivas G. and Velez M. *FtsZ polymers bound to lipid bilayers through ZipA form dynamic two dimensional networks.* Biochim Biophys Acta, 2012. 1818 (3): 806-13.
62. Meier E.L. and Goley E.D. *Form and function of the bacterial cytokinetic ring.* Curr Opin Cell Biol, 2014. 26 19-27.
63. Meinhardt H. and de Boer P.A. *Pattern formation in Escherichia coli: a model for the pole-to-pole oscillations of Min proteins and the localization of the division site.* Proc Natl Acad Sci U S A, 2001. 98 (25): 14202-7.
64. Menendez M., Rivas G., Diaz J.F. and Andreu J.M. *Control of the structural stability of the tubulin dimer by one high affinity bound magnesium ion at nucleotide N-site.* J Biol Chem, 1998. 273 (1): 167-76.
65. Milam S.L., Osawa M. and Erickson H.P. *Negative-stain electron microscopy of inside-out FtsZ rings reconstituted on artificial membrane tubules show ribbons of protofilaments.* Biophys J, 2012. 103 (1): 59-68.
66. Mingorance J., Rivas G., Velez M., Gomez-Puertas P. and Vicente M. *Strong FtsZ is with the force: mechanisms to constrict bacteria.* Trends Microbiol, 2010. 18 (8): 348-56.
67. Mingorance J., Tadros M., Vicente M., Gonzalez J.M., Rivas G. and Velez M. *Visualization of single Escherichia coli FtsZ filament dynamics with atomic force microscopy.* J Biol Chem, 2005. 280 (21): 20909-14.
68. Monteiro J.M., Pereira A.R., Reichmann N.T., Saraiva B.M., Fernandes P.B., Veiga H., Tavares A.C., Santos M., Ferreira M.T., Macario V., VanNieuwenhze M.S., Filipe S.R. and Pinho M.G. *Peptidoglycan synthesis drives an FtsZ-treadmilling-independent step of cytokinesis.* Nature, 2018. 554 (7693): 528-532.
69. Monterroso B., Ahijado-Guzman R., Reija B., Alfonso C., Zorrilla S., Minton A.P. and Rivas G. *Mg(2+)-linked self-assembly of FtsZ in the presence of GTP or a GTP*

analogue involves the concerted formation of a narrow size distribution of oligomeric species. Biochemistry, 2012. 51 (22): 4541-50.
70. Monterroso B., Alfonso C., Zorrilla S. and Rivas G. *Combined analytical ultracentrifugation, light scattering and fluorescence spectroscopy studies on the functional associations of the bacterial division FtsZ protein.* Methods, 2013. 59 (3): 349-62.
71. Moran U., Phillips R. and Milo R. *SnapShot: key numbers in biology.* Cell, 2010. 141 (7): 1262-1262 e1.
72. Mosyak L., Zhang Y., Glasfeld E., Haney S., Stahl M., Seehra J. and Somers W.S. *The bacterial cell-division protein ZipA and its interaction with an FtsZ fragment revealed by X-ray crystallography.* EMBO J, 2000. 19 (13): 3179-91.
73. Nanninga N. *Morphogenesis of Escherichia coli.* Microbiol Mol Biol Rev, 1998. 62 (1): 110-29.
74. Natale P., Pazos M. and Vicente M. *The Escherichia coli divisome: born to divide.* Environ Microbiol, 2013. 15 (12): 3169-82.
75. Niu L. and Yu J. *Investigating intracellular dynamics of FtsZ cytoskeleton with photoactivation single-molecule tracking.* Biophys J, 2008. 95 (4): 2009-16.
76. Ortiz C., Natale P., Cueto L. and Vicente M. *The keepers of the ring: regulators of FtsZ assembly.* FEMS Microbiol Rev, 2016. 40 (1): 57-67.
77. Osawa M., Anderson D.E. and Erickson H.P. *Curved FtsZ protofilaments generate bending forces on liposome membranes.* EMBO J, 2009. 28 (22): 3476-84.
78. Osawa M., Anderson D.E. and Erickson H.P. *Reconstitution of contractile FtsZ rings in liposomes.* Science, 2008. 320 (5877): 792-4.
79. Osawa M. and Erickson H.P. *Chapter 1 - Tubular liposomes with variable permeability for reconstitution of FtsZ rings.* Methods Enzymol, 2009. 464 3-17.
80. Osawa M. and Erickson H.P. *Inside-out Z rings--constriction with and without GTP hydrolysis.* Mol Microbiol, 2011. 81 (2): 571-9.
81. Osawa M. and Erickson H.P. *Liposome division by a simple bacterial division machinery.* Proc Natl Acad Sci U S A, 2013. 110 (27): 11000-4.
82. Osawa M. and Erickson H.P. *Turgor Pressure and Possible Constriction Mechanisms in Bacterial Division.* Front Microbiol, 2018. 9 111.
83. Park K.T., Dajkovic A., Wissel M., Du S. and Lutkenhaus J. *MinC and FtsZ mutant analysis provides insight into MinC/MinD-mediated Z ring disassembly.* J Biol Chem, 2018. 293 (16): 5834-5846.
84. Pazos M., Natale P. and Vicente M. *A specific role for the ZipA protein in cell division: stabilization of the FtsZ protein.* J Biol Chem, 2013. 288 (5): 3219-26.
85. Pichoff S. and Lutkenhaus J. *Escherichia coli division inhibitor MinCD blocks septation by preventing Z-ring formation.* J Bacteriol, 2001. 183 (22): 6630-5.
86. Pichoff S. and Lutkenhaus J. *Identification of a region of FtsA required for interaction with FtsZ.* Mol Microbiol, 2007. 64 (4): 1129-38.
87. Pichoff S. and Lutkenhaus J. *Tethering the Z ring to the membrane through a conserved membrane targeting sequence in FtsA.* Mol Microbiol, 2005. 55 (6): 1722-34.
88. Pichoff S. and Lutkenhaus J. *Unique and overlapping roles for ZipA and FtsA in septal ring assembly in Escherichia coli.* EMBO J, 2002. 21 (4): 685-93.
89. Pichoff S., Shen B., Sullivan B. and Lutkenhaus J. *FtsA mutants impaired for self-interaction bypass ZipA suggesting a model in which FtsA's self-interaction competes*

with its ability to recruit downstream division proteins. Mol Microbiol, 2012. 83 (1): 151-67.
90. Potluri L.P., Kannan S. and Young K.D. *ZipA is required for FtsZ-dependent preseptal peptidoglycan synthesis prior to invagination during cell division.* J Bacteriol, 2012. 194 (19): 5334-42.
91. RayChaudhuri D. *ZipA is a MAP-Tau homolog and is essential for structural integrity of the cytokinetic FtsZ ring during bacterial cell division.* EMBO J, 1999. 18 (9): 2372-83.
92. Reija B., Monterroso B., Jimenez M., Vicente M., Rivas G. and Zorrilla S. *Development of a homogeneous fluorescence anisotropy assay to monitor and measure FtsZ assembly in solution.* Anal Biochem, 2011. 418 (1): 89-96.
93. Renner L.D. and Weibel D.B. *MinD and MinE interact with anionic phospholipids and regulate division plane formation in Escherichia coli.* J Biol Chem, 2012. 287 (46): 38835-44.
94. Richter R.P., Berat R. and Brisson A.R. *Formation of solid-supported lipid bilayers: an integrated view.* Langmuir, 2006. 22 (8): 3497-505.
95. Rico A.I., Garcia-Ovalle M., Mingorance J. and Vicente M. *Role of two essential domains of Escherichia coli FtsA in localization and progression of the division ring.* Mol Microbiol, 2004. 53 (5): 1359-71.
96. Rico A.I., Krupka M. and Vicente M. *In the beginning, Escherichia coli assembled the proto-ring: an initial phase of division.* J Biol Chem, 2013. 288 (29): 20830-6.
97. Rigaud J.L. and Levy D. *Reconstitution of membrane proteins into liposomes.* Methods Enzymol, 2003. 372 65-86.
98. Rivas G., Alfonso C., Jimenez M., Monterroso B. and Zorrilla S. *Macromolecular interactions of the bacterial division FtsZ protein: from quantitative biochemistry and crowding to reconstructing minimal divisomes in the test tube.* Biophys Rev, 2013. 5 (2): 63-77.
99. Rivas G., Lopez A., Mingorance J., Ferrandiz M.J., Zorrilla S., Minton A.P., Vicente M. and Andreu J.M. *Magnesium-induced linear self-association of the FtsZ bacterial cell division protein monomer. The primary steps for FtsZ assembly.* J Biol Chem, 2000. 275 (16): 11740-9.
100. Rivas G., Vogel S.K. and Schwille P. *Reconstitution of cytoskeletal protein assemblies for large-scale membrane transformation.* Curr Opin Chem Biol, 2014. 22 18-26.
101. Romberg L. and Levin P.A. *Assembly dynamics of the bacterial cell division protein FTSZ: poised at the edge of stability.* Annu Rev Microbiol, 2003. 57 125-54.
102. Rouser G., Siakotos A.N. and Fleischer S. *Quantitative analysis of phospholipids by thin-layer chromatography and phosphorus analysis of spots.* Lipids, 1966. 1 (1): 85-6.
103. Rowlett V.W. and Margolin W. *The bacterial Min system.* Curr Biol, 2013. 23 (13): R553-6.
104. Rueda S., Vicente M. and Mingorance J. *Concentration and assembly of the division ring proteins FtsZ, FtsA, and ZipA during the Escherichia coli cell cycle.* J Bacteriol, 2003. 185 (11): 3344-51.
105. Samson R.Y., Obita T., Freund S.M., Williams R.L. and Bell S.D. *A role for the ESCRT system in cell division in archaea.* Science, 2008. 322 (5908): 1710-3.
106. Schuck P. *Size-distribution analysis of macromolecules by sedimentation velocity ultracentrifugation and lamm equation modeling.* Biophys J, 2000. 78 (3): 1606-19.

107. Shen B. and Lutkenhaus J. *The conserved C-terminal tail of FtsZ is required for the septal localization and division inhibitory activity of MinC(C)/MinD.* Mol Microbiol, 2009. 72 (2): 410-24.
108. Sobrinos-Sanguino M., Zorrilla S., Monterroso B., Minton A.P. and Rivas G. *Nucleotide and receptor density modulate binding of bacterial division FtsZ protein to ZipA containing lipid-coated microbeads.* Sci Rep, 2017. 7 (1): 13707.
109. Soderstrom B. and Daley D.O. *The bacterial divisome: more than a ring?* Curr Genet, 2017. 63 (2): 161-164.
110. Soderstrom B., Mirzadeh K., Toddo S., von Heijne G., Skoglund U. and Daley D.O. *Coordinated disassembly of the divisome complex in Escherichia coli.* Mol Microbiol, 2016. 101 (3): 425-38.
111. Soderstrom B., Skoog K., Blom H., Weiss D.S., von Heijne G. and Daley D.O. *Disassembly of the divisome in Escherichia coli: evidence that FtsZ dissociates before compartmentalization.* Mol Microbiol, 2014. 92 (1): 1-9.
112. Suefuji K., Valluzzi R. and RayChaudhuri D. *Dynamic assembly of MinD into filament bundles modulated by ATP, phospholipids, and MinE.* Proc Natl Acad Sci U S A, 2002. 99 (26): 16776-81.
113. Sundararaj S., Guo A., Habibi-Nazhad B., Rouani M., Stothard P., Ellison M. and Wishart D.S. *The CyberCell Database (CCDB): a comprehensive, self-updating, relational database to coordinate and facilitate in silico modeling of Escherichia coli.* Nucleic Acids Res, 2004. 32 (Database issue): D293-5.
114. Szwedziak P., Wang Q., Bharat T.A., Tsim M. and Lowe J. *Architecture of the ring formed by the tubulin homologue FtsZ in bacterial cell division.* Elife, 2014. 3 e04601.
115. Szwedziak P., Wang Q., Freund S.M. and Lowe J. *FtsA forms actin-like protofilaments.* EMBO J, 2012. 31 (10): 2249-60.
116. Thanedar S. and Margolin W. *FtsZ exhibits rapid movement and oscillation waves in helix-like patterns in Escherichia coli.* Curr Biol, 2004. 14 (13): 1167-73.
117. Tonthat N.K., Milam S.L., Chinnam N., Whitfill T., Margolin W. and Schumacher M.A. *SlmA forms a higher-order structure on DNA that inhibits cytokinetic Z-ring formation over the nucleoid.* Proc Natl Acad Sci U S A, 2013. 110 (26): 10586-91.
118. Vicente M., Rico A.I., Martinez-Arteaga R. and Mingorance J. *Septum enlightenment: assembly of bacterial division proteins.* J Bacteriol, 2006. 188 (1): 19-27.
119. Wagstaff J.M., Tsim M., Oliva M.A., Garcia-Sanchez A., Kureisaite-Ciziene D., Andreu J.M. and Lowe J. *A Polymerization-Associated Structural Switch in FtsZ That Enables Treadmilling of Model Filaments.* MBio, 2017. 8 (3):
120. Weimann L., Ganzinger K.A., McColl J., Irvine K.L., Davis S.J., Gay N.J., Bryant C.E. and Klenerman D. *A quantitative comparison of single-dye tracking analysis tools using Monte Carlo simulations.* PLoS One, 2013. 8 (5): e64287.
121. Wiseman P.W. and Petersen N.O. *Image correlation spectroscopy. II. Optimization for ultrasensitive detection of preexisting platelet-derived growth factor-beta receptor oligomers on intact cells.* Biophys J, 1999. 76 (2): 963-77.
122. Wu L.J. and Errington J. *Nucleoid occlusion and bacterial cell division.* Nat Rev Microbiol, 2011. 10 (1): 8-12.
123. Yang X., Lyu Z., Miguel A., McQuillen R., Huang K.C. and Xiao J. *GTPase activity-coupled treadmilling of the bacterial tubulin FtsZ organizes septal cell wall synthesis.* Science, 2017. 355 (6326): 744-747.

124. Zieske K., Chwastek G. and Schwille P. *Protein Patterns and Oscillations on Lipid Monolayers and in Microdroplets.* Angew Chem Int Ed Engl, 2016. 55 (43): 13455-13459.
125. Zieske K. and Schwille P. *Reconstitution of pole-to-pole oscillations of min proteins in microengineered polydimethylsiloxane compartments.* Angew Chem Int Ed Engl, 2013. 52 (1): 459-62.
126. Zieske K. and Schwille P. *Reconstitution of self-organizing protein gradients as spatial cues in cell-free systems.* Elife, 2014. 3